ORGANIC-INORGANIC NANOCOMPOSITE MEMBRANES FROM HIGHLY ORDERED MESOPOROUS THIN FILMS FOR SOLUBILITY-BASED SEPARATIONS

A Dissertation

by

SUK JOON YOO

Submitted to the Office of Graduate Studies of
Texas A&M University
in partial fulfillment of the requirements for the degree of

DOCTOR OF PHILOSOPHY

December 2006

Major Subject: Chemical Engineering

ORGANIC-INORGANIC NANOCOMPOSITE MEMBRANES FROM HIGHLY ORDERED MESOPOROUS THIN FILMS FOR SOLUBILITY-BASED SEPARATIONS

A Dissertation

by

SUK JOON YOO

Submitted to the Office of Graduate Studies of
Texas A&M University
in partial fulfillment of the requirements for the degree of

DOCTOR OF PHILOSOPHY

Approved by:

Co-Chairs of Committee,	David M. Ford
	Daniel F. Shantz
Committee Members,	Victor M. Ugaz
	Eric E. Simanek
Head of Department,	Kenneth R. Hall

December 2006

Major Subject: Chemical Engineering

ABSTRACT

Organic-Inorganic Nanocomposite Membranes from Highly Ordered Mesoporous Thin Films for Solubility-Based Separations. (December 2006)

Suk Joon Yoo, B.S., Korea University;

M.S., Texas A&M University

Co-Chairs of Advisory Committee: Dr. David M. Ford
Dr. Daniel F. Shantz

Solubility-based membrane separation, in which the more soluble species preferentially permeates across the membrane, has attracted considerable recent attention due to both economic and environmental concerns. This solubility-selective mode is particularly attractive over a diffusivity-selective mode in applications in which the heavier species are present in dilute concentrations. Examples include the recovery of volatile organic components (VOCs) from effluent streams and the removal of higher hydrocarbons from natural gas. Recently, nanocomposites have shown great promise as possible membrane materials for solubility-selective separations. The chemical derivatization of inorganic mesoporous substrates has been explored to synthesize organic-inorganic nanocomposite membranes. The most exciting feature of this approach is that it enables the rational engineering of membrane nano-architecture with independent control over the free volume and chemistry to create membranes with highly customizable permselectivity properties.

In this study, we synthesized the organic-inorganic nanocomposite membranes by decorating the surfaces of commercially available mesoporous alumina substrates, and surfactant-templated highly ordered mesoporous silicate thin films placed on commercially available macroporous inorganic substrates, with a selective organic material that is physically or chemically anchored to the porous surfaces. Hyperbranched melamine-based dendrimers, with nanometer dimension and chemical composition designed to target certain components, were used as filling agents. We evaluated these membranes for several environmentally relevant separations, such as the recovery of the higher hydrocarbon from air and the removal of trace VOCs from air or water, while exploring the impact of organic oligomer size, chemistry, and surface coverage, as well as substrate pore size and structure, on membrane performance. First, we did a model study to verify the feasibility of dendrimer growth inside mesopores by using ordered mesoporous silica. Alumina-ordered mesoporous silica (alumina-OMS) hybrid membranes were prepared as new inorganic porous substrates. Finally, we synthesized dendrimer-ceramic nanocomposite membranes by growing several generations of melamine-based dendrimers with diverse functional groups directly off the commercial alumina membranes. Composite membranes show very high propane/nitrogen selectivity up to 70.

DEDICATION

To God

To My Family

ACKNOWLEDGEMENTS

The work with this dissertation has been extensive and challenging, but first of all exciting and instructive. Without help, support, and encouragement from many people, I would never have been able to accomplish my doctoral study. I would like to acknowledge the guidance and support of many people during my doctoral study, research, and writing of this dissertation.

First of all, I would like to express my deepest regard and appreciation to my advisor, Prof. David M. Ford, for his inspiring and encouraging way of guiding me to a deeper understanding of knowledge, invaluable comments, patience, and encouragement throughout my graduate studies. His depth and understanding in separation process is truly admirable and has inspired me in many ways.

I am greatly indebted to Prof. Daniel F. Shantz for his strong involvement in this research. His critical acumen, broad range of expertise and insight, as well as persistent encouragement of intellectual rigor have exerted a magnetic pull on my thinking and sustained me through graduate study.

I am also fortunate to have Prof. Eric E. Simanek and Prof. Victor M. Ugaz as committee members. Their flexibility, help, and suggestions have been greatly appreciated.

I am grateful to my colleagues for this study. I thank Dr. Sergio Gonzales and Dr. Robert Sherman in the Simanek group for a fruitful collaboration on the dendrimer

project. I also thank my colleagues in the Ford and Shantz group. It was a wonderful experience working with them.

Especially, I am also grateful to the student workers Lindsey Moore, Karl Debney, Jennifer Ritsch, Iara Hernadez, and Jennifer Carvajal Diaz for all their help on this study.

I owe a special gratitude to my parents, Byungchul Yoo and Jongsoon Lee, who always supported and believed in me. Their encouragement and indispensable love made possible what I have today. I save the last acknowledgement for my wife Yunyoung Oh, who has always inspired me to be a better person and reminded me to have fun, and for my sons, Jeemin and Jeeseung, who have always been a source of joy.

TABLE OF CONTENTS

CHAPTER Page

LIST OF FIGURES

FIGURE Page

FIGURE Page

LIST OF TABLES

CHAPTER I

INTRODUCTION

Membrane technology provides an economical and reliable separation process in many industrial applications. In recent times, membrane-based separation processes have been increasingly employed due to their inherent advantages over energy-intensive traditional separation methods such as distillation[1-3]. These advantages include low capital and operating costs, low energy requirement and ease of operation. Tailoring membranes with better separation characteristics for specific industrial applications is important to the continued development of this technology.

Membrane-based gas separations occur due to the differences in the permeabilities of the components through the membrane [4, 5]. Generally, the permeability of a gas through the membrane can be thought of as the product of diffusivity and solubility. Therefore gas separation through membranes can be broadly categorized into diffusivity-based or solubility-based separation.

Most membrane separations are currently based on diffusivity differences such as size sieving effects, which is the concept we usually have for the membrane separation. For chemically similar species, such as O_2 and N_2, the difference in solubility is quite small, and therefore the difference in diffusivity of the two species through the

---

This dissertation follows the style and format of the Journal of Membrane Science.

membrane plays the dominant role in achieving separation. In such cases, the diffusivity of the smaller species is typically greater, and thus membranes used in diffusivity-based separation preferentially permeate the smaller, more mobile species.

However, in solubility based separations, the preferential permeation of the largest molecule is enabled by choosing the membrane material so that the largest or most condensable species has the highest solubility; it can leave the smaller molecules behind, contrary to diffusion based separation. This solubility-selective mode is particularly attractive over diffusivity-selective mode in applications where a dilute heavy molecular weight species contaminates a light gas feed stream [6]. Examples include the recovery of volatile organic components (VOCs) from effluent streams and the removal of higher hydrocarbons from natural gas. In such examples the preferential permeation of the larger species would greatly reduce the membrane surface area requirement and operating costs because a much smaller percentage of the total feed will cross the membrane. And also, in certain processes, it is extremely advantageous to keep the "cleaned" lighter component on the high-pressure side.

Both polymeric and porous inorganic materials have been considered for solubility-selective membranes. Inorganic porous materials have been modified to become permselective for the larger species by enhancing surface effects like surface flow and capillary condensation [7-9]. Inorganic porous membranes generally exhibit high permeabilities, and even very high selectivities in some cases; however, their transport mechanisms such as surface diffusion and/or capillary condensation are very

sensitive to process variables. So it is difficult to get the consistent separation performance from the inorganic porous membrane.

Polymeric materials also provide a practical route to solubility-selective membranes. Solubility-selectivity for larger species arises naturally by solution-diffusion mechanism. So, it des not need to rely on a capillary condensation mechanism. We can get the more consistent performance than inorganic membrane. For these reasons, polymer is currently the main material commercially used for solubility-based separation in industry. However polymeric materials tend to leads to a low overall permeability due to low free volumes and neck-cavity structures. And also it is difficult to do rational modification for its different applications. In addition to this issue, polymer materials can be prone to swelling [10], which may greatly reduce their selectivity.

An alternative approach for the optimum material for a solubility-based separation is to design membranes that combine the best aspects of both polymeric and inorganic porous materials, by forming organic-inorganic composite membranes. One method of generating organic-inorganic composites is the chemical derivatization of mesoporous inorganic substrates by tethering organic oligomers to the inorganic surface. This approach of forming organic-inorganic composites has shown great promise as possible materials for solubility-based separation [11-13]. Several research works including ours showed that the composite membranes had significantly different (better) permselectivity properties than their pure-polymer analogues, proving the viability of this design concept of composite materials for solubility based separation [11, 14, 15].

The most exciting feature of this approach is that this architecture can give us a degree of simultaneous control over both the chemistry and free volume of the membrane, which is difficult to attain in purely polymeric or purely inorganic membranes.

The ideal materials for a solubility-based separation will have a diffusivity-selectivity very close to unity, in addition to having a significant solubility-selectivity. In general, this means that high free volume and/or flexibility is required for the membrane material with the high solubility. Dendrimers are particularly attractive for the present application. Dendrimers are highly branched, monodispersed polymers with dimensions ranging from one to ten nanometers. They can be engineered for chemically specific interaction and their size may be altered in generations with exact chemical similarity. The above discussion suggests that dendrimer may lead to frustrated packing and a resulting high free volume when deposited on a porous surface.

Precise control of pore size and structure of the inorganic porous support is also very important for composites to achieve consistent and high separation performance. In previous work by Javaid and coworkers, they manipulated the pore size of inorganic support by choosing different commercially available alumina membranes with sizes of 5nm and 10nm [11]. Mesoporous film in these membranes is made by compacting nano- or micron- sized dense crystallities such in as γ- or α-alumina crystals with slip-casting. This synthesis method is called as sol-gel process. Their pore structure is defined by the crystallite size and the manner in which they are packed. The pores of these films are not arranged in an ordered fashion and it has the multilayer structure with the broad range of pore size, which makes it hard to provide the precise control of pore

size and structure for the consistent membrane performance. Furthermore, it is difficult to obtain analogous powder samples from the manufacturer to perform the detailed characterizations such as adsorption measurements. These drawbacks from the commercial slip-cast membranes can be overcome by in-house synthesis of ordered mesoporous inorganic thin films as inorganic supports. Surfactant-templated ordered mesoporous inorganic thin films are attractive for our applications: (1) their well ordered pore structures and narrow pore size distributions are expected to provide better membrane performance, (2) pores of controllable size and different pore connectivities provide tailorability, and (3) all of the well-known silane chemistry developed for functionalizing silica surfaces can be implemented on ordered mesoporous silica films. Many studies have characterized thin films grown on non-porous supports by using surfactant-templated methods. But, a porous support is required for membrane applications of these materials. Therefore, a key issue for this work is whether defect-free films can be fabricated on porous supports [16-18].

In this study, we synthesize the organic-inorganic nanocomposite membranes by decorating the surfaces of commercially available mesoporous alumina substrates, and surfactant-templated highly ordered mesoporous silicate thin films placed on commercially available macroporous inorganic substrates, with a selective organic material that is physically or chemically anchored to the porous surfaces. Hyperbranched melamine-based dendrimers, with nanometer dimension and chemical composition designed to target certain components, are used as filling agents [19]. We evaluate these membranes for several environmentally relevant separations, such as the

recovery of the higher hydrocarbon from air and the removal of trace VOCs from air or water, while exploring the impact of organic oligomer size, chemistry, and surface coverage, as well as substrate pore size and structure, on membrane performance.

The outline of this dissertation is as follows. Chapter II provides a background on the theory of gas separations in membranes and a review of previous work done in this field. Chapter III describes the procedures for the synthesis of composite materials, the synthesis of supported mesoporous thin film membrane, the synthesis of dendrimer-ceramic nanocomposite membranes, the single gas permeation experiments, the vapor permeation experiments, and several analytical methods. The model study about dendrimer synthesis inside mesoporous material by using powder ordered mesoporous silica (OMS), SBA-15, are given in Chapter IV. Chapter V details the synthesis of supported ordered mesoporous thin film (SOMTF) membrane and its gas permeance characteristics. The results and discussion of the gas permeation experiments of dendrimer-ceramic nanocomposite membranes are given in Chapter VI. Finally, Chapter VII discusses our major conclusions and gives the summary of the work conducted.

CHAPTER II

LITERATURE REVIEW

2.1 Membrane Based Separations

The separation of gases by thin barriers termed "membranes" is a dynamic and rapidly growing field during the last 30 years. A membrane may be simply defined as a selective barrier between two bulk phases [1]. Membranes are used to separate gases from their mixtures by the differential permeation of the components through the membrane material. Membrane separation processes offer a number of significant advantages over traditional separation processes, like cryogenic distillation and pressure swing adsorption. First, energy requirements, and in some cases also capital investment costs, are lower than those for conventional separation processes in important industrial applications. Second, the necessary process equipment is simple, compact, and relatively easy to operate and control. Moreover, this equipment is modular and can be easily scaled up or operated at partial capacity. As a result, the process has acquired a significant industrial role in the industry in terms of economical considerations, as gases occupy a central position in the central feed stock industry.

The foundation of gas separations was laid by Thomas Graham in 1829, who performed the first recorded experiment on the transport of gases in polymeric membrane by showing air can be enriched in O_2 by permeation through nonporous polymer membranes, natural rubber films. In 1866, he also developed concepts for gas

permeation in terms of a ‘solution-diffusion mechanism’[20]. In 1855, Fick emplyed cellulose nitrate membranes to propose a quantitative description of material transport through boundary layers [21]. These two model concepts have contributed significantly to the understanding of gas permeation phenomena across membrane. The first series of microfiltration membranes of graded pore structure was synthesized by Benchold in 1907. He first defined the relationship between the membrane performance and the physical properties such as pore radius and surface tension [22]. Kalplus developed the concept of pore size distribution and improved the technique to prepare nitrocellulose membrane and commercialize microporous colloidan membranes in the 1930s[23]. During the next 20 years, many other polymer materials were found and tried in a substantial number of important applications and subsequent studies were done about diffusion across various kinds of membranes with porous, non-porous, glassy and rubbery characteristics. By 1960, the elements of modern membrane science had been developed and sufficient knowledge was available on the relationships between structure and function in gas separation membrane. However, the available membranes were generally unreliable and were minimally selective with low fluxes, and were also expensive. The separation of gas mixtures of industrial interest with membranes became economically competitive, for certain applications, only in the late 1970s. This was made possible by the development of the high flux asymmetric and composite polymer membranes for water desalination by Loeb and Sourirajan in the 1960s [24]. The first large-scale separation plant based on membranes was installed by the Monsanto Co. in 1977 for the separation of hydrogen from the product stream of ammonia [25]. The

progress in membrane science and technology was accelerated during the 1980s by the development and refinement of synthetic polymeric membranes. During this period, membrane gas separation emerged as a commercial process on a large scale and significant progress was made in every aspect of membrane-based separations, including membrane formation processes, chemical and physical structures, configuration and applications. Considerable work is presently in progress in academic and industrial laboratories in order to improve the economics of extant membrane processes, as well as to extend the range of applications of this technology.

The transport is a non-equilibrium processes, and separation of chemical species result from differences in permeabilities of the species flowing through the membrane. Differential transport can occur under a variety driving forces including pressure, concentration and electrical potential across the membranes. The most general driving force in membrane separation is pressure difference. Pressure differences across the membrane can facilitate microfiltration, ultrafiltration, reverse osmosis (RO), gas separation, and pervaporation. Temperature differences across the membrane can be utilized for distillation, whereas concentration differences can facilitate dialysis and extraction. Electrodialysis can also be performed with the help of membranes when an electric potential across the membrane is maintained.

Other than the driving force, membranes are normally classified according to the pore size or the size of materials they are used to separate. Membranes with pore sizes of 5000 nm or greater are particulate filters. Microfiltration membranes have pore sizes in the range of 100 – 5000 nm and are capable of removing suspended particles like

blood cells and latex emulsions. Ultrafiltration membranes have pore sizes in the range of 2 – 100 nm and can remove large molecules like albumin or pepsin within this range. Nanofiltration membranes can separate small molecules like divalent salts, dissociated acids and sugar, and have pore sizes less than 10 Å. RO membranes separate ions like sodium and chloride on the molecular level and have pore sizes in the range of a few Angstroms.

Today membrane processes are used in a wide range of applications and the number of such applications is still growing. From the economic point of view, the present time is intermediate between the development of the first generation membrane processes such as microfiltration (MF), ultrafiltration (UF), hyperfiltration (HF) or reverse osmsis (RO), electrodialysis (ED) and dialysis and second generation membrane processes such as gas separation (GS), pervaporation (PV), membrane distillation (MD), and separation by liquid membrane (LM).

2.2 Types of Membranes

A membrane can be thick or thin, homogeneous or heterogeneous, symmetric or asymmetric, charged or uncharged, dense or porous, and solid or liquid. Membranes can be also classified by nature, i.e. natural biological or synthetic membranes. Synthetic membranes can be subdivided into organic (polymeric or liquid) and inorganic membranes. In principle, all materials that form sufficiently thin and stable films can be used as membranes. This includes metal, glass, ceramic, and polymers as well as molecular monolayers of liquids. Three basic types of membrane can be distinguished

based on structure and separation principles: porous membranes (microfiltration, ultrafiltration), nonporous membranes (gas separation, pervaporation), and liquid membranes (carrier-mediated transport). This approach of classification is very useful to understand the basic principles such as membrane formation, transport through membranes and membrane characterization more readily.

For the porous membrane the dimension of the pore mainly determines the separation characteristics, the type of membrane material being of crucial importance for chemical, thermal and mechanical stability but not for flux and rejection. On the other hand, for nonporous membranes, the intrinsic properties of the material are mainly responsible for the separation. Some major characteristics of the two basic types are given below.

2.2.1 Porous Membranes

Porous membranes have a rigid, well-defined static pore structure, which depending on the formation process can be highly connected and torturous or non-connected and straight. Pores in membranes can be classified according to their size as macropores (>500 Å), mesopores (500-20 Å) or micropores (<20 Å) [26]. A porous membrane is very similar in its structure and function to a conventional filter. Membranes of this class induce separation by discriminating between particle sizes. Such membranes are used in microfiltration and ultrafiltration. In general, porous membranes can exhibit very high level of flux. High selectivity can be obtained when solute size is large relative to the pore size in the membrane.

Porous inorganic membranes are usually amorphous in nature and formed from metals, ceramics, or pyrolyzed carbon [27, 28]. To obtain high enough permeances for the inorganic membranes to be practically useful, the membrane thickness needs to be quite small (on the order of microns). Amorphous inorganic materials do not typically have the inherent mechanical strength to form self-supported membranes in this size range, and therefore thick macroporous supports made of alumina, zirconia, glass, or stainless steel are used to provide the desired mechanical strength. There a number of processes employed for the formation of amorphous porous inorganic membranes, however among them the most widely used are sol-gel method, chemical vapor deposition (CVD) and pyrolysis method for the formation of carbon membranes [27-29].

The sol-gel process involves the coating a porous support with a suitable colloidal solution (sol), followed by drying and thermal treatment [30-33]. The colloidal particles in the coating sol may be dense or polymeric in nature. A sol of dense particles is widely used to form mesoporous γ-Al_2O_3 layers on top of macroporous α-Al_2O_3 supports. The sol-gel technique has been widely adopted for the formation of silica and alumina based inorganic membranes. Supported carbon membranes are created by heating precursors like poly furfuryl alcohol (PFA) or phenolic resins at high temperature in an inert environment [34, 35]. The heat treatment leads to the formation of nongraphitizing carbon, which is well cross-linked. Zeolite membranes are generally formed by a hydrothermal deposition method on suitable porous supports like α-Al_2O_3 [36-38]. The main advantages of this class of crystalline inorganic membranes are high

chemical stability and very narrow pore size distribution; however, it is very difficult to create a defect free zeolite membrane with practically useful thickness.

2.2.2 Nonporous Membranes

The use of nonporous or dense polymer membranes has generated an ever-increasing interest in the field of gas separation [5, 39]. Polymers are available in a wide array of chemistries that can be used to suit particular applications. However, polymers show a low overall permeability as compared to porous materials. And also, generally, polymers cannot withstand high temperatures and harsh chemical environments like inorganic membranes. An important property of nonporous dense membrane is that it is capable of separating molecules of approximately the same size from each other. Separation takes place through differences in solubility and/or differences in diffusivity in polymer materials. The intrinsic prosperities of the polymeric material determine the extent of selectivity and permeability.

For diffusivity-based separations, polymers show what has been commonly termed in literature as the "inverse permeability/selectivity" behavior. Robeson investigated this inverse relationship and suggested that there exists a hypothetical "upper bound" in the relationship between permeability and selectivity [40]. Much of the present research has focused on pushing the polymer performance above the upper bound and into the economically attractive region currently enjoyed by inorganic membranes (Fig. 2-1).

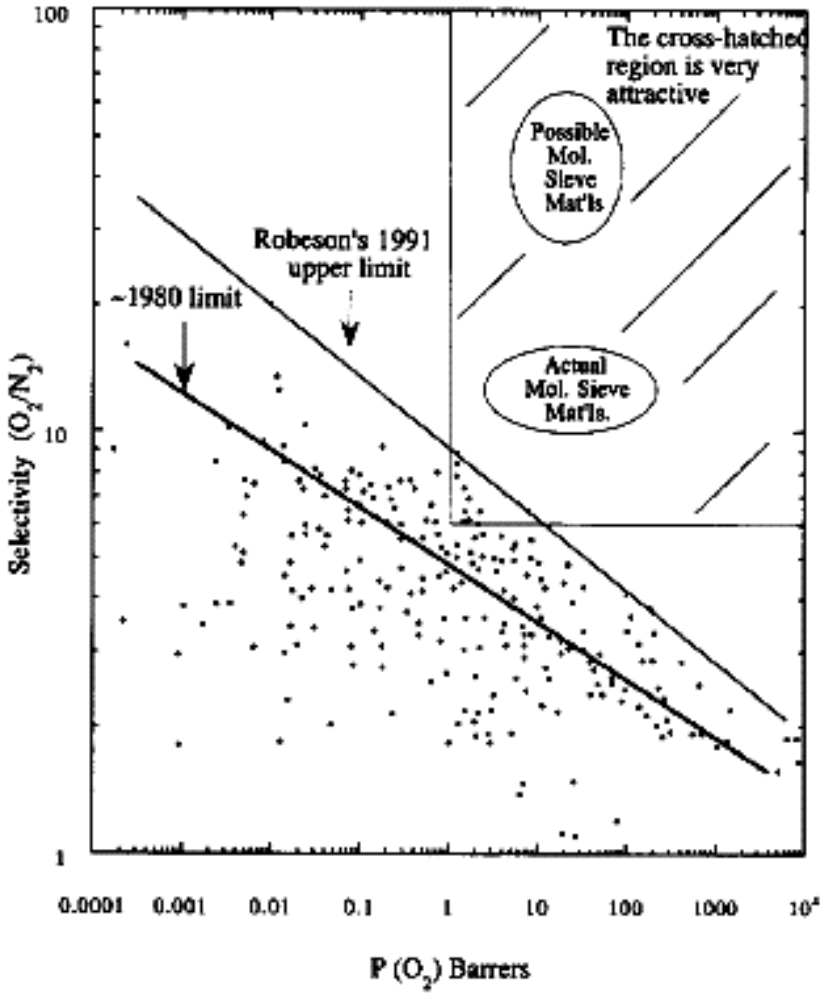

Fig. 2-1. Trade off curve for oxygen permeability and oxygen/nitrogen selectivity for polymer materials. [41]

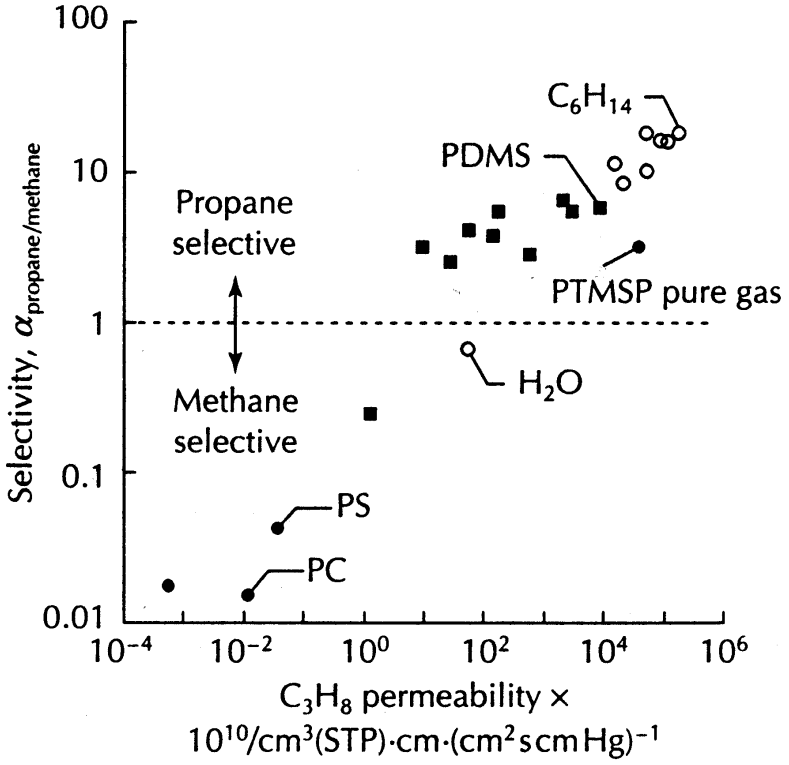

Fig. 2-2. Correlation between propane/methane selectivity and propane permeability. [6]

For solubility-based separations, polymers show the possibility of having a positive correlation between permeability and selectivity to provide a practical route to solubility-selective membranes [6]. Several polymers have been explored for this. Polydimethysiloxane (PDMS) and poly(1-trimethylsilyl-1-propyne) (PTMSP) have shown promising results for solubility-based separation (Fig. 2-2).

2.3 Transport Mechanism in Membranes

Various mechanisms for gas transport across the membranes have been proposed depending on the properties of both the permeant and the membrane. These include Knudsen diffusion, molecular sieving, and solution-diffusion. Most of these models, however, have been found to be applicable to only a limited number of gas/material systems. Transport through the membrane takes place as a result of driving force acting on the individual components in the feed. In many cases the permeation rate through the membrane is proportional to the driving force. When the pressure difference is a driving force, transport of molecule through membrane can be expressed by Darcy's law

$$J = -P\left(\frac{dp}{dx}\right) \tag{2-1}$$

where J is the flux of the gas through the membrane, P is the permeability and dp/dx is the pressure gradient of the gas across the membrane. At steady state, the flux is a constant. If we also assume P to be constant, Eq. (2-1) can be integrated to give

$$J = P\frac{(p_o - p_l)}{l} = P\frac{\Delta p}{l} \tag{2-2}$$

2.3.1 Porous Membranes

Across pore size regimes, gas transport in porous membranes may occur via a host of different mechanisms. A description of the commonly occurring mechanisms is given below.

2.3.1.1 Molecular Diffusion. In molecular diffusion, the mean free path of the gas molecules, as given by λ in Eq. (2-3), is smaller than the pore size and diffusion occurs primarily through molecule-molecule collisions.

$$\lambda = \frac{3\eta}{2P}\left(\frac{\pi RT}{2M}\right)^{1/2} \tag{2-3}$$

where η is the viscosity of the gas and R the universal gas constant, T the temperature, M the molecular weight, and P the pressure.

In molecular diffusion, the driving force is the composition gradient. If a pressure gradient is applied in such pore regimes bulk (laminar) flow occurs, as given by Poiseuille's equation [31, 42]. Such transport is often referred to as Poiseuille flow or viscous flow. The Poiseuille permeance $P_{0,p}$ can be evaluated using Eq. (2-4).

$$P_{0,p} = \frac{\varepsilon\, \mu_p r^2}{8\, R\, T\, \eta\, L} P_m \tag{2-4}$$

where $P_{0,k}$ is the Poiseuille permeance (mol m^{-2} sec^{-1} Pa^{-1}), ε the porosity, μ_p the shape factor which is equal to the inverse of tortuosity, r the modal pore radius (m), R the

universal gas constant (J mol^{-1} K^{-1}), T the absolute temperature (K), L the thickness of the porous medium, η the viscosity of the gas (N sec m^{-2}) and P_m the mean pressure (Pa).

2.3.1.2 Knudsen Diffusion. This mode of transport is important when the mean free path of the gas molecules is greater than the pore size. In such situations the collisions of the molecules with the pore wall are more frequent than the collisions among molecules. Separation selectivities with this mechanism are proportional to the ratio of the inverse square root of the molecular weights. This mechanism is often predominant for light gases in mesoporous membranes [26, 43, 44]. Knudsen diffusion can be calculated using Eq. (2-5) [31, 42] .

$$P_{0,k} = \frac{2\,\varepsilon\,\mu_k r\,\bar{v}}{3\,R\,T\,L} \tag{2-5}$$

where $P_{0,k}$ is the Knudsen permeance (mol m^{-2} sec^{-1} Pa^{-1}), ε the porosity, μ_k the shape factor which is equal to the inverse of tortuosity, r the modal pore radius (m), R the universal gas constant (J mol^{-1} K^{-1}), T the absolute temperature (K), L the thickness of the porous medium and $\bar{v}$ the average molecular velocity given by

$$\bar{v} = \sqrt{\frac{8\,R\,T}{\pi\,M}} \tag{2-6}$$

where M is molecular mass of the gas molecule (kg mol^{-1}).

2.3.1.3 Surface Diffusion. Surface diffusion occurs when the permeating species exhibit a strong affinity for the membrane surface and adsorb along the pore walls. Adsorbed molecules may have considerable mobility, resulting in an additional transport along the surface in the direction of decreasing surface concentration. In this mechanism, separation occurs due to differences in the amount of adsorption and surface diffusion rates of the permeating species. Surface diffusion often occurs in parallel with other transport mechanisms such as Knudsen diffusion [26, 43]. Mechanism of surface flow is rather complicated and has been treated in many papers [7, 8, 45]. For low surface concentrations, the surface flow for a single gas can generally be described by the two dimensional form of the Fick's law [31, 45, 46].

$$J_s = -\rho(1-\varepsilon)\frac{D_s}{\tau}\frac{dq}{dl} \tag{2-7}$$

where J_s is the flux due to surface flow (mol m^{-2} sec^{-1}), ρ is the true density of material (kg m^{-3}), ε is the porosity, D_s is the surface diffusion coefficient, τ is the tortuosity and dq/dl is the concentration gradient of the adsorbed species.

Generally in the limit of a small pressure gradient, D_s and dq/dp can be assumed constant, therefore Eq. (2-7) can be integrated to obtain the surface permeance $P_{0,s}$ as given by

$$P_{0,s} = \frac{J_s}{\Delta p} = \rho(1-\varepsilon)\frac{D_s}{\tau L}\frac{dq}{dp} \tag{2-8}$$

where D_s is the surface diffusion coefficient, Δp is the pressure difference, L is the thickness of the membrane and the term dq/dp can be obtained from the adsorption isotherm.

2.3.1.4 Capillary Condensation. Capillary condensation is one form of surface flow that may occur when one of the gases is condensable. Typically in mesopores and small macropores, at certain critical relative pressures that may be determined by the Kelvin equation, as given in Eq. (2-9), the pore gets completely filled by the condensed gas. Due to the formation of menisci at both ends of the pore, transport can take place through hydrodynamic flow driven by capillary pressure difference between the two ends. This mechanism of gas transport can be thought of as the ultimate limit of the process of adsorption as pressure is increased. In theory, capillary condensation can be used to achieve very high selectivities, as the formation of the liquid layer of the condensable gas will block and prevent the flow of the non-condensable gas [43, 44, 47].

$$p = p^* \exp\left(\frac{2\gamma}{r}\frac{M}{RT\rho_l}\right) \tag{2-9}$$

where p is the equilibrium vapour pressure of a liquid when it is dispersed as droplets of radius r, and p^* is the equilibrium vapour pressure over a plane surface, γ is the surface tension of the liquid and ρ_l is the densities of liquid, M is the molecular weight, R is the gas constant and T is the temperature.

2.3.1.5 Configurational or Micropore Diffusion. This type of diffusion may be considered as surface diffusion in the limit where the pore size becomes comparable to the molecular size. In this mechanism, diffusion is perceived as an "activated" process and separation is a strong function of molecular shape and size, pore size, and interactions between the pore wall and gas molecules. This type of mechanism is dominant in microporous zeolite membranes and carbon molecular sieves [44].

2.3.2 Dense Polymeric Membranes

The mechanism for gas separation by nonporous membrane is different from that of porous membranes. In dense polymeric materials, solution-diffusion is widely accepted to be the main mechanism of transport [4-6]. This mechanism is generally considered to be a three-step process. In the first step the gas molecules are absorbed by the membrane surface on the upstream end. This is followed by the diffusion of the gas molecules through the polymer matrix down a concentration gradient. In the final step the gas molecules evaporate on the downstream end. In glassy polymers, the sorption of gases becomes a complex process, which has been described by a combination of Henry's law and Langmuir expressions. This has been referred to as "dual mode sorption theory" [39]. Diffusion in glassy polymers is usually an activated process and, Arrhenius relations may be used to express the permeability, diffusivity and solubility coefficients.

A simplified development of the theory of gas transport across a dense polymeric membrane is followed. We focus on single gas species and several assumptions will be

made to simplify the presentation, but these are discussed later. The diffusion of gas through the membrane can be expressed by Fick's first law

$$J = -D\left(\frac{dC}{dx}\right) \tag{2-10}$$

where J is the flux of the gas through the membrane, D is the diffusion coefficient and dC/dx is the concentration gradient of the gas across the membrane. At steady state, the flux is a constant. If we also assume D to be constant, Eq. (2-10) can be integrated to give

$$J = D\frac{C_o - C_l}{l} \tag{2-11}$$

where C_o and C_l are the concentration of the gas on the upstream and downstream ends respectively, and l is the thickness of the membrane. At low pressures Henry's law is often adequate to express the concentration of the gas in the membrane

$$C = Sp \tag{2-12}$$

where S is the Henry's solubility constant and p is the pressure of the gas. By substituting Eq. (2-12) into Eq. (2-11) we get

$$J = DS\frac{(p_o - p_l)}{l} = \overline{P}\frac{(p_o - p_l)}{l} \tag{2-13}$$

where $\overline{P}$ is permeability of the gas and according to Eq. (2-13) can be defined as

$$\overline{P} = DS \tag{2-14}$$

The permeability is therefore a product of the diffusivity and solubility coefficients of the gas species. In real systems, the diffusion coefficient *D* and the solubility coefficient *S* may both be function of concentration, so the theoretical analysis becomes more complicated. However, the idea of the permeability being the product of a solubility term and a diffusivity term is quite general.

In gas separation with membranes, selectivity is defined as the ratio of the individual gas permeabilities. Based on single gas permeabilities of species "A" and "B" we may write an ideal selectivity as

$$\alpha_{A/B} = \frac{\overline{P_A}}{\overline{P_B}} = \frac{D_A}{D_B}\frac{S_A}{S_B} \tag{2-15}$$

The selectivity can therefore be viewed as a function of differences in both the diffusivity and solubility coefficients of the two gases. Eq. (2-15) indicates that membrane separations can be based on either diffusivity or solubility differences. Diffusivity-based gas separation is generally employed for chemically similar species like O_2 and N_2, where separation occurs due to the preferential permeation of the smaller more mobile species. In fact most membrane separations are currently based on diffusivity differences such as size sieving effects, which is the concept we usually have for the membrane separation. However, in certain industrial applications, it is preferable to achieve separation based on solubility differences.

2.4 Solubility-based Gas Separations

Differences in solubility arise from differences in the molecular-level interactions of the membrane material with the permeating species. The exploitation of "chemically-specific" energetic interactions such as hydrogen bonding may lead to greater selectivity; however even simple van der Waals dispersion forces, which tend to be stronger for the larger molecules, may lead to significant selectivity. In certain applications, like the removal of volatile organic compounds (VOCs) from effluent streams or the removal of higher hydrocarbons from natural gas, process economics dictate that membranes should be designed to preferentially permeate the larger molecular weight species. In these examples the heavier species are present in dilute concentrations and preferential permeation of the heavier species translates into lower surface area requirements; furthermore, the "cleaned" lighter component is kept on the high-pressure side, which may be advantageous [6, 48].

Freeman and Pinnau outlined the design criteria for solubility-selective polymeric membranes [6]. They point out that for separation of dilute heavy molecular weight species from light gases, such as the removal of organic vapors from air, generally the diffusivity selectivity is in favor of the smaller more mobile species. Therefore to achieve separation with the preferential permeation of the larger species, one would like the polymer to have a high enough free volume so that the ratio of diffusivities of the two species is driven close to unity as possible. The solubility-selectivity is greater for the larger species simply due to van der Waals interactions, resulting in an overall higher selectivity for the larger species. For example, to design a

membrane separation system for organics/light gas that is more selective for the organics, the ideal membrane would have the ratio of the diffusivity coefficients of the two gases in the membrane close to unity

$$\frac{D_{organics}}{D_{light\ gas}} \leq 1 \tag{2-16}$$

The propane/nitrogen solubility ratio based on the discussion above would be significantly higher than one

$$\frac{S_{organics}}{S_{light\ gas}} >> 1 \tag{2-17}$$

leading to an overall higher propane permeability as given by Eq. (2-18) below

$$\frac{P_{organics}}{P_{light\ gas}} > 1 \tag{2-18}$$

Both inorganic and polymeric membranes can be designed to achieve solubility-based gas separations. Both materials have certain advantages and disadvantages. Presently research effort is concentrating on designing membranes that provide high permeance and high selectivity.

2.4.1 Inorganic Membranes

Porous inorganic materials can be made permselective for the larger species for solubility-based separation by enhancing surface effects like surface flow and capillary condensation.

Several groups reported inorganic porous membranes to show the good performance for solubility-based separation. Rao and Sircar developed nanoporous carbon membranes, which they called selective surface flow (SSF) membranes [7]. Selective separation of the hydrocarbons from hydrogen stream was achieved on the basis of preferential adsorption and diffusion of the hydrocarbons. As the feed pressure increases the membranes performance showed a significant improvement due to higher adsorption of hydrocarbons at higher partial pressures [8]. Hassan *et al.* reported the study of the gas separation properties of silica hollow fiber membranes [49]. They conducted both single and mixed gas experiments using light gases and hydrocarbons. They observed large separation factors for carbon dioxide/methane mixtures, which was attributed to surface diffusion as being the primary transport mechanism. The mixed gas selectivity was higher than single gas selectivity, which they concluded was due to the competitive adsorption effects. Huang *et al.* modified γ-alumina membranes to enhance multilayer diffusion and capillary condensation transport mechanisms for recovery of acetone from nitrogen [9]. The modified membranes showed higher acetone permeability and higher separation factors as compared to polymeric membranes; however, the performance was strongly influenced by temperature and feed composition. Depending on the temperature and the feed composition, the separation factor varied from being less than 10 to as high as 1200.

Inorganic membranes typically have the advantage of higher permeabilities as compared to polymeric membranes, and selectivities are high when certain transport mechanisms such as surface flow and capillary condensation are dominant. Inorganic

membranes also exhibit good resistance to harsh chemical conditions and can withstand high pressures and temperatures. However one major drawback of inorganic membranes is that selectivity tends to be a strong function of process conditions, especially temperature, pressure and mole fraction of the condensable species in the feed.

2.4.2 Polymeric Membranes

Polymeric materials also provide a practical route to solubility-selective membranes. It shows the possibility of having a positive correlation between permeability and selectivity, which is in contrast to diffusivity-based separation [6]. Polydimethysiloxane (PDMS) and poly(1-trimethylsilyl-1-propyne) (PTMSP) have shown promising results for solubility-based separation, primarily because they exhibit diffusivity selectivity near unity for a wide range of gas species [6, 10].

PDMS is a rubbery silicone polymer that has one of the lowest glass transition temperatures. PDMS has been investigated extensively as a suitable material for removal of different solvents from air or nitrogen. The permeabilities of different solvents and gases through PDMS were studied by several groups [50, 51]. Their study showed that solvent permeabilities strongly depend on the solvent concentration and that it is much related with the sorption of the solvent into the polymer. Leemann *et al.* investigated the performance of PDMS membrane in the removal of toluene from nitrogen. Their study showed that within certain regimes of purity and flow the PDMS membrane system could be an economical alternative to the conventional processes [48].

PTMSP is a glassy polymer that was first synthesized by Masuda *et al.* in 1983 [52]. PTMSP has one of the highest free volume known of any glassy polymers, which has been attributed to its unique structure [53-55]. PTMSP has shown very high permeabilities and very low selectivities for lighter gases. For this reason initially PTMSP was considered as having little use in gas separation [5, 39]. However the low diffusivity-selectivity property of PTMSP makes it a good candidate for solubility-based separation. Pinnau and Toy studied the transport of light gases and organic vapors through PTMSP [56]. They observed higher permeability coefficients for the more condensable gases than the lighter non-condensable gases. The mixed gas selectivities in general showed higher values as compared to ideal selectivities suggesting blocking effects by the condensable species during mixed gas permeation. Merkerl *et al.* performed mixed gas permeation of synthesis gas on both PDMS and PTMSP [57]. Their study again showed that both PDMS and PTMSP exhibit higher permeability for the more condensable gas (carbon monoxide and hydrogen sulfide) as compared to hydrogen, and demonstrated the suitability of these materials for solubility-based separations.

Polymeric membranes have several potential advantages over porous inorganic membranes. In polymeric materials, since target species actually become solvated by the polymer, there is no need to rely on a capillary condensation mechanism. Therefore selectivity is less dependent on feed conditions and good performance may be achieved over a wide range of process conditions. Furthermore, there is a much wider variety of chemistries that can be used to suit particular applications. However polymeric

materials tend to have low free volumes and neck-cavity structures that restrict transport. This leads to a low overall permeability as compared to porous materials and a high diffusivity-selectivity for the smaller gas species over the larger. The latter effect acts in opposition to the desired solubility-selectivity and may partially or completely negate it. And also, generally, polymers cannot withstand high temperatures and harsh chemical environments like inorganic membranes. In addition to this issue, polymer materials can be prone to swelling, which may greatly reduce their selectivity when exposed to gas mixtures under actual conditions. PDMS has been shown to be prone to plasticization, which may greatly reduce its selectivity when exposed to actual gas mixtures [10]. A major drawback of PTMSP is that this polymer, like most glassy polymers, is prone to aging effects and shows a decrease in permeability over time. This has been attributed to relaxation of the polymer chains and possible attack by impurities on the unsaturated double bonds in the polymer backbone [58].

2.4.3 Composite Membrane Materials

The discussion in the previous section suggests that an alternative approach for the optimum material for a solubility-based separation is to design membranes that combine the best aspects of both polymeric and porous materials, by forming organic-inorganic composite membranes. Different types of composites have been proposed to enhance membrane performance. Organic-inorganic composites have been formed by incorporating zeolites into a polymer matrix, dispersing intercalated clay dispersed in polymer matrix, covering a porous substrate with organic-inorganic sol-gel materials,

forming layers of polymeric material on the surface of a porous substrate, and by plasma polymerization on the surface of an inorganic support [41, 59-65].

Another approach for generating organic-inorganic composites is the chemical derivatization of mesoporous inorganic substrates by tethering organic species to the inorganic surface. This approach of forming organic-inorganic composites has shown great promise as possible materials for solubility-based separations [11-13]. It allows one to design and build membranes that simultaneously deliver the desired chemistry and the desired free volume thereby making the membrane formation process quite versatile. Furthermore, the composites should be largely resistant to swelling, due to the rigid ceramic framework. The most exciting feature of this approach is that it enables the rational engineering of membrane nano-architecture with independent control over the free volume and chemistry to produce high performance membranes for the specific applications, which is especially attractive relative to 'purely organic' or 'purely inorganic' systems. By rationally selecting the pore size and structure of porous inorganic support, organic filler size and chemistry, surface coverage, and other properties, we can create membranes with highly customizable permselectivity properties.

The chemical derivatization of inorganic substrates with organic layers has been a field of interest for a number of applications, such as wetting, electrochemistry, bioactive surfaces, and catalysis [66]. More recently this approach has been applied to membranes. Paterson and co-workers published a series of papers on the surface modification of inorganic membranes [67-69]. Their modifications were based on wet

chemistry routes rather than the vapor deposition as employed by Miller and Koros [70]. They modified titanium and alumina membranes with several organics to test composite membranes for several applications such as bovine serum albumin (BSA) filtration or several gas separations. They concluded that with such modifications made it possible to change the nature of the inorganic surface and improved solubility-based separation characteristics of membranes.

In our previous work we also have focused on the development of solubility-based composite membrane by the surface-derivitization of inorganic membrane. Javaid and co-workers modified 5 and 10 nm commercial alumina membranes, Membralox® membranes obtained from USFilter Ceramic Membrane Products (DeLand, FL), using different alkyltrichlorosilanes, linear chain structure molecules with chain lengths ranging from C4 to C28 [11]. Single gas studies with propane and nitrogen showed a significant increase in propane/nitrogen ideal selectivity, accompanied by a loss in permeance, after modification of the membrane. In comparison to PDMS, one of the best-known polymers for solubility-based separations, the hybrid membranes exhibited equal or greater propane/nitrogen selectivity although at lower propane permeance. The mixed gas separation performance was superior to that predicted by the single gas permeances [14]. The membrane performance may be manipulated by controlling the surface coverage of organic oligomer with changing synthesis conditions such as hydration states and chlorosilane functionality [15]. The selectivity increase was much higher for 5 nm membranes and was positively correlated with alkyl chain length and was attributed to the effective filling of pores with oligomer. However, this positive

correlation was not extended to a very dense coating. As surface coverage is increased, the diffusion barriers by a dense film exceed the solubility effect, which makes the diffusion based selectivity dominant in separation.

All previous works including ours showed that the composite membranes had significantly different (better) permselectivity properties than their pure-polymer analogues [13], proving the viability of this design concept of nanocomposites materials for solubility based separation. In this study, we develop this concept of engineering the membrane nano-architecture more by exploring new organic molecule architecture and chemistry, melamine-based dendrimers, and new inorganic support, ordered mesoporous thin film.

2.5 Melamine-based Dendrimers

The ideal materials for a solubility based separation will have a diffusivity-selectivity very close to unity, in addition to having a significant solubility-selectivity. In general, this means that high free volume and/or flexibility is required for the membrane material. On the basis of this, a highly branched structure can be thought to have the advantage over a linear alkyl chain if it has the similar solubility effect. Dendrimers are particularly attractive for the present application due to their hyperbranched nature and structural and chemical diversity.

Dendrimers are highly branched, monodispersed polymers with dimensions ranging from one to ten nanometers, in which branching emanates from a center core. The term “dendrimer” is derived from the Greek word for “tree” (dendron) and the

scientific suffix for “unit” (mer, as in polymer). Dendrimers are built in a step-wise manner. The central unit of a dendrimer is called the “core”. From the core, linking groups radiates to the periphery or surface, which are referred as “peripheral groups” or “surface groups”. Their structure is unique in several ways. Their exteriors typically have a very high density of surface groups that are available for surface sorption or chemical reaction. Their interior branches can be chemically specific as well although the cores have lower density than the exteriors. These structural features have led to the consideration of dendrimers for applications like molecular encapsulation, catalysis and drug delivery [71].

Dr. Simanek’s laboratory developed novel techniques of synthesizing dendrimers based on melamine in 2000 and explored several cases of their applications. [72-79]. Melamine is a 1,3,5-triazine substituted with three amines. Melamine is also commonly known as cyanuramide or triaminotriazine. Melamine-based dendrimers are synthesized by using differential reactivity of triazines (Fig. 2-3). Triazine core are interconnected with diamine linkers. High generation dendrimers are synthesized by the iterative synthesis between triazine ring and diamine linker molecules. Significant structural diversity is obtained by varying the amines that interconnect the triazine rings at each generation. We can incorporate a variety of linker groups with different polarities, hydrophobicities, and rigidities for the particular applications. The different peripheral functional groups can be attached finally for the specific applications such as surface sorption or chemical reaction.

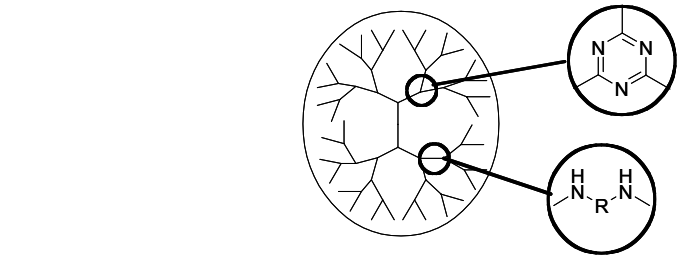

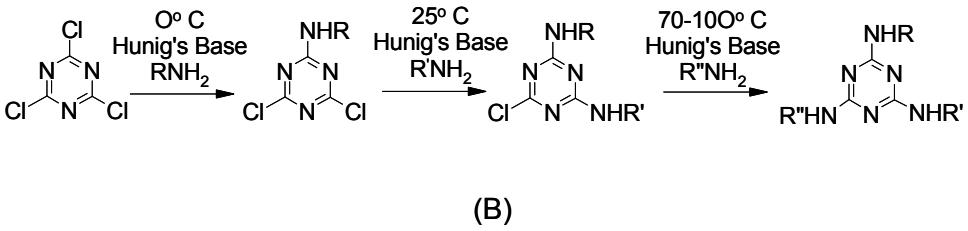

Fig. 2-3. Melamine-based dendrimers. (A) Structural diversity by the interconnection between triazine core and diamine linker. (B) Differential reactivity of triazine. [76]

Melamine-based dendrimers are especially attractive as filling agents for our application of organic-inorganic nanocomposite membranes [80]. They can be engineered for chemically specific interaction and the structural diversity. Their size may be altered in generations with exact chemical similarity. Their hyperbranched structure may lead to frustrated packing and a resulting high free volume when deposited on a porous surface. Finally, they may allow the composite membrane to have a nanostructure with both a high free volume and a high solubility for the target component.

2.6 Ordered Mesoporous Inorganic Thin Films Membranes

The precise control of pore size and structure of the inorganic porous support is very important for composites to achieve consistent and high separation performance. So far, we manipulated the pore size of inorganic support by choosing different commercially available alumina membranes, e.g. with sizes of 5 nm and 10 nm. These mesoporous membranes are amorphous in nature and are made by compacting nano- or micron- sized dense crystallities such as γ- or α-alumina crystals. Their pore structure is defined by the crystallite size and the manner in which they are packed. The pores of these films are not arranged in an ordered fashion and it has the multilayer structure with the broad range of pore size, which makes it hard to provide the precise control of pore size and structure for the consistent membrane performance. Furthermore, it is difficult to obtain analogous powder samples from the manufacturer to perform the detailed

characterizations such as adsorption measurements. These drawbacks from the previous membrane can be overcome by introducing the ordered mesoporous inorganic thin film as new inorganic support.

The synthesis of surfactant-templated ordered mesoporous silica materials has developed rapidly over the past decades. Ordered mesoporous materials share characteristics of both microporous zeolites and gels. They contain ordered uniform pore systems similar to those of the microporous zeolites, but the pores are larger, allowing larger molecules to diffuse inside. The uniform controlled pore sizes created by this method show promise as catalyst supports, sensors, filtration membranes and in a variety of optoelectronic applications.

Ordered mesoporous materials are synthesized by using arrays of surfactant molecules rather than single molecules (as in the case of zeolites) as structure-directing agents around which inorganic species can polymerize. This concept of surfactant-templated inorganic materials was suggested by researchers at Mobil over a decade ago when reporting the first ordered mesoporous materials, M41S [81, 82]. This mesoporous aluminosilicate material with well-defined pore sizes up to 33 nm exceeds the pore-size constraint (<1.5 nm) of microporous zeolites. The extremely high surface areas (>1000 m^2/g) and precise tuning of pore sizes are among the many desirable properties that have made such materials the focus of great attention. Since the initial discovery of the M41S materials, many other ordered pore structures corresponding to different surfactant assemblies have been synthesized.

In the simplest form, these syntheses require a surfactant template that will form lyotropic liquid crystal phases in the solvent (usually water) and an inorganic species that will interact with the surfactant micelles and polymerize to form a continuous solid network encapsulating the micelles. The liquid crystalline arrangement of the surfactant micelles within the solid creates the ordering in these materials on the mesoscale. Porosity is created by removal of the surfactant template through liquid extraction or calcinations. The pore structure, volume, surface area and wall composition can be tailored by careful choice of inorganic source materials, surfactants, molar compositions, the type of inorganic-organic interaction and polymerization process [83-88]. Ordered pore structures have been synthesized as corresponding to many different surfactant liquid crystal phases. The most common ordered mesoporous structure is the two-dimensional hexagonal phase with the *P*6*mm* symmetry, consisting of close-packed hexagonal arrays of cylindrical surfactant micelles [81, 89-91]. Lamellar silicate-surfactant phases are also obtained, which are not stable to the removal of the surfactant which leads to a collapse of the silica layers [82]. Various cubic phases have also been reported. The bicontinuous cubic gyroid phase with the *Ia*3*d* symmetry is found in alkaline-catalyzed syntheses [82]. This phase with its network of interconnected pores is much more attractive than the two-dimensional hexagonal phase for applications requiring diffusion of species into and out of the pore network. The *Pm*3*n* phase composed of spherical micelles in a cubic close-packed arrangement is found in both acid- and alkaline-catalyzed preparations [92].

The initial work of Beck *et al.* [82] and Kresge *et al*. [81] involved only alkaline-catalyzed preparations and materials reported in these papers are referred to as MCM-41 (*P*6*mm* two-dimensional hexagonal phase), MCM-48 (*Ia*3*d* cubic phase) and MCM-50 (lamellar phase). Two-dimensional hexagonal mesoporous materials prepared by Inagaki and co-workers [89, 90] from surfactant-intercalated kanemite are referred to as FSM-16. Subsequent preparation of materials in acidic medium led to ordered mesoporous materials with similar symmetries, but distinct wall properties: SBA-1 (*Pm*3*n*, cubic phase), SBA-2 ($P6_3/mmc$, three-dimensional hexagonally packed spherical micelle phase) and SBA-3 (*P*6*mm*, two-dimensional hexagonally packed cylinders) [92]. Other surfactant-templated phases include disordered materials with a worm-like network of channels: KIT-1 [93], MSU-1 [86], a well-defined intergrown cubic hexagonal phase STAC-1 [94] and ordered non-ionic alkyl-EO_x-templated materials, e.g. cubic SBA-11 (*Pm*-3*m*), three-dimensional hexagonal SBA-12 ($P6_3/mmc$) [95]. Using the same methodology, triblock-copolymer-templated materials with much larger pores have also been synthesized in acidic systems, e.g. two-dimensional hexagonal SBA-15 (*P*6*mm*) [88] and SBA-16 cubic cage structure (*Im*3*m*) [95].

The technological potential of mesoporous materials for chemical separations and heterogeneous catalysis was recognized at the time of their discovery. An important feature of mesoporous materials is the recently discovered ability to form thin films [96, 97]. While the early work focused on the synthesis of bulk materials, methods for preparation of mesoporous materials in a thin film configuration at a thickness range of tens of nanometers to micrometers were reported in the last few years. The motivation

for synthesis of mesoporous thin films originates from the appreciation of their technological potential as membranes[91], sensors [98-101], heterogeneous catalysts [102], and insulating layers of low dielectric constant for microelectronics [103, 104]. These applications require the ordered material in the form of thin film.

Especially, formation of these materials in a thin film is attractive for membrane applications: (1) their well ordered pore structures and narrow pore size distributions are expected to provide better membrane performance, (2) pores of controllable size and different pore connectivities provide tailorability, and (3) mesoporous thin films or membranes are characterized by bulk properties, such as symmetry, pore diameter, surface area and stability, and film-related parameters, such as pore orientation, film thickness, continuity and surface roughness. Many studies have characterized thin films grown by using surfactant-templated methods [105-107].

Solvent evaporation techniques are mostly used for the formation of ordered mesoporous inorganic films and membranes [108]. In this method, a liquid film containing the solvent, surfactant and silica precursor is formed on substrates. And then evaporation of the solvent is followed, which induces the organization of surfactant species into mesoscale aggregates (i.e. lamellar, hexagonal, and cubic) around which condensation of silicates species take place [109]. Various mesostructured inorganic films and membranes are prepared by the solvent evaporation techniques, which include dip-, spin-coating and film casting.

Spin-coating has been widely used for the preparation of mesostructured films by solvent evaporation [109, 110]. Four stages of spin-coating can be distinguished:

deposition of the surfactant/inorganic solution, spin-up, spin-off and evaporation [111]. Initially, an excess of liquid is deposited on the surface of the substrate during the first stage. In the spin-up stage, the liquid flows radially outward by centrifugal force. In the spin-off stage, the excess of liquid flows to the perimeter and leaves in a form of droplets. In the final stage, evaporation takes place leading to the formation of uniform thin films. One of the most important advantages of this method is that the film tends to become very uniform in thickness. The main disadvantage of this method is that it can only be used with flat substrates.

Casting is another solvent evaporation method that has been used for the preparation of mesostructured films [112]. In this method, the solution is dropped on to the substrate and allowed to solidify, resulting in much thicker films.

The mesostructured films can be prepared by a dip-coating method [113, 114]. In this method, the substrates are withdrawn from a homogeneous precursor solution and the dip-coated solution is allowed to drain to a particular thickness [111]. The thickness of the film is mainly determined by the rate of evaporation of the solvent and the viscosity of the solution. One of the advantages of this method is the facile formation of films on non-planar surfaces.

Different pore structures (i.e. hexagonal, cubic, rectangular) and pore symmetries (*P*6*mm* two-dimensional hexagonal, *Ia*3*d* cubic, $P6_3/mmc$ three-dimensional hexagonally packed spherical micelle, etc.) with one-, two- and three-dimensional pores have been observed on the films prepared by these three methods [109, 110, 112-114]. Most

studies have characterized thin films grown on non-porous supports. But, synthesis of film on a porous support is required for membrane applications.

Several papers were published about the filling of ordered mesoporous silica within porous support. But their main application is synthesis of mesoporous silica nanowire by confined assembly [115-120]. For membrane application, Yang *et al.* recently reported the synthesis of the ordered mesoporous silica thin film membrane on the porous support and examined the molecular transport across the membrane using a series of molecules with different molecule sizes [121]. Currently, many studies have explored the synthesis of solid substrate-supported ordered mesoporous thin films membranes [17, 18, 122]. A key issue of this study is whether defect-free films can be fabricated on porous supports.

2.7 Summary

Solubility-based gas separations for applications such as the removal of VOCs from air, in recent times have become important due to environmental and economic driving forces. Either inorganic or polymeric membranes can be designed to achieve solubility-based gas separations with each type having certain advantages and disadvantages. An alternative approach is to design membranes that combine the best aspects of both polymeric and porous materials, by forming organic-inorganic composite membranes. One method of generating organic-inorganic composites is the chemical derivatization of mesoporous inorganic substrates by tethering organic moieties to the inorganic surface. This approach is especially useful in designing membranes for

solubility-based separations, as the membrane formation process is quite versatile to address a wide variety of feed compositions and conditions, and also this approach has the advantage of varying free volume and surface chemistry independently. All previous works including ours showed that the composite membranes had significantly better permselectivity properties than their pure-polymer analogues, proving the viability of this design concept. In the research reported here, we further develop this concept of engineering the membrane nano-architecture by exploring new organic molecule architecture and chemistry, especially melamine-based dendrimers, and new inorganic support, ordered mesoporous inorganic thin film. Melamine-based dendrimers are attractive for this application due to their hyperbranched nature and structural and chemical diversity. Ordered mesoporous inorganic thin films shows promising characteristics as inorganic porous supports because of their well ordered pore structure and uniform pore size distribution, which can lead the precise control of membrane performance.

CHAPTER III

EXPERIMENTAL PROCEDURE

This chapter describes the experimental procedures for the synthesis of the dendrimer-SBA15 hybrids, the synthesis of supported ordered mesoporous thin film (SOMTF) membranes, the synthesis of Dendrimer-ceramic nanocomposite membranes, single gas permeation experiments, and vapor permeation experiments. Details of analytical methods of organic and inorganic characterization are also given.

3.1 Synthesis of Dendrimer-SBA15 hybrids

Dendrimer/SBA-15 hybrids are synthesized by growing melamine-based dendrimers on powder ordered mesoporous silica (OMS), SBA-15, in order to prove the feasibility of dendrimer synthesis inside mesoporous materials. OMS/dendrimer hybrids can be promising materials that can be used for catalysis, separations, molecular recognition, or as scaffolds to build more complex structures.

3.1.1 Synthesis of SBA-15

SBA-15, the hexagonally ordered (*p6mm*) mesoporous silica, was chosen as the mesoporous support for this application. SBA-15 was synthesized using a method comparable to that reported previously [95]. 4.0 g of Pluronic P123 were dissolved in 60

mL of 4M HCl and 85 mL of deionized water by stirring for 5 hours at room temperature. Then 8.5 g of TEOS were added to that solution and stirred for 24 hours at 35 °C. The mixture was aged at 80 °C for 24 h under static conditions. The solid product was filtered, washed with copious quantities of deionized water and air-dried overnight. The solid product was calcined to remove the Pluronic used in the synthesis. The calcination procedure was as follows: the sample was heated from room temperature to 100 °C at a rate of 1 °C/min; held at 100 °C for 1 hour; increased from 100 °C to 500 °C at a rate of 1 °C/min; and then held at 500 °C for 5 hours.

3.1.2 Synthesis of Dendrimer-SBA15 Hybrids

A series of melamine-based dendrimers of various generations were grown directly off the mesopore surface of SBA-15 via the stepwise synthesis [123]. Several linker molecules with various sizes were also used to control dendrimer size in the same generation (Fig. 3-1A). The synthesis of these composites is illustrated in Fig. 3-1B. Commencing with amine functionalized silica, iterative reactions with triazine trichloride, rinsing, and diamine produced the first generation dendrimer. Subsequent reactions yielded the higher generations of dendrimers.

First, SBA-15 was amine-functionalized by using post-synthetic grafting. An aliquot of APTES 16 μL (0.1 mmol), 80 μL (0.5 mmol), 160 μL (1.0 mmol) or 320 μL (2.0 mmol), depending on the desired amine loading, was added to 1 g of calcined SBA-15 in 100 ml of anhydrous toluene under nitrogen. This mixture was stirred overnight

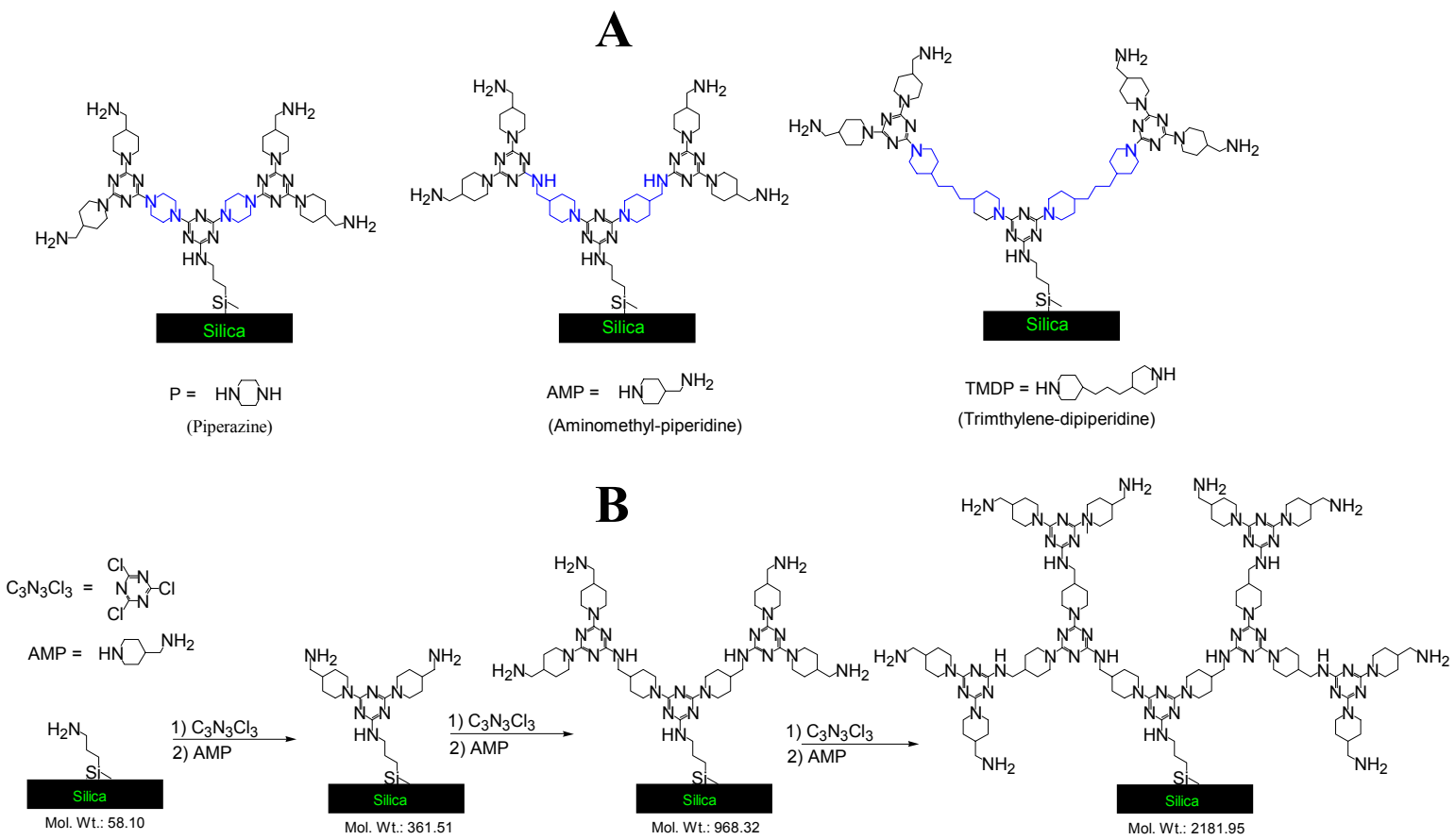

Fig. 3-1. Iterative synthesis of melamine-based dendrimer on mesoporous surfaces. (A) The second generation dendrimer with the different linker molecule, and (B) Stepwise synthesis of a series of generation by using 4-aminomethylpiperidine (AMP) linker molecule.

in a closed container at room temperature. The product was collected by filtration, washed with 1 L deionized water and air-dried. One gram of amine-functionalized SBA-15 was placed in a 30 mL vial and 25 mL of the prepared CC solution are added. A 0.3 M cyanuric chloride (CC) solution was prepared by adding 1.25g CC and 2.5 mL diisopropylethylamine (DIPEA) (8mmol) to 25 mL of tetrahydrofuran (THF). The vial was shaken for approximately 24 hours at room temperature. The solution was filtered to remove the silica from the solution and the silica was then rinsed with 50 mL portions of methanol, dichloromethane, and THF sequentially. The silica was transferred back into a clean vial, 25 mL of a 0.4 M diamine linker molecule solution were added, and the vial is again shaken for 24 hours. A 0.4 M 4-(aminomethyl)piperidine (AMP) solution was prepared by adding 1.25 g AMP to 25 mL of THF. 0.4 M solutions were also prepared of piperazine (P) and 4,4'-trimethylenedipiperidine (TMDP). The material was filtered and rinsed as described above. The same procedure was followed to increase the dendrimer generation. So that every dendrimer has the same functionality on the outer periphery (primary amine), the final linker molecule used was AMP.

3.2 Synthesis of Supported Ordered Mesoporous Thin Film (SOMTF) Membrane

The precise control of pore size and structure of inorganic porous support is very important to achieve the consistent and high separation performance. Surfactant-templated ordered mesoporous inorganic thin films shows promising characteristics as inorganic porous support because of their well ordered pore structure and uniform pore size distribution, which can lead the precise control of membrane performance. While

numerous studies have characterized thin films grown on non-porous supports, in this study, we synthesized a defect free supported ordered mesoporus thin film membrane by depositing ordered mesoporous silica thin film into macropores of commercial alumina membrane.

3.2.1 Anopore® Aluminum Oxide Membrane

Anopore® aluminum oxide (AAO) membranes were purchased from Whatman and used as received. The literature consensus [124-129] is that all of Anodic aluminum membranes, irrespective of nominal pore size, have an asymmetric structure. The structure comprises a relatively thin (0.5 to 1.0 micron) layer on top of a thicker (59 to 59.5 micron) support. The asymmetry appears to be a natural consequence of the way the materials are made by anodic oxidation [129]. The thin "active" (A) layer generally has the smaller average pore size, as compared to the thicker "support" (S) layer. Anopore® membrane of nominal pore size 200 nm has the thin active layer of 104 nm pore size and the thicker support layer of 240 nm pore size. The summary of data about several Anopore® membranes is given in Table 3-1.

Table 3-1 Summary of data about Anopore® aluminum oxide membranes

Label	Nominal pore diameter (nm)	Porosity	Average pore diameter (nm)	Source
A02 (A)	200	0.359	104 (±32)	[126] (SEM)
A02 (S)		0.43	240	[126] (SEM)
A01 (A)	100	0.29	83 (±25)	[126] (SEM)
A01 (S)		0.41	220	[126] (SEM)
A002 (A)	20	0.13	25	[124] (voltammetry); [128] (SEM)
A002 (S)		0.35	150	[124] (voltammetry); [128] (SEM)

Thicknesses: For all membranes, A=0.5 microns and S=59.5 microns are generally reported. However, A may be as large as 1.0 micron in some cases.
Tortuosity: Essentially no investigations of this property. We assume it to be 1.0.

3.2.2 Synthesis of SOMTF Membrane

We synthesized cubic (Ia3d) mesoporous thin film on a macroporous Anopore® aluminum oxide membrane of nominal pore size 200 nm by simple dip coating with evaporation induced self assembly (EISA) [108]. AAO membrane was immersed in an acidified ethanol-based precursor solution containing a surfactant template and silica precursor. Brij56 is used as the surfactant template and TEOS is used as a silica source. Brij-56 (Aldrich) and TEOS (Aldrich, 98%) were used as received and HCl (Aldrich, 37 wt%) was diluted to 0.032 N stock solutions for subsequent use. The solution used for dip coating was prepared based on previous work by Hayward and coworkers [106]. 1.15 g of Brij-56 was dissolved in 2.0 g of ethanol for 2 hrs. 3.0 g ethanol, 2.6 g TEOS, and 1.35 g of HCl (0.032 N) were mixed together for 20 min. The two solutions were then combined and mixed for 10 minutes. Anodic alumina membranes were submerged into the precursor solutions for 15 min and the AAO macropores were filled by the precursor solution. And then membranes are drawn out slowly from solution for film formation. The dip-coated membranes are immediately transferred to an oven at 45 ºC and subsequently maintained at that temperature for 15 min. As the solvent evaporates, the microstructure is formed by EISA. After drying at room temperature the surfactant was removed from the inorganic matrix by ethanol extraction for 48 hrs. Multiple dip-coating/surfactant extraction cycles were carried out to achieve a membrane that had the separation characteristics (i.e. selectivities) of a 5 nm membrane.

3.3 Synthesis of Dendrimer-ceramic Nanocomposite Membrane

Dendrimer-ceramic nanocomposite membranes were prepared by growing the melamine-based dendrimer directly off the commercial alumina membrane with 5 nm mesopores. We engineered the nanostructure of composite membranes by controlling the structure and chemistry of dendrimers to achieve high permselectivity.for the propane recovery.

3.3.1 Membralox® Alumina Membrane

The membranes used in this part of research were Membralox® T1-70-25G-Bare, γ-alumina membranes with an average pore size of 5 nm (Part# S700-01227). They were obtained from US Filter Ceramic Membrane Products, DeLand, Florida. The mesoporous film in these membranes is made by compacting nano- or micron- sized dense crystallities such as γ- or α-alumina crystals. Their pore structure is defined by the crystallite size and the manner in which they are packed. The pores of these films are not arranged in an ordered fashion and have a multilayer structure with the broad range of pore size. These membranes have been discussed in detail by Liu and co-workers who have described and characterized them in a two part series [130, 131]. The membranes have an extruded tubular macroporous α-alumina support with a thickness of 2 mm and an average pore size of 10 μm. The macroporous support is coated by slip casting and firing two more layers of α-alumina with average pore diameters of 0.8 and

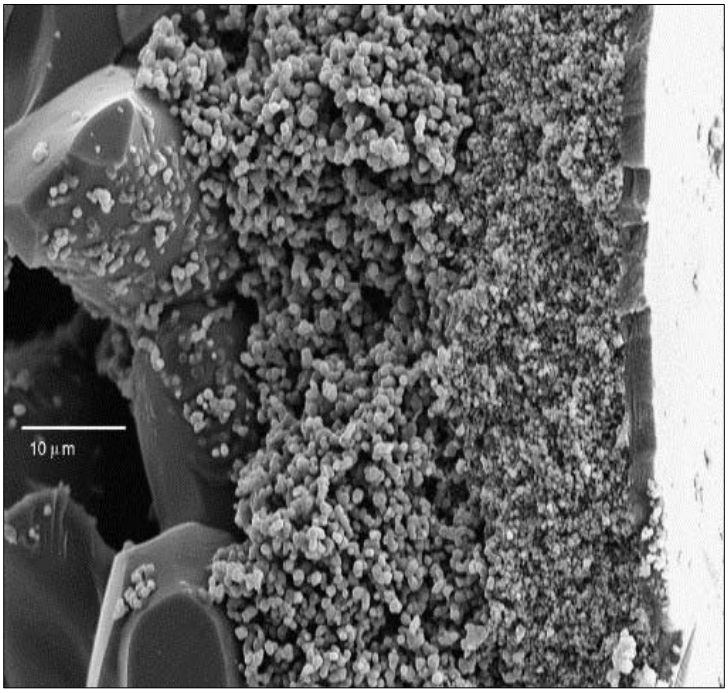

Fig. 3-2. SEM image of a 5 nm Membralox® alumina membrane. [15]

0.2 μm, respectively. The final layer, which is 3-5 μm thick, is a γ-alumina layer that is slip-cast and fired to yield an average pore size of 5 nm and a porosity of 50% [130]. Fig. 3-2 shows a scanning electron micrograph (SEM) of the membrane cross-section [15].

The membrane tube outer and inner diameters were 1 cm and 0.7 cm respectively. The tubes were received in 25 cm lengths, and for our experiments we cut them into 1 inch long pieces, using a laboratory glass cutter. After cutting, the membranes were cleaned by soaking in 2:1 ethanol/water solution for 24 hours at ambient temperature. The ethanol used for cleaning purposes was obtained from EM Science and was used without any further purification. The membranes were then dried at 60 ^{o}C for 30 min and stored in the laboratory environment. Single gas permeation data for nitrogen, propane, methane, and butane were obtained according to the procedure described in sections 3.4. Toluene-nitrogen mixture data at different toluene feed mole percents were also obtained for the untreated membranes according to the procedure described in section 3.5.

3.3.2 Synthesis of Dendrimer-Ceramic Nanocomposite Membrane

Dendrons were grown divergently from the surface of mesoporous alumina membranes by the stepwise synthesis (Fig. 3-3). The dendrons were grown by first attaching 3-aminopropyl dimethylsilane to the surface of the alumina as an anchor. These surface amines were then allowed to react with cyanuric chloride to give the dichlorotriazine intermediate, branch-point. The dichlorotriazine was then allowed to

react with either a monoamine or a diamine. The monoamines acted as a capping group that provided function to the membranes, while the diamine acted as a reactive spacer that continued the polymerization process. In this manner generation 1, 2 and 3 triazine based dendrons capped with either dodecylamine or aminobenzylamine groups were produced.

Purification of the membranes between each reaction was very important. If not fully cleaned, excess cyanuric chloride or piperazine would result in the formation of poorly soluble hyperbranched oligomers that would clog the 5 nm mesopores. The salt of Hunig's base also was found to crystallize on and in the membranes so, a solvent other than THF was necessary. It was found that the most efficient method of purification was to sequentially rinse the membranes with three different solvents: THF, methanol and dichloromethane. Other methods of purification including rinsing only with THF resulted in pores clogged with polymer, while sonication was found to damage the membrane by removing attached dendrons. Only by using a three solvent cleaning method could nonclogged pores with reproducible permselectivies be produced.

3.3.2.1. General Methods. All reagents were purchased from EMD, Aldrich or Fisher and used without purification. 3-aminopropyldimethyethoxysilane was purchased from Gelest Inc and was used without purification. Mesoporous alumina membranes with 5 nm pores were purchased from US Filter, cut into 1 in pieces and cleaned as described. Water was purified using a Barnstead EASY pure water purification system. Shaking was carried out using a GCA Precision shaker.

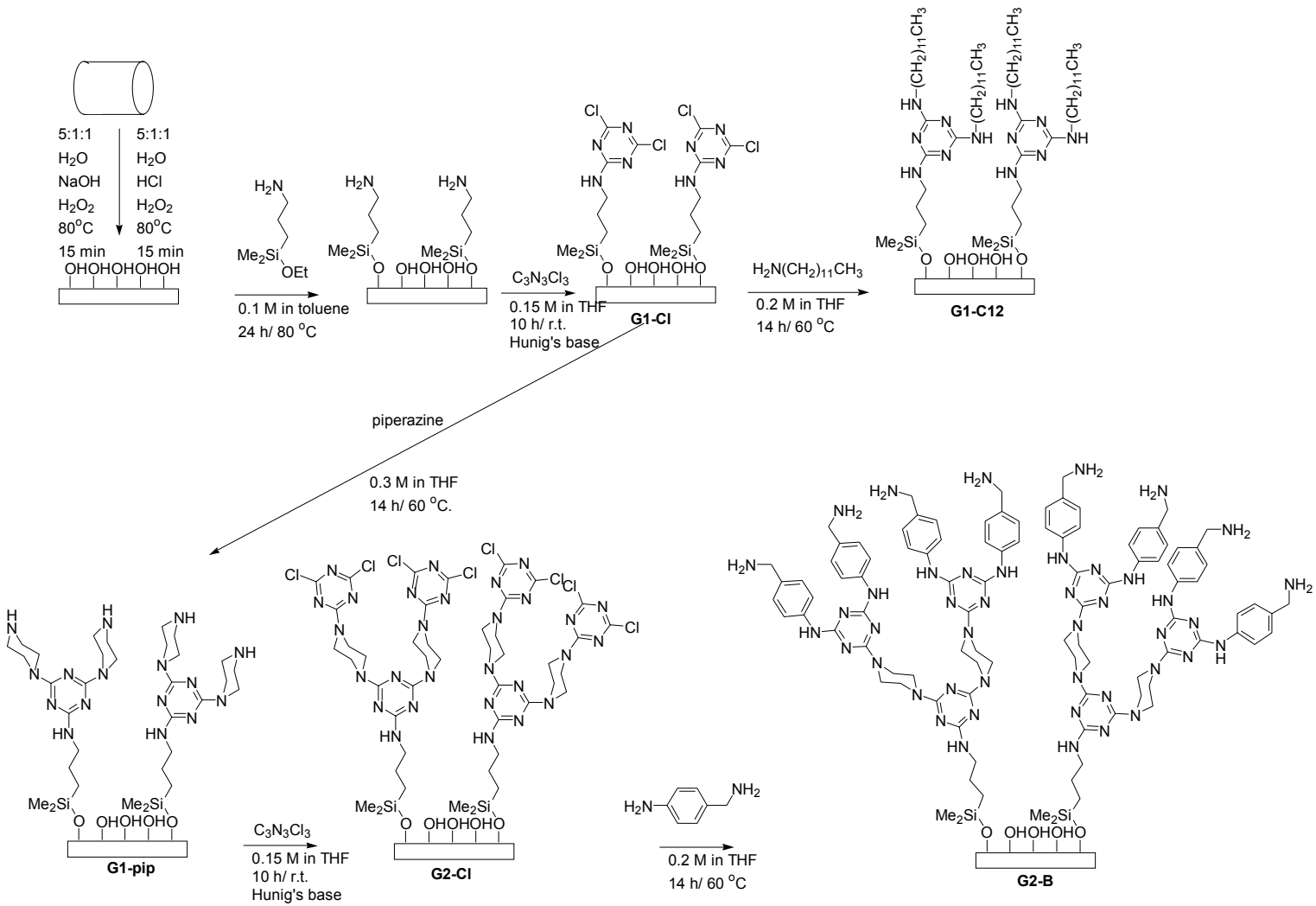

Fig. 3-3. Growth of melamine-based dendrimer on the surface of the mesoporous alumina membrane.

3.3.2.2. RCA (Radio Corporation of America) Cleaning of the Membranes. In a 100 mL beaker a membrane was submerged in 75 mL of 5:1:1 H_2O: H_2O_2: NH_4OH (organic cleaning solution) and then heated to 80 ^oC for 15 min on a hotplate. The membranes were rinsed 7 x with 100 mL of deionized water. The membranes were treated and rinsed in the same manner using 75 mL of 6:1:1 H_2O, H_2O_2, HCl (ionic cleaning solution). The treated membranes were stored in an oven at 100 ^oC for at least 4 h or until used. This drying process in 100 ^oC oven before the amine-functionalization is important to control the hydration states of the alumina surface, which enables membrane surface has the optimum density of amine anchor groups for the further organic synthesis. Both normal and superhydrated surfaces [15] result in a high density of dendrimer on the surface that would completely block the 5 nm mesopores and produce no permeance. Membranes also should used immediately for the amine-functionalization after they were taken out from the oven. If not, surface hydration states return to the normal state by cooling down to room temperature, which result in the similar effects as described above.

3.3.2.3. Amine-functionalization Treatment. In a 100 mL capped round-bottomed flask, 0.8 g (5 mmol) of 3-aminopropyldimethylethoxysilane was dissolved in 50 mL of toluene (0.1 M). A clean membrane was submerged in the solution and heated for 24 h in an 80 ^oC oil bath. The siloxane treated membrane was then rinsed (5 min soak) 3 times with 20 mL of toluene and rinsed 4 times with 20 mL of THF. The cleaned membranes were then used immediately.

3.3.2.4. Cyanuric Chloride Treatment. In a capped 100 mL round-bottomed flask, 1.4 g (7.5 mmol) of cyanuric chloride was dissolved in 50 mL of THF (0.15 M) with 1 mL (6 mmol) of diisopropylethylamine. A silane treated membrane was then inserted into the solution, the flask was capped and the solution was slowly rocked (approx. 30 rpm) for 10 h. The cyanuric chloride treated membranes were rinsed 3 times with 20 mL of THF, 2 times with 20 mL of methanol, 2 times with 20 mL of dichloromethane, and 2 times with 20 mL of THF. The final THF rinse was checked by TLC (Thin Layer Chromatography) for trace amounts of triazine and amine. The membranes were then used immediately.

3.3.2.5. Piperazine Treatement of Cyanuric Chloride Treated Membranes. In a capped 100 mL round-bottomed, 1.3 g (15 mmol) of piperazine was dissolved in 50 mL (0.3 M) of THF. A cyanuric chloride treated membrane was submerged in the solution and the solution was heated in a 60 ^{o}C oil bath for 14 h. The treated membrane was rinsed 3 times with 20 mL of THF, 2 times with 20 mL of methanol, 2 times with 20 mL of dichloromethane, and 2 times with 20 mL of THF. The final THF rinse was checked by TLC for trace amounts of triazine and amine. The cleaned membranes were used immediately.

3.3.2.6. Amine Capping of Cyanuric Chloride Treated Dendrons. In a capped 100 mL round-bottomed flask 1.8 g (10 mmol) of dodecylamine or 1.2 g (10 mmol) of *p*-aminobenzylamine was dissolved in 50 mL (0.2 M) of THF. A cyanuric chloride treated

membrane was placed in the solution and heated in a 60 ^{o}C oil bath for 14 h. The treated membrane was then rinsed 3 times with 20 mL of THF, 2 times with 20 mL of methanol, 2 times with 20 mL of dichloromethane, and 2 times with 20 mL of THF. The final THF rinse was checked by TLC for trace amounts of triazine and amine. The cleaned membranes were then air-dried and stored in a vial until used.

3.4 Single Gas Permeation Experiments

3.4.1 Procedure

Permeation measurements on the individual gases were performed using an in-house unit. Pure helium (99.996%), nitrogen (99.998%) and propane (99.5%) gases were used as received from Praxair Distribution, Inc. Fig. 3-4 shows our set up for the single-gas experiments. The membrane was held in a steel module. Two different membrane modules were used for different membrane types. A shell-tub module was used For the Membralox® cylinder membrane and a disc module was used for Anopore® disc membrane. Each membrane module has two openings for feed and permeate side (a shell-tube module, which was dead-ended on one of the tube ends). Screw caps and rubber O-rings were used for proper sealing.

The pure gas was supplied to the feed inlet and flowed across the membrane and through the permeate outlet, which is connected to a bubble flow meter vented to a fume hood. The pressure on the feed side was controlled with a pressure regulator. The pressure difference was monitored with a digital pressure transducer from Omega.

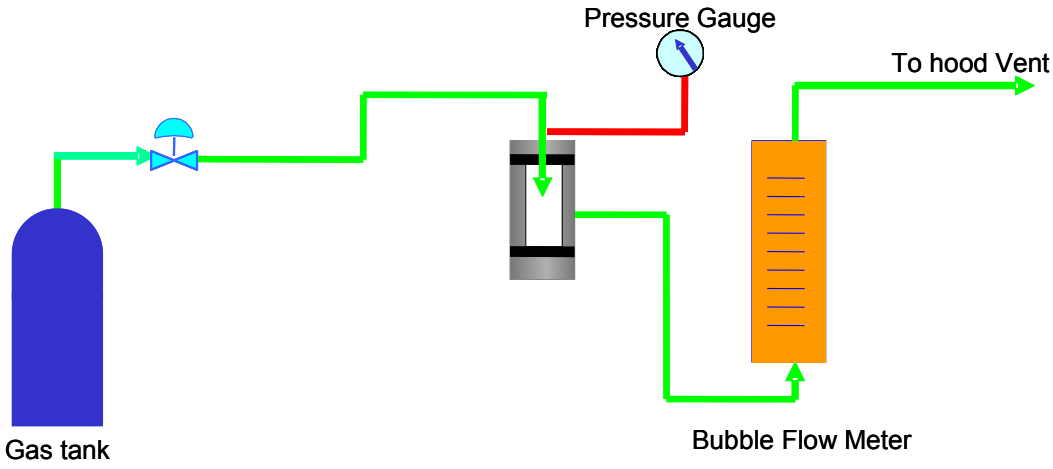

Fig. 3-4. Schematic of the dead-end ideal single gas experiments.

Since the shell side was at atmospheric pressure, the gauge pressure reading was considered as the pressure drop across the membrane. The volumetric flow rate was measured at several pressure differences ranging from 5 to 90 psi.

A leak test was performed prior to each single gas permeation experiment. The membrane was placed inside the module, and feed gas was introduced to the module with the retentate valve closed. When the pressure drop across the membrane was around 1 bar, the feed and permeate valves were closed to isolate the membrane module. A continuous drop in the pressure would indicate the presence of a leak, in which case a soap solution was used to detect the source of the leak. If no pressure drop was observed within a period of five minutes, the apparatus was considered to be free of any leaks.

Once the leak test was satisfactorily completed, the feed and the permeate valves were opened. The retentate was closed for a shell-tube module so that a "dead-end" experiment could be done. Pressure drop across the membrane was set to the desired value by adjusting the regulator on the gas cylinder. The pressure drop was monitored until it reached the set-point value, after which permeate volumetric flow rate was measured using the bubble flow meter and a stopwatch. After it reaches the stabilization, the average value of the final four measurements was taken in order to determine a value of the permeate flow rate. For the organic treated membrane, it usually takes a longer time for the pressure to stabilize (up to 24 hrs) than one of the bare membrane (around 15 min). At least 4 different pressure readings were tested for the measurement of flow rate; however, depending on the nature of the experiments, more readings were often taken.

After completing the set of readings for one gas, the gas flow from the cylinder was stopped and the retentate valve was opened to quickly release the gas from inside the module. The feed tubing was then connected to the next gas cylinder and with the retentate valve open, gas was slowly introduced into the module. The retentate valve was kept open for about 30 seconds after which it was closed. This procedure was done to ensure that no gas from the previous experiment was left inside and the system had been completely flushed with the new gas. Volumetric flow rate was again monitored at different feed pressure readings. This procedure was then repeated until all the data needed for the different gases had been obtained. During the permeation experiment, room temperature and barometric pressure were noted to make the necessary correction for converting volumetric flow rate to molar rate using the ideal gas equation. Humidity of the laboratory was also checked.

3.4.2 Permeance Calculation

This section describes the procedure for calculating the single gas permeances. As noted above, volumetric flow rate was measured for different pressure readings. The volumetric flow rates were converted to molar flow rate assuming ideal gas behavior, as given by Eq. (3-1) below:

$$N(gmol/sec) = Q\left(\frac{ml}{sec}\right)\times\left(\frac{1l}{1000ml}\right)\times\left(\frac{1gmol}{22.4l}\right)\times\left(\frac{T_0}{T}\right)\times\left(\frac{p}{p_0}\right) \qquad (3\text{-}1)$$

where

T_0 =273 K

T = ambient room temperature (K)

p_0 = 1.01 bar

p = ambient pressure reading (bar)

The internal surface area of the membrane was calculated using Eq. (3-2)

$$Area(m^2) = \pi \times D \times L \quad for \quad a \quad cylider \quad membrane$$
$$or \quad \pi \times R^2 \quad for \quad a \quad disc \quad mebrane \tag{3-2}$$

where

D = internal diameter of the cylinder membrane (m)

L = length of the cylinder membrane (m)

R = radius of the disc membrane

The membrane flow area was determined to be 0.000346 m^2 for Anopore® disc membranes and to be 0.000559 m^2 for Membralox® cylinder membrane by using Eq. (3-2).

The gas flux J through the membrane was calculated by dividing the molar flow rate with the membrane flow area

$$J(\frac{gmol}{sec\ m^2}) = \frac{N}{Area} \tag{3-3}$$

Permeance is related to flux through Eq. (3-4).

$$P\ (\frac{gmol}{sec\ m^2 bar}) = \frac{J}{\Delta p} \tag{3-4}$$

where

Δp= pressure drop across the membrane (bar)

Permeance was obtained directly using Eq. (3-4). The intrinsic property of "permeability" is a product of the permeance and the thickness of the membrane. We have no direct data on the thickness of the active layer, which controls transport in our membranes, so therefore we report permeances instead of permeabilities. During the course of this study the room temperature ranged from 18 to 22 ^{o}C, while the ambient pressure varied between 0.97 to 1.02 bars.

3.5 Vapor Permeation Experiments

3.5.1 Procedure

The schematic for the toluene-nitrogen permeation experiments is shown in Fig. 3-5. The membrane piece is placed in a cylindrical steel module or a flat steel module, as for the gas separations. A constant flow of nitrogen gas and toluene vapor flow are achieved by using a mass flow controller and a liquid injection syringe pump to make

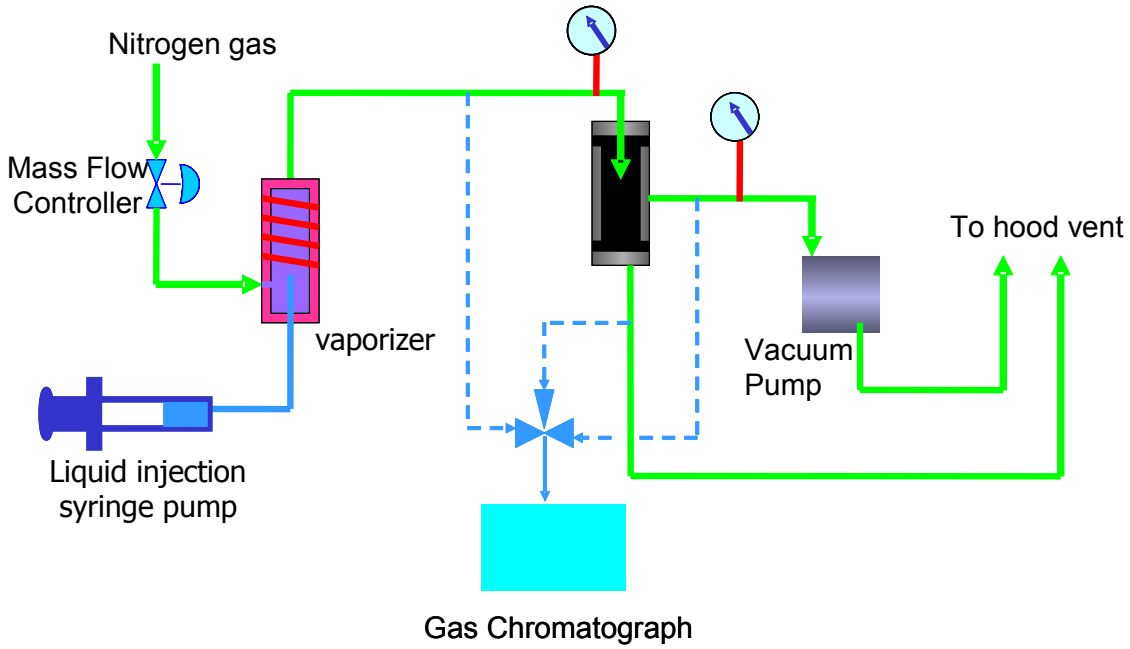

Fig. 3-5. Schematic of the vapor permeation experiments.

the constant feed concentration. Nitrogen gas and the injected liquid toluene are mixed well in a vaporizer, which has α-alumina particles packed inside and is heated up to 250 ^{o}C. To prevent any condensation of toluene inside the flow line, all lines were heated to 150 ^{o}C using heating tape connected to a power regulator or temperature controller. This feed stream passes through the membrane module. Feed pressure was controlled by means of the retentate control valve.

The feed gauge pressure during the course of the experiments varied between 0.022-0.027 bars. Due to the low feed pressures, a vacuum pump was used downstream of the permeate line to generate the necessary driving force for permeate flow. For our experiments, the permeate pressure varied between 0.8-0.88 bars below atmospheric pressure. Sample lines from feed, permeate, and retentate streams were taken to a gas chromatograph (a Varian 3800 GC) to analyze their molar compositions. The retentate flow in the toluene-nitrogen was kept high enough so that there was no significant difference between the feed and retentate compositions. The cold trap with liquid N_2 cooling is used to collect the condensed toluene in the permeate side. The amount of condensed toluene in cold traps is measured to calculate the permeate flow rate

3.5.2 Permeance Calculation

The permeate volumetric flow rate for toluene was calculated by converting the amount of the condensed toluene to the mol fraction of propane in the permeate as given below

$$N_i(gmol/\sec) = Q\left(\frac{ml}{sec}\right)\times\left(\frac{0.865g}{ml}\right)\times\left(\frac{1gmol}{92.14g}\right) \quad (3\text{-}5)$$

where

N_i = molar flow rate for component *i*

The partial pressure drop for component *i* was calculated by subtracting the permeate partial pressure from the inlet partial pressure for component *i* as given in Eq. (3-6)

$$\Delta p_i = p_{i,f} - p_{i,p} \quad (3\text{-}6)$$

where

Δp_i= partial pressure drop for component *i* across the membrane (bar)

$p_{i,f}$ = partial pressure for component *i* in feed gas (bar)

$p_{i,p}$ = partial pressure for component *i* in permeate (bar)

The flux J_i and permeance P_i were calculated by writing Eq. (3-3) and Eq. (3-4) for species *i* as detailed below

$$J_i\left(\frac{gmol}{sec\ m^2}\right) = \frac{N_i}{Area} \quad (3\text{-}7)$$

$$P_i\left(\frac{gmol}{sec\ m^2 bar}\right) = \frac{J_i}{\Delta p_i} \quad (3\text{-}8)$$

For the mixed gas we also calculated the separation factor (S_F) as defined by Eq. (3-9)

$$S_F(A/B) = \frac{(y_{A,p} / y_{B,p})}{(y_{A,f} / y_{B,f})} \quad (3\text{-}9)$$

where

$y_{i,p}$ = mol fraction of component *i* in permeate

$y_{i,f}$ = mol fraction of component *i* in feed

3.6 Analytical Methods

Several analytical methods were applied to characterize the inherent properties of organic-inorganic nanocomposite materials and membranes.

3.6.1 Powder X-ray diffraction

Powder X-ray diffraction (PXRD) is used to determine structural ordering of materials. Powder X-ray diffraction measurements were performed using a Bruker-AXS D8 powder diffractometer with Cu Kα radiation over a range of 0.8 to 5° 2θ. Peak intensities and 2θ values were determined using the Bruker program EVA. Powder X-ray diffraction measurements were also performed using a Bruker NanoSTAR system with a Nonius rotating anode (FR591) and a copper target (1.5417 Å) [132].

3.6.2 Nitrogen Adsorption

Porosimetry experiments give useful information about the pore size distribution, pore volume, and surface area of the materials. Nitrogen adsorption experiments were performed on a Micromeritics ASAP 2010 micropore system using approximately 0.1 g of sample. The samples were degassed under vacuum at room temperature for 2 h, then at 40 °C for 4 h, then at 60 °C for 4 h before analysis. The micropore and mesopore volumes were determined using the α_s-method [133, 134]. The mesoporous size distributions were calculated from the adsorption branch of the isotherm using the Barret-Joyner-Halenda (BJH) method [135] with a modified equation [136] for the statistical film thickness.

3.6.3 Electron Microscopy

Electron microscopy is also essential for characterizing material shape, size, and surface. Transmission electron microscopy (TEM) produces a real space image of the mesoporous nature that can be used to examine the structural ordering, complementing PXRD results. Scanning electron microscopy (SEM) is used to determine the particle size and surface morphology.

Transmission electron microscopy (TEM) was performed on a JEOL 2010 microscope with a lanthanum hexaboride (LaB_6) filament and an excitation voltage of 200 kV. Energy Dispersive X-Ray Analysis (EDX) was performed using an Oxford

instrument eXL EDS system. The samples were dispersed in methanol (100%, Aldrich) and placed on a 400-mesh copper grid.

Field-Emission Scanning Electron Microscopy (FE-SEM) measurements were performed using a Zeiss Leo-1530 microscope operating at 1-10 kV. The microscope employs a GEMINI electron optical column with a Schottky-type field emitter, single condenser, crossover-free beam path, large specimen chamber with two chamber ports for EDS or WDS adaptation, four accessory ports on the chamber and three on the door, fail-safe vacuum system, digital image store and processor.

3.6.4 Organic Characterization

Infrared spectroscopy is used to verify the presence of organics attached in the materials. Infrared spectroscopy was performed using an Nexus 670 FT-IR Spectrometer from Thermo Nicolet.

Solid-state NMR spectroscopy provides evidence for hybrid formation. ^{29}Si MAS and CP-MAS and ^{13}C CP-MAS were performed on a Bruker Avance operating at 79.49 and 100.61 MHz. All spectra were acquired using a 7 mm probe with ZrO_2 rotors and a spinning rate of 5080 Hz. ^{29}Si MAS spectra were acquired using a 2 μs 50° pulse, high-power proton decoupling, and a 90 s recycle delay. ^{29}Si{^{1}H} CP-MAS spectra were acquired with a 5 ms contact time, a ^{1}H 90° pulse length of 4 μs, and a 5 s recycle delay. 13C{^{1}H} CP-MAS spectra were acquired with a 2.5 ms contact time, a ^{1}H 90° pulse length of 4 μs, and a 5 s recycle delay.

The organic content is quantified using thermal gravimetric analysis (TGA) and elemental analysis. Thermal gravimetric analyses (TGA) were performed using a TG 209C Iris Instrument from Netsch over a temperature range of 25 to 515 °C using oxygen as a carrier gas and temperature ramping rate of 5 °C min^{-1}. Elemental analysis (C, H, N analysis) was performed by Galbraith labs.

MALDI-MS was performed on the organic groups to further study the identity of the organic groups formed. Mass spectra were acquired using MALDI-MS on an Applied Biosystems Voyager-DE STR Biospectrometry Workstation. Matrix-assisted laser desorption/ionization time-of-flight (MALDI-TOF) spectra were recorded in refelected ion mode with an Applied Biosystems Voyager DE-STR mass spectrometer (ABI, Framingham, MA). Positive ions were generated by using a nitrogen laser pulse (y= 337 nm, 20Hz) and accelerated under 25 kV using delayed extraction (190 nsec) before entering the time-of-flight mass spectrometer. Laser strength was adjusted to provide minimal fragmentation and optimal signal-to-noise ratio. An average of 100 laser shots was used for each spectrum, and data were processed with the accompanying Voyager software package. The sample was prepared using the dry drop method with 2,4,6-trihydroxyacetophenone (THAP) as has been described previously. The analysis solution, approximately 1 μM dendrimer and 10 mg/ml THAP solution in methanol, was spotted in 1 μl aliquots on top of a Teflon coated plate.

To characterize the effects of surface treatments X-ray photoelectron spectroscopy (XPS) was performed on the inner active surface of the bare and treated membranes. For this purpose, the membrane had to be split open to expose the inside

surface. The XPS work was carried out using a Kratos analytical Axis HIS 165 instrument with a monochromatic aluminum X-ray source and an electron flood gun for charge neutralization. Photoelectron peaks for carbon (C 1s), oxygen (O 1s), silicon (2p) and aluminum (Al 2p) were collected and the relative molar compositions were calculated using integrated analysis software.

CHAPTER IV

ENGINEERING NANOSPACES: OMS/DENDRIMER HYBRIDS POSSESSING CONTROLLABLE CHEMISTRY AND POROSITY [*]

The synthesis and characterization of melamine-based dendrimer/SBA-15 hybrids is reported in Chapter IV. We did the model study by using powder ordered mesoporous silica (OMS), SBA-15 in order to prove the feasibility of dendrimer synthesis inside mesoporous materials. The results from this study provide the fundamental idea about how dendrimer synthesis affects the porosity of inorganic mesoporous support when the same oligomers are applied on the synthesis of organic-inorganic nanocomposite membranes. It is shown that OMS/dendrimer hybrids can be promising materials that can be used for catalysis, separations, molecular recognition, or as scaffolds to build more complex structures.

This study demonstrates the ability to fabricate hybrid materials containing a high loading of organic moieties (~30-35 weight percent) that possess a well-defined structure. Numerous characterization methods including X-ray diffraction, electron microscopy, infrared spectroscopy, solid-state NMR spectroscopy, thermal gravimetric analysis, MALDI-MS, elemental analysis and nitrogen porosimetry have been used to

---

[*] Reprinted with permission from "Engineering Nanospaces: OMS/Dendrimer Hybrids Possessing Controllable Chemistry and Porosity" by S. Yoo, J. D. Lunn, S. Gonzalez, J. A. Ristich, E. E. Simanek, D. F. Shantz, Chem. Mater. 18 (2006) 2935-2942. © 2006 by American Chemical Society

characterize the microstructure of the hybrids obtained. Based on thermal gravimetric analysis and elemental analysis the average conversion between generations is between 70-75% and highly reproducible. MALDI-MS verifies that a significant fraction of the organic groups on the OMS surface possess the desired structure, consistent with IR and NMR results. The porosity of the hybrid can be modified either by using dendrimers of different generation, using different linkers in the dendrimer structure, or by controlling dendrimer loading. Porosimetry measurements indicate that the effective pore size of the hybrid and the total pore volume of the material can be controlled independently of one another. Copper sequestration was used as a probe to demonstrate that the amines of the dendrimer are accessible and able to bind Cu(II). Given the ability to tune chemistry and porosity independently the current work shows these hybrid materials have potential use in many areas including separations, sensing, and catalysis.

4.1 Introduction

Organic-inorganic hybrid materials have long attracted interest from the scientific and engineering communities [137-140]. These materials hold great promise in areas including sensing, separations, optics, and catalysis, given that they combine the features of both organic (e.g. chemical diversity) and inorganic (e.g. good mechanical/thermal properties) materials. Ordered mesoporous silicas (OMS) [81, 82, 88, 95, 141-144] have been studied extensively as supports for hybrid materials given that they possess an ordered pore structure containing uniformly sized pores, a variety of pore connectivities, and surfaces that can be easily functionalized using a the wealth of

previously developed silane chemistry [145]. These material properties facilitate analysis of the hybrid material by microscopy, powder X-ray diffraction (PXRD), and porosimetry, and allow a relatively straightforward determination of how organic incorporation modifies the porosity and other properties of the parent OMS.

Numerous works have investigated incorporating organic functional groups into OMS [145-150]. These works have studied approaches including direct synthesis of hybrid materials, post-synthetic grafting, covalent versus non-covalent linkage, etc [145-149]. While most investigations have studied the grafting of simple silanes, more recent work has expanded to functional groups prepared by multistep reactions [150-155]. For hybrids to achieve their full potential, it is necessary to be able to synthesize complex organic structures containing multiple functional groups and well-defined spatial arrangements directly on the mesoporous support. Such properties are of relevance in applications such as bi-functional catalysis and molecular recognition that require multiple functional groups or precise control over the spatial arrangement of functional groups. For emerging applications utilizing OMS such as drug delivery and sensing it will be necessary to control particle size, chemical functionality, and porosity, ideally in an independent manner [156].

The fabrication of OMS-hybrids with high densities of functional groups is particularly problematic. At high loading (> 0.25 mmol/g) heterogeneity of sites is often observed [157] and the formation of polymeric layers of the tethering agent is often problematic as well [158]. Recent work by the Jones lab has shown that surface patterning approaches can be used to circumvent this issue [159, 160], and work by the

Katz lab has shown the potential of molecular imprinting to achieve higher (0.3 – 0.4 mmol/g) densities of organic functional groups on amorphous silica [161-164]. Another possible route to high functional group densities is the use of surface-tethered dendrimers. These highly uniform hyper-branched polymers [165-167] present unique opportunities given that increasing the dendrimer generation doubles the number of peripheral functional groups on the dendrimer. Further, dendrimers have shown promise in applications including catalysis, separations, and molecular recognition. Though physisorption of dendrimers into OMS has been successfully achieved [168-170], covalent attachment is preferable in many applications.

The literature on dendrimers covalently attached to OMS is relatively sparse. Acosta *et al.* synthesized melamine-based dendrimer of various generations on SBA-15 mesoporous silica to bring the controllable chemistry and porosity to OMS [123]. Additionally collaboration between the Alper and Al Sayari labs has produced three publications on PAMAM dendrimer-MCM-41 hybrids [171-173]. The current investigation, building off our preliminary report, expands the scope to other linkers in the dendrimers, as well as demonstrating that these materials can be used in such applications as metal sequestration. A thorough characterization study is presented using a battery of methods to determine the hybrid microstructure.

4.2 Experimental Section

4.2.1 Materials

Tetraethoxysilane (TEOS, ≥99%) was purchased from Fluka. Pluronic P123 ($EO_{20}PO_{70}EO_{20}$, MW=5800) was obtained from BASF. Ethanol and toluene (ACS reagent grade) were purchased from EM Science. 3-aminopropyltriethoxysilane (APTES, 99%), Piperazine (P, 99%), 4,4'-Trimethylenedipiperidine (TMDP, 97%), and N,N-diisopropylethylamine (DIPEA, 99%) were purchased from Aldrich. 4-(aminomethyl)piperidine (AMP, ≥98%) was purchased from TCI America. Cyanuric Chloride (CC, 99%) was purchased from ACROS. Tetrahydrofuran (THF), methanol, and dichloromethane (DCM) (all ACS reagent grade) were purchased from EMD. Copper(II)sulfate pentahydrate (Cupric Sulfate, ≥99%) was purchased from J.T. Baker. Ethylenediamine-tetraacetic acid disodium salt (EDTA, ≥99%) was purchased from EM Science. Murexide (Ammonium Purpurate) was purchased from Acros. All chemicals were used as received.

4.2.2 Synthesis of Dendrimer-SBA15 Hybrids

Dendrimer-SBA-15 hybrids were synthesized by methods described in Chapter III. The synthesis of the composites is illustrated in Fig. 4-1. Amine-functionalized SBA-15 was extended to the high generation dendriemr by the iterative synthesis of cyanuric chloride and diamine linnker. So that every dendrimer has the same functionality on the outer periphery (primary amine), the final linker molecule used was

AMP. Several linker molecules with various sizes were also used to control dendrimer size in the same generation. Fig. 4-2 shows a second-generation dendrimer for each linker molecule.

4.2.4 Analytical

Several analytical methods such as powder X-ray diffraction (PXRD) measurements, transmission electron microscopy (TEM), infrared spectroscopy, solid-state NMR spectroscopy, thermal gravimetric analyses (TGA), mass spectroscopy, and nitrogen adsorption experiments were done as described in Chapter III.

4.2.5 Copper (II) Sequestrations

30 mg of the following samples were placed in vials: bare SBA-15, 0.5 mmol/g amine-SBA-15, and G1, G2, and G3 AMP-based composites (0.5 mmol/g amine loading). To these vials 6.6 mL of 14.4mM cupric sulfate in purified water (360.0 mg of cupric sulfate pentahydrate per 100 mL water) were added. The mixtures were then shaken for 14 hours. The resulting solutions were filtered and 2 mL of each were titrated with 5.4mM Na2EDTA using murexide as the indicator (50.2 mg per 100mL purified water). Each solution was titrated twice including the stock cupric sulfate solution.

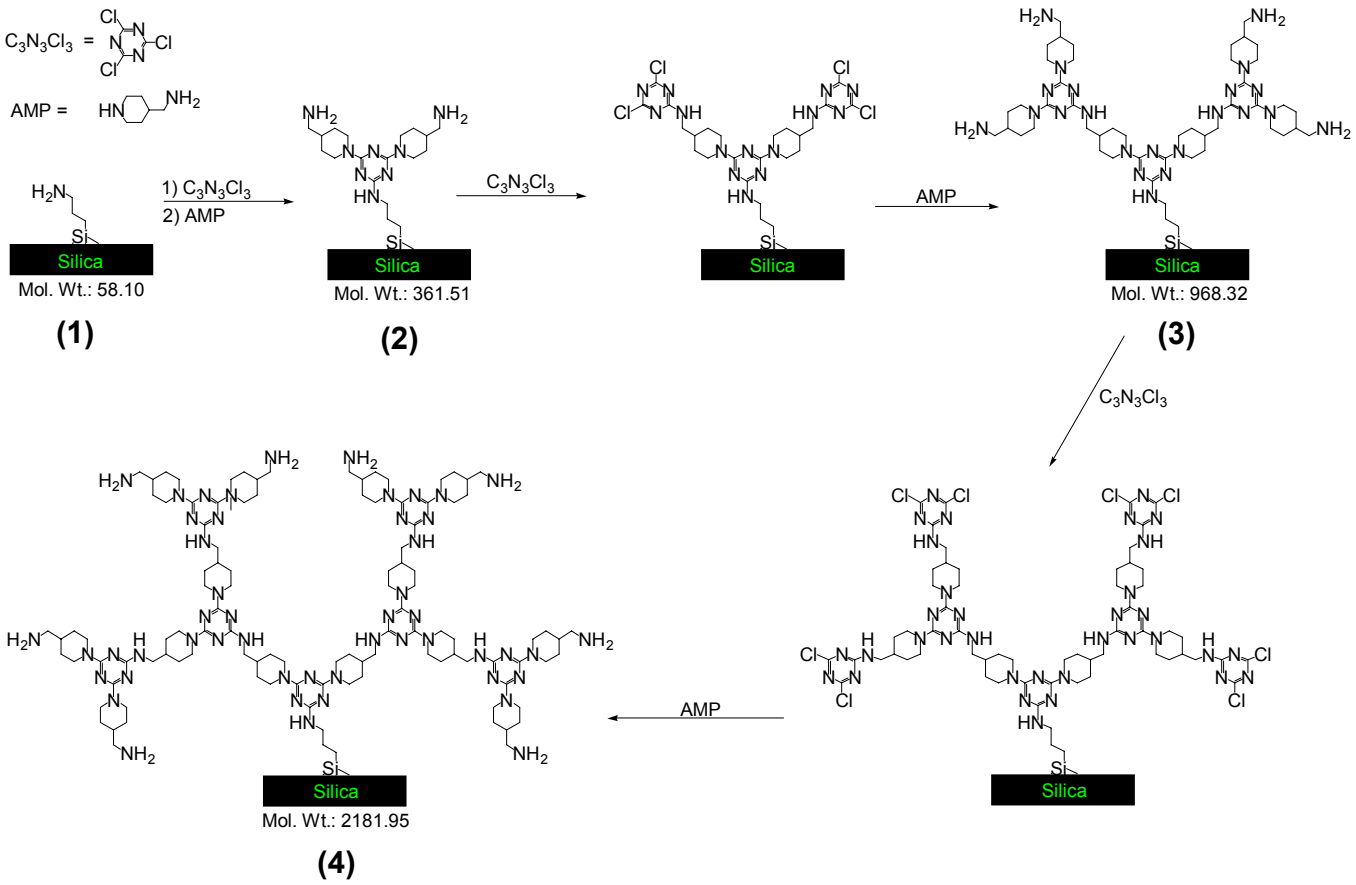

Fig. 4-1. Iterative synthesis of melamine-based dendrimers of various generations on amine-functionalized SBA-15. Shown is the synthesis using 4-aminomethylpiperidine (AMP) as the linker molecule: (1) Amine-functionalized SBA-15, (2) G1-AMP dendrimer, (3) G2-AMP dendrimer, (4) G3-AMP dendrimer.

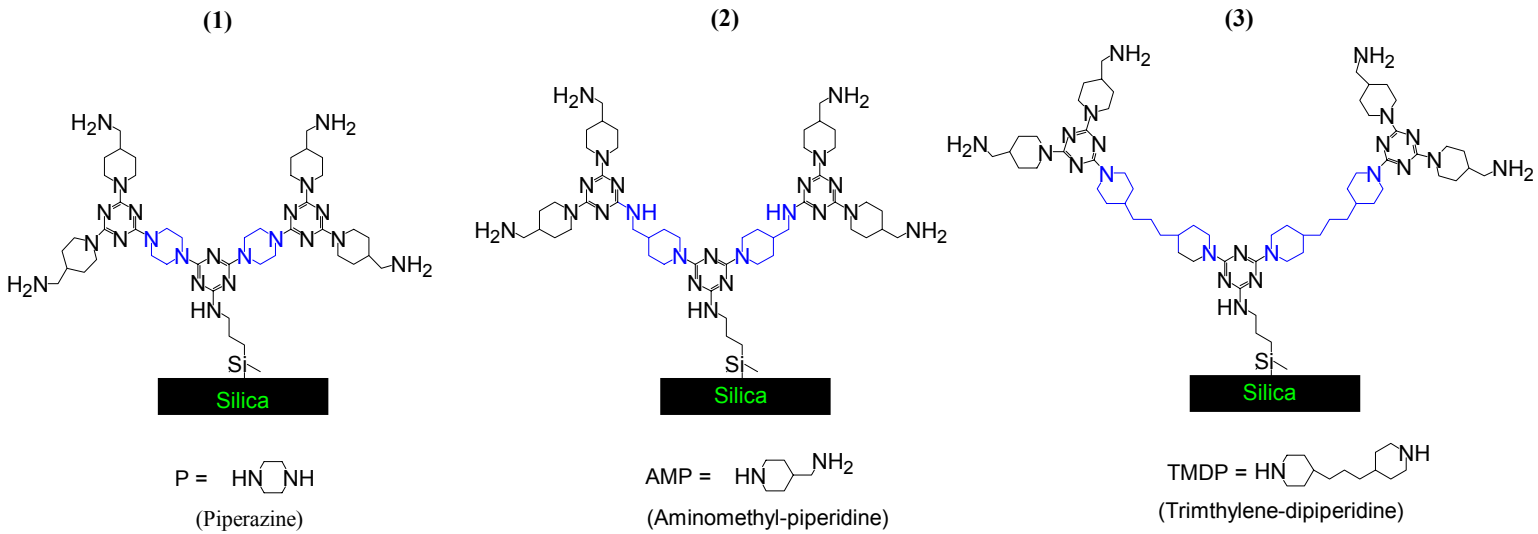

Fig. 4-2. Synthesis of dendrimer-SBA15 hybrids using different linker molecules. (1) piperazine (P), (2) 4-(aminomethyl)piperidine (AMP) and (3) 4,4'-trimethylenedipiperidine (TMDP). Second generation dendrimers are shown in all cases.

4.3 Results

4.3.1 Analytical Characterization

Powder X-ray diffraction was used to verify the hexagonal mesostructure of the SBA-15 (Fig. 4-3). The parent SBA-15, amine-SBA-15 and G1-hybrid materials show three well-defined peaks at 2θ values between 0.8 to 5° that can be indexed as the (100), (110), and (200) Bragg peaks, typical of hexagonal (*p6mm*) SBA-15 [88]. The (100) peak is clearly observed as the dendrimer generation increases, however the intensity of (110) and (200) peaks decrease for the G2 and G3 hybrids. Subsequently TEM was used to verify the SBA-15 retained its structural ordering (Fig. 4-4). The images show the mesostructure is hexagonally ordered as expected.

Infrared spectroscopy was used to verify the presence of dendrimers in the materials. Fig. 4-5 shows the spectra for SBA-15, amine-functionalized SBA-15 and the G3 composites of each linker molecule. The spectra show the G3 composites are chemically different from SBA-15, the amine-SBA-15, and each other. The spectra exhibit the characteristic peaks for the primary, secondary and tertiary carbon C-H bond stretches between 2800 and 3000 cm^{-1}. These peaks are not observed in the parent SBA-15 sample, and are very weak for the amine-SBA-15 hybrid. The intensity differences between the samples are due to the different linker molecules in the dendrimers. The dendrimer-composites also show aromatic peaks between 1400 and 1600 cm^{-1}. The results are qualitative evidence for hybrid formation.

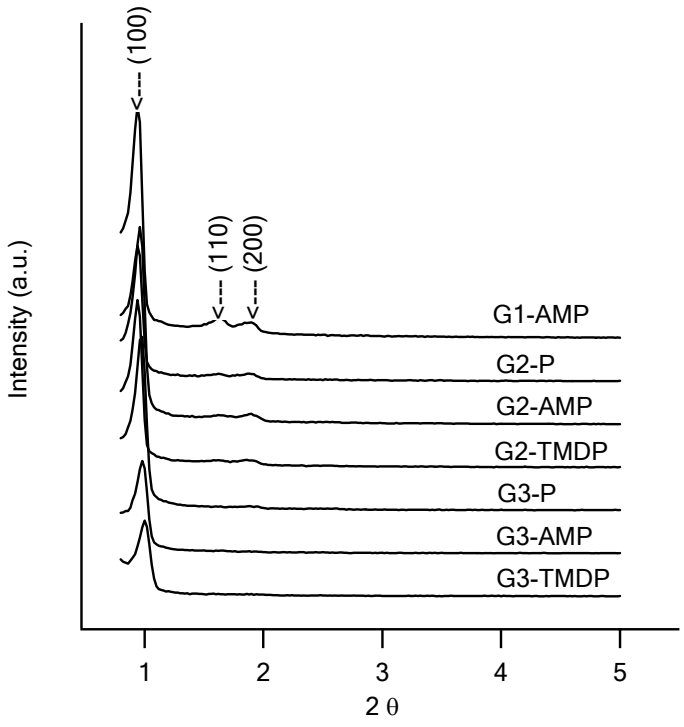

Fig. 4-3. Powder X-ray diffraction patterns of the dendrimer-SBA15 hybrids.

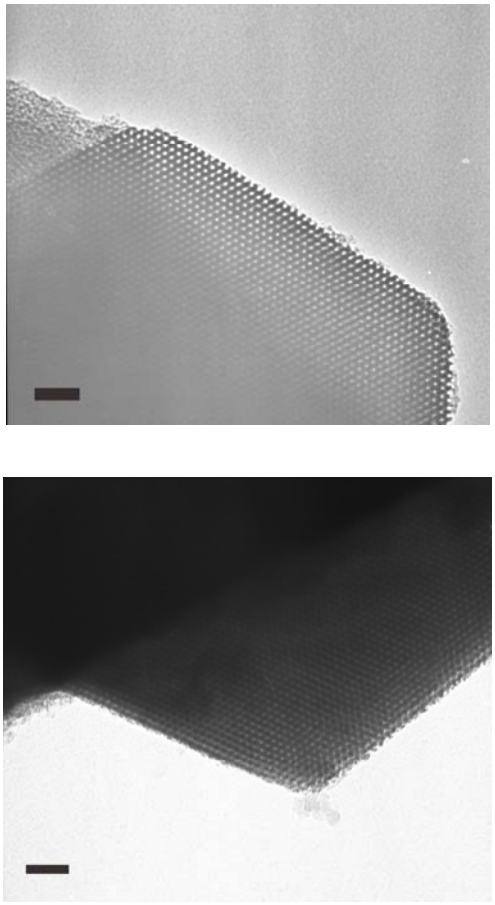

Fig. 4-4. Transmission electron micrographs of dendrimer-SBA15 hybrids. (Top) G3-AMP-SBA15 and (Bottom) G3-TMDP-SBA15 samples. The scale bars in the figures are 50 nm.

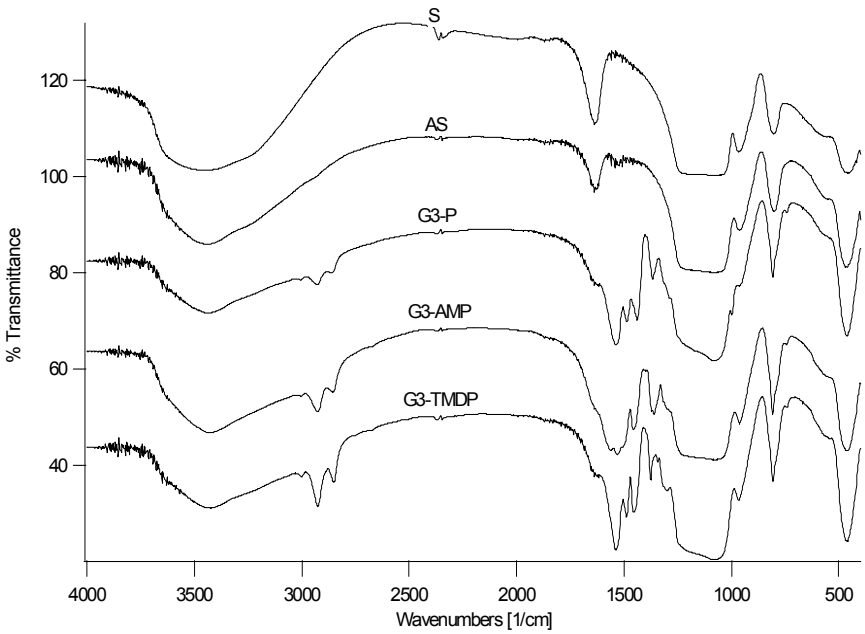

Fig. 4-5. IR spectra of dendrimer-SBA15 hybbrids. SBA-15 (S), 0.5mmol/g NH_2-SBA-15 (AS), G3-P composite, G3-AMP, composite, and G3-TMDP composite.

Further evidence for hybrid formation is obtained from solid-state NMR spectroscopy. Fig. 4-6 shows the ^{29}Si MAS and ^{29}Si{^{1}H}CP-MAS spectra for the G3-AMP sample. Both spectra contain three broad sets of peaks between –90 and –110 ppm, consistent with Q^2, Q^3, and Q^4 silicon centers. The main differences between the spectra are the change in the relative intensities of the Q^3 and Q^4 lines, and the resonance centered at approximately –67 ppm in the CP-MAS due to Si-C linkages, which is not observed in the one-pulse MAS spectra. The ^{29}Si NMR indicates that the silane is successfully grafted to the surface via the resonance observed at –67 ppm. The ^{13}C{^{1}H} CP-MAS (Fig. 4-7) provides further evidence for the incorporation of the organic group. There is a line at 163 ppm due to the aromatic carbons, and the two resonances at 40 ppm and 27 ppm are due to the aliphatic carbons on the 4-aminomethylpiperidine. The carbons on the aminopropyl silane are obscured by these resonances, but a weak signal can be seen at approximately 6 ppm that is the methylene group attached to the silicon center. Also note that the aromatic carbons are quite rigid based on the spinning side bands observed (marked with an asterisk). These results are consistent with the IR results. While it is not possible to rule out the presence of some reaction side products with NMR (see below), the results qualitatively indicate the presence of dendrimer; this is studied further below via MALDI-MS.

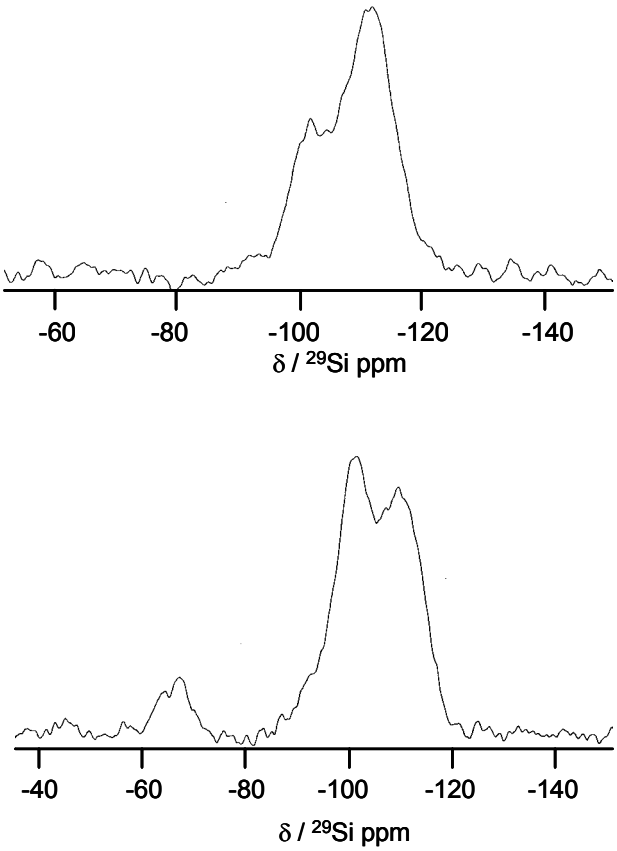

Fig. 4-6. ^{29}Si MAS (top)and ^{29}Si{^{1}H} CP-MAS (bottom) of the G3-AMP hybrid.

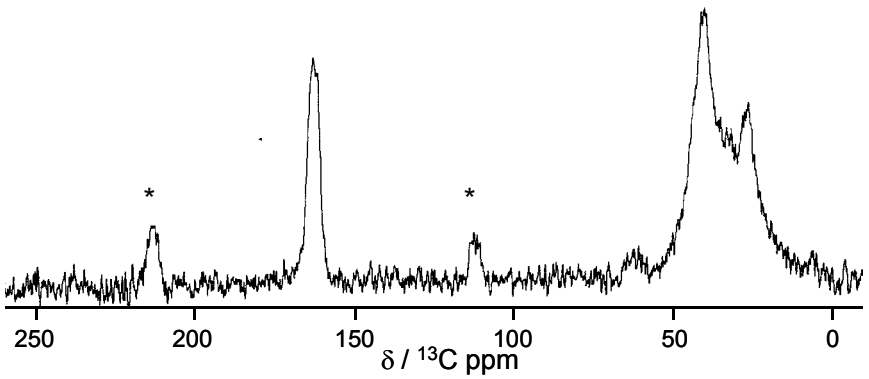

Fig. 4-7 $^{13}C\{^{1}H\}$ CP-MAS spectrum of the G3-AMP hybrid. Spinning sidebands are denoted with asterisks.

The organic content is quantified using thermal gravimetric analysis (TGA) and elemental analysis. The TGA results are summarized in Fig. 4-8. The weight percent of organic increases by approximately 10% for each generation increase of AMP: 11*wt*% for G1, 20*wt*% for G2, and 31*wt*% for G3. Based on these values the theoretical conversion at each stage is 31% (amine-SBA → G1), 75% (G1 → G2), and 83% (G2 → G3). A summary of the elemental analysis and TGA data is included in Table 4-1 and Table 4-2. Using the elemental analysis data to estimate the conversions between the G1 → G2 → G3 gives reasonable agreement with this. These values are consistent with previous work [123], but merit a few comments. First, the data shown is not corrected for the approximately 3.9% weight loss observed for the parent SBA-15, likely due to silanol condensation at elevated temperatures. This number was not subtracted from the subsequent samples as many of the silanol groups that contribute to the weight loss react during the aminosilane functionalization step. However, not correcting the data results in the appearance that there is an excess of amine groups on the amine SBA-15 material. This in part contributes to the low conversion in going from the amine-SBA-15 material to the G1 hybrid.

Two other factors that contribute to the low conversion in going from the amine SBA-15 material to the G1 hybrid are that the some of the amines are simply not reactive, and that some of the amines preferentially site in the micropores inhibiting their subsequent reactivity. Three points appear consistent with this. First, the TGA data indicates the amine grafting to the parent SBA-15 is essentially quantitative.

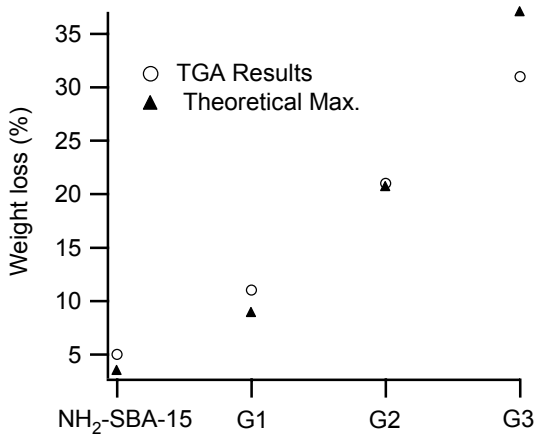

Fig. 4-8. TGA results for the dendriemr-SBA-15 composite materials.

Table 4-1 Elemental analysis results

	G1 AMP			G2 AMP			G3 AMP		
	TGA* (wt%)	EA (wt%)		TGA* (wt%)	EA (wt%)		TGA* (wt%)	EA (wt%)	
C	*6.6*	7.14	7.13	*11.9*	12.90	12.82	*18.4*	19.41	19.44
H	*1.0*	1.50	1.45	*1.7*	2.18	2.11	*2.6*	3.03	2.90
N	*3.4*	2.90	2.91	*6.4*	5.93	5.95	*10.0*	9.77	9.83
Total	11	11.54	11.49	20	21.01	20.88	31	32.21	32.17

	G2 P			G2 TMDP		
	TGA* (wt%)	EA (wt%)		TGA* (wt%)	EA (wt%)	
C	*11.0*	11.72	12.19	*12.8*	14.25	13.82
H	*1.6*	2.00	2.11	*1.9*	2.29	2.41
N	*6.4*	5.94	5.87	*5.3*	5.17	5.13
Total	19	19.66	20.17	20	21.71	21.36

Carbon/Nitrogen Ratios

	Pure Product	EA	
G1 AMP	1.93	2.46	2.45
G2 AMP	1.87	2.18	2.15
G3 AMP	1.85	1.99	1.98
G2 P	1.71	1.97	2.08
G2 TMDP	2.42	2.76	2.69

* C, H, and N values for TGA are based on the assumption that the products are completely pure.

Table 4-2 TGA data: (a) Dendrimers size effects; (b) Amine loading effects

(A)

Sample	Weight Loss [132]	Organic [mmol/g SBA-15]	Step Yield
Bare SBA-15			-----
0.5 mmol Amine	5%	0.97	-----
G2 P	19%	0.24	71%
G3 P	27%	0.21	91%
G1 AMP	11%	0.34	31%
G2 AMP	20%	0.25	75%
G3 AMP	31%	0.21	83%
G2 TMDP	20%	0.24	70%
G3 TMDP	29%	0.27	115%

(B)

Sample	Organic [wt%]	Organic [mmol/g SBA-15]
0.1 mmol Amine	3%	0.54
G3 AMP (0.1 mmol)	17%	0.10
1.0 mmol Amine	8%	1.41
G3 AMP (1.0 mmol)	38%	0.28
2.0 mmol Amine	8%	1.48
G3 AMP (2.0 mmol)	39%	0.29

* The step yield is calculated based on the initial amount of the previous dendrimer (i.e. in going from G1 → G2, it is based on the G1 content as determined by TGA)

** These numbers do not reflect that the bare SBA-15 has an average weight loss of 3.9 wt% in the same temperature range. The numbers have not been "subtracted" or "corrected" for this.

Table 4-3 TGA data of amine SBA-15 with and without micropores

Sample	Organic [wt%]	Organic [mmol/g SBA-15]	Step Yield
0.5 mmol Amine	5%	0.97	-----
G1 AMP	11%	0.34	31%
0.5 mmol Amine (No Micropores)	2%	0.43	-----
G1 AMP (No Micropores)	7%	0.20	45%

Second, nitrogen adsorption (see below) of the parent material indicates a micropore volume of approximately 0.06 cm^3/g, whereas the amine-functionalized SBA-15 has no micropores that can be detected by α_s-analysis. Third a sample of SBA-15 was calcined at 900ºC to collapse the micropores and the G1 AMP-based composite was synthesized as described above. TGA performed on this sample showed a yield of 45% of the G1 material, higher than the 35% yield for the sample with micropores (Table 4-3). That this value is still much lower than the other generations is likely due to a result of the post-synthetic grafting method leading to inhomogeneity of the amine sites, rendering a fraction of them either inaccessible or unreactive. Elemental analysis (Table 4-1) is in good agreement with the TGA results.

TGA results for dendrimers made with the other two linkers show also clear trends. The increase in organic content per generation is approximately 8*wt*% for P, 10*wt*% for AMP, and 9*wt*% for TMDP (Table 4-2). The result for piperazine is consistent with its lower molecular weight as compared to AMP. TMDP, however, does not behave as expected, as the organic content for a given dendrimer generation should be larger for this linker than with AMP or P. This result indicates the TMDP is not as effective of a linker as AMP under the conditions used. This is likely due to side reactions (e.g. reactions between chloro groups on adjacent dendrimers) being more prevalent for the TMDP linkers. TGA results for samples with different initial amine-loadings (Table 4-2) show that the amine loading can be increased or decreased without greatly influencing the overall yield of the G3 dendrimer growth: 24% for 0.1 mmol/g and 20% for 2.0 mmol/g. However, it is worth noting that the amount of amine

deposited in the 1.0 mmol/g sample is the same as that for the 2.0mmol/g sample, indicating an upper bound for effective amine deposition. All of these materials were made in duplicate and the TGA data are reproducible. Finally, it should be noted that the synthesis described above has not been optimized to maximize the dendrimer yield on the silica substrate. The results show that this chemistry, which has been shown to proceed efficiently in solution [76], can be extended to a solid support.

To further study the identity of the organic groups formed on the OMS surface, MALDI-MS was performed on the organic groups removed from the OMS. Fig. 4-9 shows the MALDI-MS results for the samples G2-AMP, G2-P, and G2-TMDP. The exact masses for the G2-AMP, G2-P, and G2-TMDP dendrons are 1024, 990, and 1238, respectively. Significant peaks representing each of these masses (M+H) are present in the mass spectra. These results are consistent with the NMR, TGA, and elemental analysis that indicate that the bulk of the groups on the OMS surface are in fact the desired dendrimer moieties. While the conversion/yield at each stage is not quantitative, the mass spectrometry is the strongest evidence that the desired dendrimer groups are formed on the OMS surface.

4.3.2 Nitrogen Adsorption

Nitrogen adsorption was used to quantify the change in porosity of the OMS substrate. The porosity of the dendrimer-SBA15 composite materials can be systematically controlled by increasing the dendrimer generation, dendrimer loading,

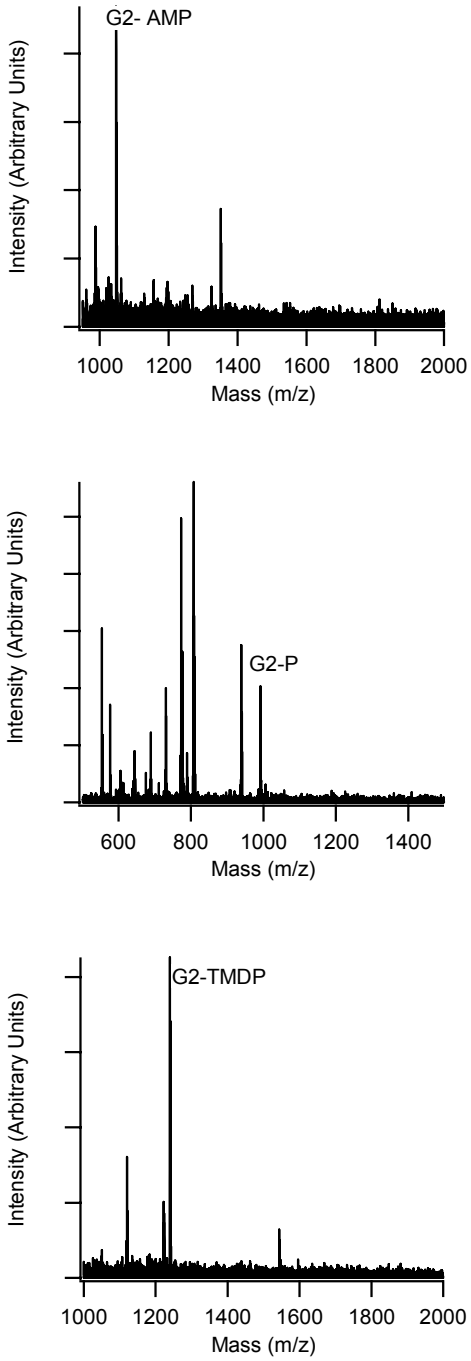

Fig. 4-9 MALDI-MS for the G2-AMP, G2-P, and G2-TMDP hybrids. Label in plot indicates position of the peak for the target dendrimer.

and using three different linker molecules (P, AMP, TMDP). Fig. 4-10 shows the nitrogen adsorption isotherms for the first three generations of the AMP-based dendrimer composite. As shown in Fig. 4-10, the relative pressure at which capillary condensation occurs, shifts systematically to lower relative pressures as the dendrimer generation increases. This is consistent with the BJH analysis which shows a decrease of the effective mesopore diameter from 7.5, to 6.7, to 5.2 nm for G1-AMP, G2-AMP, and G3-AMP, respectively. Given the large organic content of these samples and the lack of a suitable reference material it should be emphasized that the pore sizes derived from the BJH analysis are subject to some error. That said, clear trends are observed consistent with an increase of organic content in the SBA-15 mesopores and the TGA, elemental analysis, and mass spectrometry results. The pore volume also systematically decreases from 0.59, to 0.41, to 0.20 $cm^3 g^{-1}$ as the dendrimer generation increases from G1-AMP, to G2-AMP, to G3-AMP, respectively. These values are comparable to previous work [123]. These results indicate that a considerable fraction of dendrimers is formed in the mesopores and that the porosity can be controlled by changing the dendrimer generation.

The porosity of the composite materials can also be controlled using different linker molecules in the dendrimer synthesis. Fig. 4-2 shows each linker molecule and the second-generation dendrimer. The linker molecules trend in size as P < AMP < TMDP. Fig. 4-11 shows the nitrogen-adsorption isotherms for the different G1-G3 hybrids with the different linkers. A shift of the hysteresis loop to a lower pressure is observed as the size of linker molecule increases.

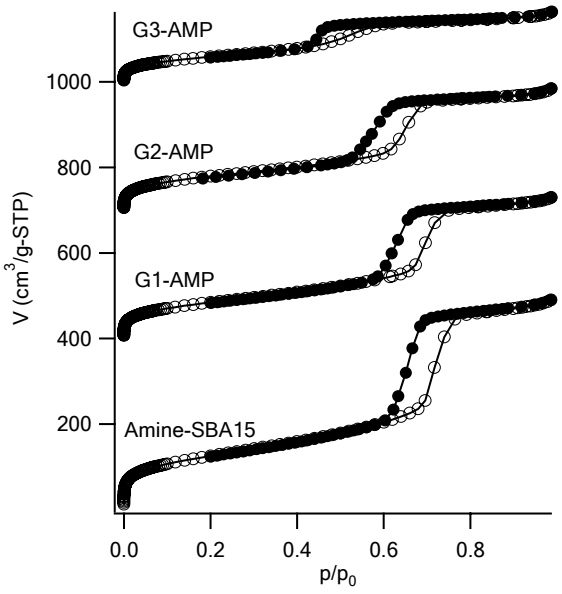

Fig. 4-10. Adsorption isotherms for the dendrimer-SBA-15 composite materials: Effect of the dendrimer generation. Adsorption branches are represented by open circles, desorption branches by solid circles. The isotherms are shifted 400, 700, and 1000 cm3/g-STP for G1-AMP, G2-AMP, and G3-AMP, respectively.

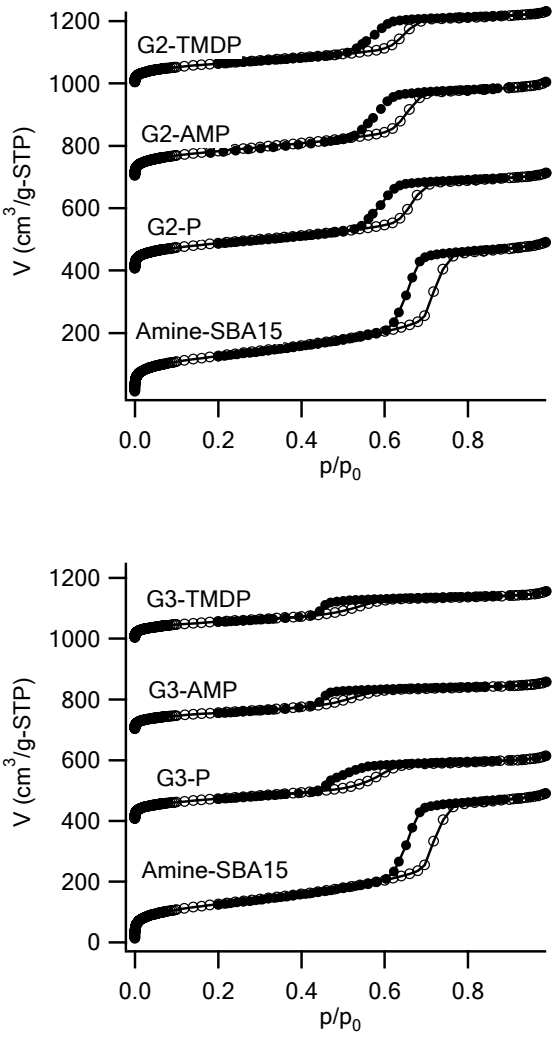

Fig. 4-11. Adsorption isotherms for the dendrimer-SBA-15 composite materials: Effect of the linker molecule. (Top) G2 hybrids, (bottom) G3 hybrids. Adsorption branches are represented by open circles, desorption branches by solid circles. The isotherms are shifted 400, 700, and 1000 cm3/g-STP for P, AMP, and TMDP in 2nd and 3rd generation, respectively.

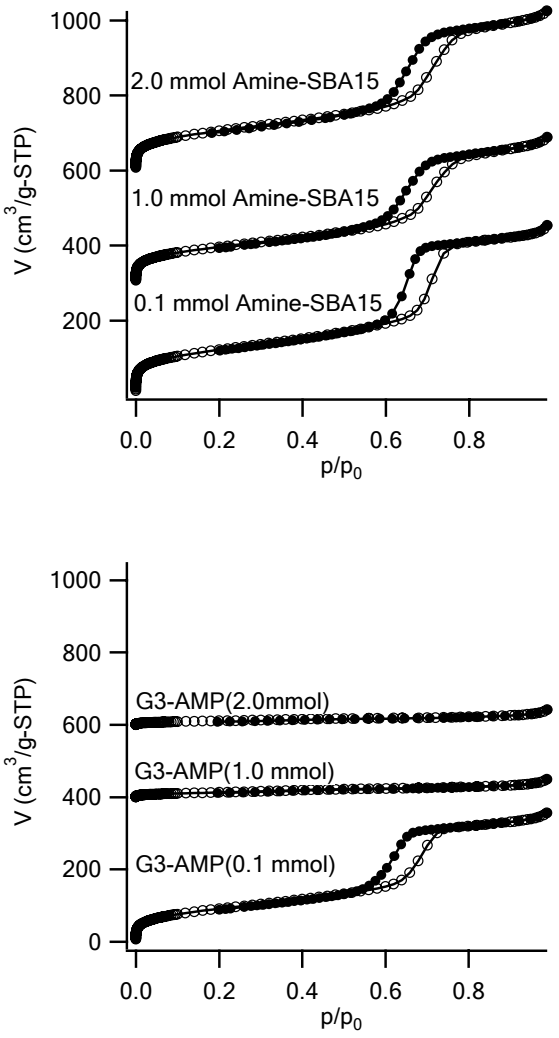

Fig. 4-12. Adsorption isotherms for the dendrimer-SBA-15 composite materials: Effect of the initial amine loading. Adsorption branches are represented by unfilled circles, desorption branches by solid circles. The isotherms are shifted 300 and 600 cm^3/g-STP for 1.0 mmol/g NH_2-SBA15 and 2.0 mmol/g NH_2-SBA15, respectively. The isotherms are shifted 400 and 600 cm^3/g-STP for G3-AMP (1.0 mmol/g) and G3-AMP (2.0 mmol/g), respectively.

Table 4-4 Adsorption data summary for the dendrimer-SBA-15 hybrids

Sample	S(BET) [m^2/g]	S(α_s) [m^2/g]	V_{meso} [cm^3/g]	D_p(BJH) [nm]
0.5 mmol Amine	438	435	0.70	7.9
G2 P	302	307	0.43	7.0
G3 P	254	256	0.27	5.9
G1 AMP	429	414	0.59	7.5
G2 AMP	286	297	0.41	6.7
G3 AMP	193	205	0.20	5.2
G2 TMDP	220	228	0.31	6.7
G3 TMDP	194	200	0.19	5.2

Sample	S(BET) [m^2/g]	S(α_s) [m^2/g]	V_{meso} [cm^3/g]	D_p(BJH) [nm]
0.1 mmol Amine	430	416	0.57	8.3
1.0 mmol Amine	335	335	0.50	7.9
2.0 mmol Amine	367	368	0.55	7.9
G3 AMP (0.1 mmol)	315	322	0.46	7.5
G3 AMP (1.0 mmol)	43	53	~0	N/A
G3 AMP (2.0 mmol)	36	42	~0	N/A

Table 4-4 summarizes the adsorption results for the different samples investigated. The effective mesopore diameter, surface area, and the volume adsorbed decrease as the dendrimer size increases by changing the linker molecule from P to AMP. But both AMP and TMDP show similar values in the pore size, surface area, and the volume adsorbed in each generation. These similar values reflect the lower yields in the TMDP dendrimers as compared to AMP system, consistent with the TGA data as stated previously. The results show that using dendrimers with different linker molecules is a route to controlling the hybrid porosity.

The initial amine loading was varied from 0.1 mmol to 2.0 mmol per gram of SBA-15 to increase the organic content of the composites. Fig. 4-12 shows the nitrogen-adsorption isotherms for the various initial amine loadings and its third generation AMP dendrimer. The isotherms indicate that the mesopores of SBA15 are completely filled by the dendrimer for the samples with high initial amine loading. The G3-AMP with higher initial amine loadings (1.0 and 2.0 mmol) show a dramatic decrease in both the surface area and the volume adsorbed values compared to the samples with lower initial amine loadings (0.1 and 0.5 mmol). The samples prepared with high initial amine loadings (1.0 and 2.0 mmol) containing the G3-dendrimers are essentially non-porous, in contrast to the samples with lower initial amine loadings (0.45 and 0.20 cm^3/g for 0.1 and 0.5 mmol respectively). Also noteworthy is that the 1 and 2 mmol/g amine-loaded samples appear very similar, consistent with the TGA data indicating they have the same amine content. This is also consistent with the TGA data that shows a substantial difference in organic content between the third generation composites grown on SBA-15

with high initial amine loadings, 38 wt%, compared with SBA-15 with the lowest amine loading, 17 wt%. This result shows that the effective porosity can be modulated for a given dendrimer chemistry and oxide substrate by adjusting the dendrimer loading.

The results above demonstrate that OMS/dendrimer hybrids can be formed by the stepwise synthesis of melamine-based dendrimers grown directly off the mesopore surface. The adsorption results indicate that the porosity of hybrids can be engineered by adjusting dendrimer generation, linker molecule, and the organic loading in a controllable way. The trends observed in the nitrogen adsorption data support this as the effective pore diameters, volumes, and surface areas decrease with increasing dendrimer generation for a fixed linker, increasing the linker size for a fixed dendrimer generation, or increasing the amine loading on the surface. The one exception to this is that AMP and TMDP show similar pore volumes and diameters even though TMDP is larger. This is consistent with TGA and elemental analysis results that show the TMDP is not as reactive/effective of a linker as AMP. Also, the high initial amine loading leads to a dramatic decrease in surface area and pore volume, which correlates with the increase of organic content determined by TGA.

4.3.3 Copper(II) Sequestration

Copper(II) sequestration was used to demonstrate the accessibility of the peripheral primary amines and the increased separation potential of higher generation dendrimer composites. Evidence for recognition of Cu(II) by melamine-based dendrimers in solution has already been reported by Zhang and coworkers [77]. Here it

is demonstrated this binding is still efficient when the dendrimers are tethered to a solid support. A 4-fold excess of cupric sulfate and a significant period of exposure (14 hours) were used in order to determine the maximum sequestering potential of the dendrimer composites. The results of this experiment are shown in Fig. 4-13. Comparing Fig. 4-13 with Fig. 4-8, which shows the organic content for these same samples, demonstrates the positive correlation between dendrimer size and the maximum amount of copper that can be sequestered. As expected, SBA-15 proved to be a very poor copper scavenger taking up a negligible amount of copper, 0.01mmol/g.

This result indicates that the copper uptake observed in the hybrids is not an artifact of copper binding to silanol groups. The amine-SBA-15 and dendrimer composites were able to sequester significant amounts of copper: 0.13 mmol/g, 0.35 mmol/g, 0.57 mmol/g, and 0.60 mmol/g for Amine-SBA-15 and the G1, G2, and G3 AMP-based composites, respectively. Ongoing work is exploring the coordination/complexation of the copper to the dendrimer. One possible explanation for the plateau in copper uptake in going from the G2 to the G3 dendrimer is that for the G3 system the copper can only complex on the outer surface (i.e. to peripheral amines). If that were the case, based on TGA data, it can be estimated there are approximately 0.58 mmol/g solid of periphery amines on the G3 dendrimer, in reasonable agreement with the uptake data. Ottaviani and coworkers studied copper binding in PAMAM dendrimers and concluded that it is possible for copper to bind amines in the dendrimer interio [174, 175]. The data for the G1 and G2 samples would seem consistent with their work.

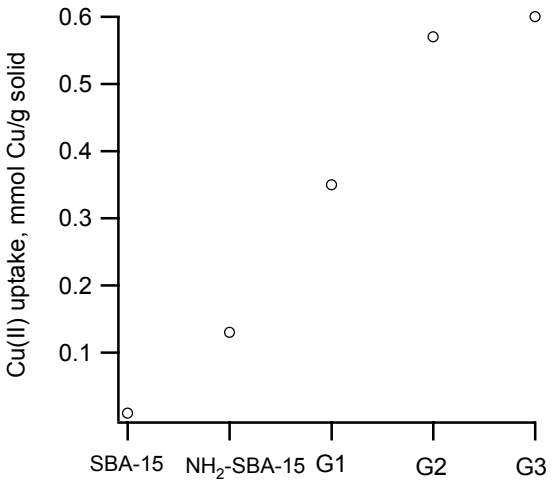

Fig. 4-13 Copper(II) sequestration results for SBA-15, 0.5 mmol/g NH_2-SBA-15, G1-AMP composite, G2-AMP composite, and G3-AMP composite.

4.4 Conclusions

Dendrimer-SBA-15 hybrids are synthesized and characterized using several analytical techniques. The hybrid porosity can be systematically altered by varying the dendrimer generation, the linker molecule, and the surface amine loading. Given the accessibility demonstrated by Cu(II) sequestration, the materials have accessible functional groups that can be used for catalysis, separations, molecular recognition, or as scaffolds to build more complex structures. Ongoing work is optimizing the synthesis conditions for higher dendrimer yields, and our results suggest the presence of micropores has a deleterious effect on dendrimer yield.

CHAPTER V

SYNTHESIS AND CHARACTERIZATION OF UNIFORM ALUMINA-ORDERED MESOPOROUS SILICA HYBRID MEMBRANES [*]

Chapter V details the synthesis of supported ordered mesoporous thin film (SOMTF) membrane and its gas permeance performances. The precise control of pore size and structure of inorganic porous support is very important for hybrids to achieve the consistent and high separation performance. Surfactant-templated ordered mesoporous inorganic thin films shows promising characteristics as inorganic porous support of hybrids because of their well ordered pore structure and uniform pore size distribution, which can lead the precise control of membrane performance. While numerous studies have characterized thin films grown on non-porous supports, porous supports are necessary for membrane applications. In this study, we synthesized a defect free supported ordered mesoporus thin film membrane by depositing ordered mesoporous silica thin film into macropores of commercial alumina membrane.

The synthesis and characterization of alumina-ordered mesoporous silica (alumina-OMS) hybrid membranes are reported. The hybrids are formed using a variation of the evaporative induced self-assembly (EISA) process reported by Hayward

---

[*] Reprinted with permission from "Synthesis and Characterization of Uniform Alumina-Mesoporous Silica Hybrid Membranes" by S. Yoo, D. M. Ford, D. F. Shantz, Langmuir 22 (2006) 1839-1845. © 2006 by American Chemical Society

and coworkers [106] based on dip-coating of an Anopore^{TM} 200 nm membrane with a Brij-56/TEOS/HCl/H_2O/EtOH solution. Numerous analytical methods are used to probe both the hybrid material and the silica phase after dissolution of the Anopore^{TM} substrate. Most importantly, He/N_2 permeation measurements show that the effective pore size of the membrane can be tuned from 20 to 5 nm based on the number of dip-coating cycles used. The observed He/N_2 permselectivity of 2.7 ± 0.11 is nearly identical to the theoretical value obtained (2.65) assuming Knudsen diffusion dominates. The selectivity of these membranes is higher than that of most commercial "5 nm" membranes (2.29), which is ascribed to the lack of pinhole defects in the materials reported here. The hybrid membranes as well as the silica obtained after dissolution of the Anopore^{TM} substrate have been characterized using scanning and transmission electron microscopy and X-ray diffraction. Those results indicate that the silica deposited in the Anopore^{TM} membrane possesses uniform pores approximately 5 nm in size, consistent with the permeation studies. The current work presents an alternative approach to materials that possess many of the properties of mesoporous silica thin films (i.e. pores of controlled size and topology) without the difficulty of growing mesoporous silica thin films on porous supports.

5.1 Introduction

Ordered mesoporous silica (OMS) has attracted considerable attention over the last ten years. Since the initial report of MCM-41 by Kresge and coworkers in 1992 [81, 82], the synthesis, characterization, and application of these materials has been intensely

explored by numerous industrial and academic labs [86, 88, 95, 147, 148, 176, 177]. These materials possess several properties of interest: (1) an ordered pore structure, (2) pores of controllable size between 2.5 – 10 nm, (3) a narrow pore size distribution, (4) different pore connectivities, and (5) all of the well-known silane chemistry developed for functionalizing silica surfaces can be implemented on OMS substrates. From a fundamental viewpoint, these points facilitate characterizing the mesostructure by microscopy, powder X-ray diffraction (PXRD), and porosimetry. From an applied viewpoint, materials with uniform pores in the 5-20 nm size range hold great promise in catalysis, separations, and once appropriately functionalized, other areas including sensors, drug delivery, etc.

While most investigations of OMS have focused on powder materials, the possibility to make thin films is particularly attractive. Such films could be used as templates for growing nanowires arrays, sensors once suitably functionalized, etc [106, 142, 143, 178-185]. Films grown on porous substrates could be used as membranes. Due to contributions from numerous labs over the last five years some general design principles for reproducibly forming high-quality films using either surfactants or polyalkylene oxide copolymers as templates are starting to emerge [16, 108, 178, 181, 183, 184]. However, all of these investigations have studied film formation on non-porous substrates. There is much less work on the synthesis of OMS membranes on porous supports [17, 18, 122]. This inspired the current investigation.

Alumina membranes formed by electrochemical etching (e.g. Anopore^{TM}, Whatman) possess many properties of interest: uniform pore sizes, a high number

density of pores, low non-specific protein adsorption, etc. As such, these materials are of great interest for use in various separations processes, and the parent membranes have been extensively studied. Anopore^{TM} membranes, irrespective of nominal pore size, have an asymmetric structure, which comprises a relatively thin (0.5 to 1.0 μm) layer on top of a thicker (59 to 59.5 μm) support. The asymmetry appears to be a natural consequence of the way the materials are made by anodic oxidation [129]. A thin active layer generally has a smaller average pore size, compared with the thicker support layer. For example, Anopore^{TM} membranes of 200 nm nominal pore size have an active thin layer of 104 nm pore size and 35.9 % porosity and a thicker support of 240 nm pore size and 43% porosity [126]. More recently, numerous investigations have reported the use of alumina membranes as containers or templates for the fabrication of interesting hybrids [115-121, 186-193]. Martin's lab in particular has been extremely active in this area, and the past few years have witnessed a dramatic increase in the number of papers in this area. Systems have ranged from the growth of inorganic nanowires [115-118, 120, 121, 187, 188, 193] (e.g. thermoelectrics, silica, etc.) to layer-by-layer assembly of organic-inorganic hybrids, to biomacromolecular nanotube-alumina hybrids [191, 192]. Given their commercial availability, the apparent homogeneity of the alumina substrate, and the relative ease of depositing other compounds in the membrane pores, this will continue to be an area of significant growth.

Consistent with this theme, several recent reports have described the synthesis of OMS phases in alumina membranes [115-118, 120, 121, 193]. In most of these reports the alumina matrix was etched away to facilitate further characterization of the silica.

As such in these investigations the "bulk" structure of the hybrid material is not clear. Recent work by Ku and coworkers [193] report permeation data of the hybrid that showed a clear decrease in the permeance of nitrogen after dip-coating; however, permeation studies of multiple gases were not reported. These experiments would provide insights about the microstructure of the silica phase, as permeation studies probe the "bulk solid", i.e., all pores (or silica) contribute to the observed results.

In the current work we report the synthesis and characterization of a series of Anopore^{TM} – OMS hybrids. This work shows that the effective pore size of the membrane after silica deposition can be tuned based on processing conditions. This is the first investigation we are aware of that reports He/N_2 and C_3H_8/N_2 comparative permeation measurements, allowing us to determine the effective pore size of the membrane after silica deposition, and clearly shows the absence of pinhole defects.

5.2 Experimental Section

5.2.1 Synthesis of Alumina-Ordered Mesoporous Silica Hybrid membrane

Anodic alumina membranes of nominal pore size 200 nm were purchased from Whatman and used as received. Brij-56 (Aldrich) and TEOS (Aldrich, 98%) were used as received, and HCl (Aldrich, 37 wt%) was diluted to 0.032 N stock solutions for subsequent use. The solution used for dip coating was prepared based on previous work by Hayward and coworkers [106]. Details about synthesis of alumina-ordered mesoporous silica hybrids were described in Chater III.

Three other commercial alumina membranes were used (without further treatment) to benchmark the permeation results of our hybrid membranes. These were Whatman Anopore™ disks with 20 nm nominal pore size and two Pall Membralox® products with 5 nm and 10 nm nominal pore sizes, respectively. Both Membralox® membranes had an asymmetric structure with a 3-4 μm thick mesoporous γ-alumina layer slip-cast on a macroporous tubular α-alumina support; the tubes were originally 20 or 25 cm in length and cut into 1 inch pieces for testing. The 5 nm membranes have been the subject of detailed characterization [130] with the conclusion that there is a distribution of pore sizes between 2 and 5.5 nm, with a maximum near 4 nm. Later work in our laboratory [11] showed the larger-pore Membralox® product to have an average pore size of about 12 nm; herein we will use the nominal value of 10 nm to denote this product.

5.2.2 Analytical

Permeation measurements on the individual gases were performed using an in-house unit. Pure helium (99.996%), nitrogen (99.998%), and propane (99.5%) gases were used as received from Praxair Distribution, Inc. Fig. 5-1 shows our set up for the single-gas experiments. The membrane was held in a steel disc module, which has two openings for feed and permeate side. Screw caps, steel meshed supports, and rubber O-rings were used for proper sealing. The pure gas was supplied to the feed inlet and flowed across the membrane and through the permeate outlet, which is connected to a

bubble flow meter vented to a fume hood (at ambient pressure). The pressure on the feed side was controlled with a pressure regulator. The pressure difference was monitored with a digital pressure transducer from Omega. The volumetric flow rate was measured at several pressure differences ranging from 5 to 30 psi. For the data presented here the ambient temperature ranged from 20 to 22 ºC. The gas flux was calculated by dividing the molar flow rate by the membrane flow area, which we determined to be 0.000346 m^2 for our Anopore^{TM} membrane pieces. For each value of the pressure difference, the permeance was obtained by dividing the gas flux by the pressure difference. In a composite membrane, helium and nitrogen showed the constant permeance but propane permeance increased as the pressure difference increased. All data presented here were obtained using a pressure difference of 20 psi, and each data point is for measurements performed on three different membranes for a given number of dip-coating cycles.

Powder X-ray diffraction (PXRD), Field-Emission Scanning Electron Microscopy (FE-SEM), Transmission Electron Microscopy (TEM), and Energy Dispersive X-Ray Analysis (EDX), were performed as described in Chapter III. The samples were dispersed in methanol (100%, Aldrich) and placed on a 400-mesh copper grid. To obtain the cross-section view, the membrane was embedded in an epoxy resin and cut orthogonally to the membrane surface by mechanical polishing, dimpling and argon-ion milling. The silica phase was isolated from the alumina matrix by dissolution of the alumina in a 10 wt% phosphoric acid solution for 24 hrs.

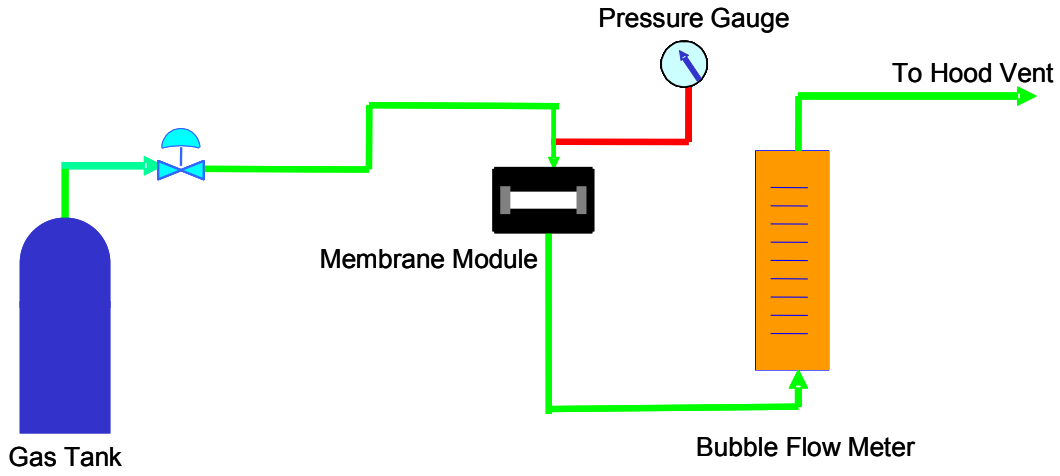

Fig. 5-1. Schematic of the dead-end ideal single gas experiments.

5.3 Results

5.3.1 Membrane Synthesis

Fig. 5-2 is a schematic of the how the hybrid membranes were fabricated. The approach uses an evaporation-induced self-assembly (EISA) process. The conditions used for the dip coating and siloxane cross-linking were taken from the work by Hayward and coworkers [106] as in our hands this was a highly reproducible synthesis methodology for making cubic mesoporous silica films with pores approximately 4-5 nm in size on glass slides. The choice of a cubic mesostructure was motivated by its high degree of pore connectivity. Before describing the results of the permeation and other characterization studies below, a few general points are worth mentioning.

First, it was observed that multiple dip-coating/surfactant extraction cycles were needed to achieve a membrane that had the separation characteristics (i.e. selectivities) of a 5 nm membrane. Second, to make useful membranes it was also essential to perform the surfactant extraction after each dip-coating step. Third, it was also observed that the mechanical properties of the hybrids deteriorated with increasing dip-coating cycles. This was particularly acute in going from the four-time coated to five-coated membrane.

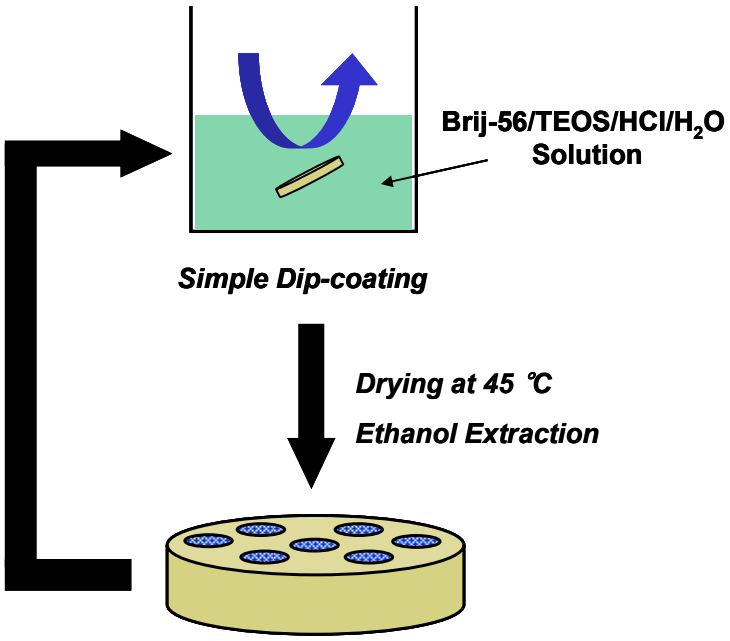

Fig. 5-2. Schematic of the membrane synthesis procedure.

5.3.2 Gas Permeation

Fig. 5-3 shows permselectivity/permeance plots for nitrogen and helium based on the single-gas experiments. Included in both figures are the benchmark data for the bare 200 and 20 nm Anopore™ membranes, as well as bare 10 nm and 5 nm Membralox® membranes (note that these numbers represents pore diameters, not pore radii). Across this pore size range, under the near-ambient conditions used in the tests, a combination of Poiseuille (viscous) and Knudsen flows is expected [26]. For the two limiting cases, a purely Poiseuille flow would result in a selectivity of 0.91 while a purely Knudsen flow would result in a selectivity of 2.65. The results for the bare membranes show that nitrogen permeance decreases and selectivity of helium over nitrogen increases incrementally as the pore size is decreased, consistent with the increasing importance of the Knudsen mechanism.

An exception is the 5 nm Membralox® membrane, which shows a slightly lower selectivity than the 10 nm Membralox® membrane (2.29 versus 2.41). This anomalous result has been observed previously [194-196], including in our lab, and is ascribed to the presence of pinhole defects in the 5 nm membranes. Theoretically, a membrane with 5 nm pores controlling flow should exhibit a He/N_2 selectivity very close to the Knudsen limit, since 99% or more of the molar flow will be due to the Knudsen mechanism. By comparison, only 75% of the nitrogen flow will be Knudsen in a 200 nm membrane. Another way of estimating the relative importance of Knudsen and Poiseuille flows is by comparing the pore size to the characteristic mean free path of the gas.

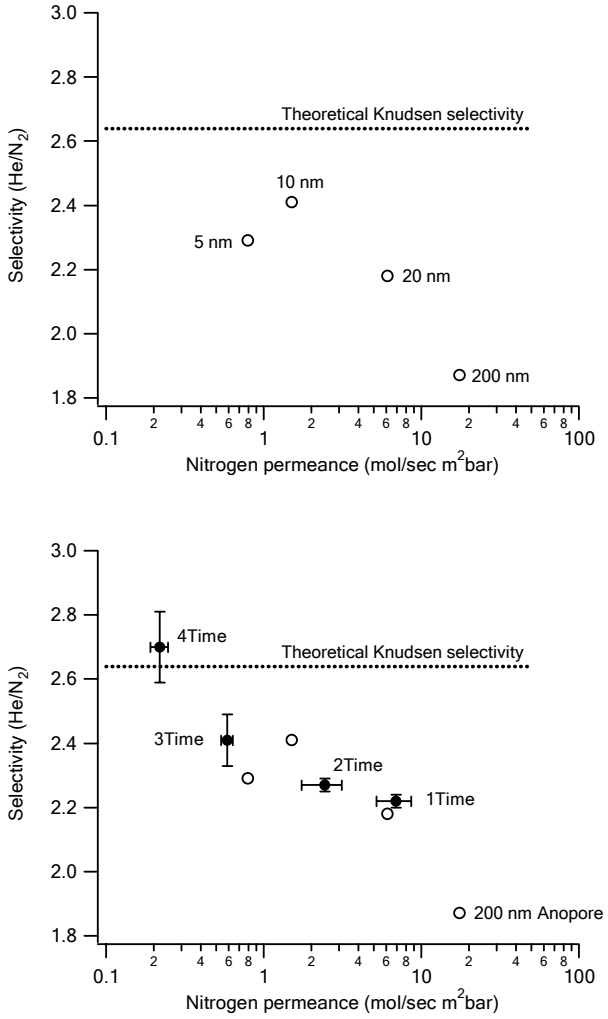

Fig. 5-3. Helium/nitrogen selectivity as a function of nitrogen permeance. (Top) the open symbols represent the commercial alumina membranes from 200 nm to 5 nm pore size, and (Bottom) the solid symbols represent Anopore^{TM}-MS composite membrane after the indicated number of dip-coating cycles.

At 20 psig and 20 ºC, the mean free paths of helium, nitrogen, and propane are 57, 28, and 16 nm, respectively. The mean free paths of helium, nitrogen, and propane are approximately 11, 5.5, and 3-times larger than the pore diameter for the case of the 5 nm pore size. These results would seem to indicate that, for helium and nitrogen at least, a Knudsen mechanism should dominate for 5 nm pores. As mentioned below, the situation for propane is more complicated. Further, the viscous flow contribution will become increasingly significant for larger pore sizes (i.e., > 10 nm).

However, in our coated membranes, as can be seen in Fig. 5-3 the nitrogen permeance decreases with a monotonic increase of He/N_2 selectivity as the multiple dip-coatings cycles are performed on the 200 nm Anopore™ membrane. The one-time coated membrane has similar properties to the 20 nm bare Anopore™ membrane. The two-time coated membrane has a lower permeance but essentially the same permselectivity as the one-time coated membrane (2.22 ± 0.02, 2.27 ± 0.03 for the one-time and two-time coated membranes, respectively). We hypothesize this is due to coating of the Anopore™ substrate with silica, but incomplete filling of the pores after one and two dip-coating cycles. By contrast, there is a substantial increase in the permselectivities of the three-time and four-time dip coated membranes, with the three-time coated membrane possessing comparable selectivities to the 10 nm Membralox® membrane (2.41 ± 0.08). The four-time dip-coated membrane has a permselectivity of 2.70 ± 0.11, which within the errors of the measurement, is identical to the theoretical selectivity of 2.65 assuming only Knudsen-type diffusion. Membranes were also made using five dip-coating cycles but had very poor mechanical properties. The permeation

data are consistent with high-quality membranes that possess very few pinhole defects and have an effective pore diameter in the small mesopore range.

We have extracted an effective diffusion coefficient [197] from the nitrogen permeance data for our four-time coated membrane. We used a membrane thickness of 60 μm (the entire thickness of the 200 nm Anopore™ membrane) to convert from permeance to permeability and an ideal gas relationship to convert from pressure to concentration (Fick's Law) driving force. The result was $D = 2.9 \times 10^{-7}$ m^2/s. A purely theoretical calculation of effective Knudsen diffusivity of nitrogen through a material with a porosity of 20%, a tortuosity of 1.0, and a mean pore diameter of 5 nm yields $D_K^{eff} = 1.6 \times 10^{-7}$ m^2/s. (note that an overall porosity of 20% is a reasonable estimate for our material, since the porosity of the 200 nm Anopore™ membranes is about 40% and the intrinsic porosity of the deposited mesoporous silica is likely near 50%.) The good agreement (within a factor of two) between the experimental and theoretical results suggests that we are probably filling most of the void space of the Anopore™ membranes with mesoporous silica.

Fig. 5-4 shows the permeance results for propane and nitrogen pure gases. Under the conditions studied, propane is expected to have significant contributions from surface flow and possibly capillary condensation mechanisms in parallel with Knudsen and Poiseuille, so interpretation of the results is not straightforward. The nitrogen permeance values are the same as those shown in Fig. 5-3.

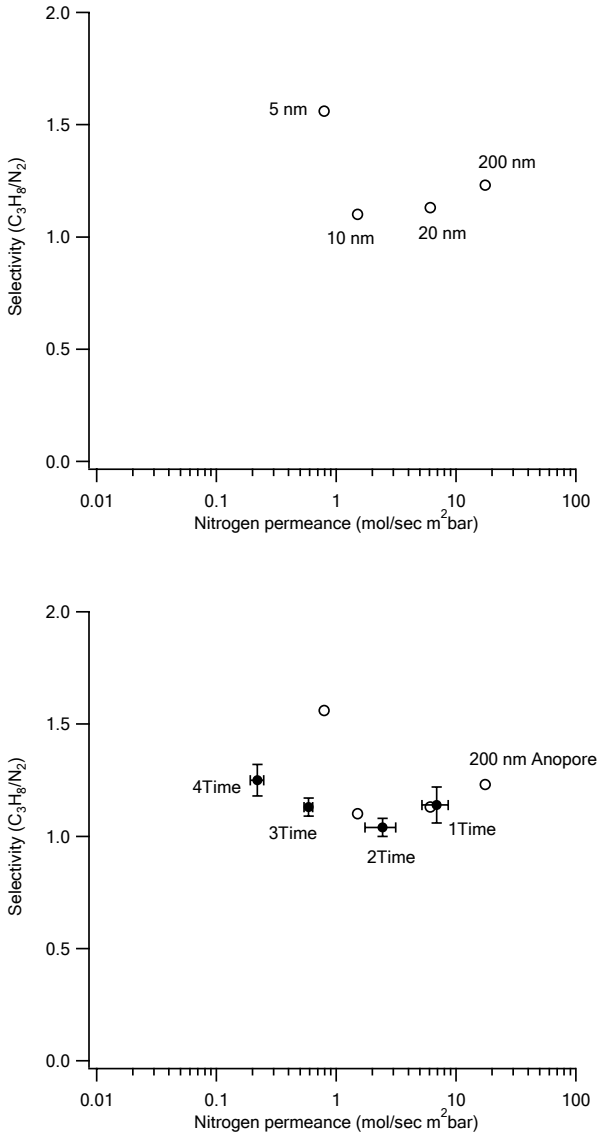

Fig. 5-4. Propane/nitrogen selectivity as a function of nitrogen permeance. (Top) the open symbols represent the commercial alumina membranes from 200 nm to 5 nm pore size, and (Bottom) the solid symbols represent Anopore^{TM}-MS composite membrane after the indicated number of dip-coating cycles.

Again the hybrid and benchmark selectivity results tracked each other closely with changing pore size, except for the 5 nm Membralox® membrane. In this case, the 5 nm membrane showed a significantly higher selectivity for propane than the other membranes. This is certainly a signature of greater surface and capillary flow contributions in these membranes, which tend to increase as the mesopore size decreases (recall that these membranes have a large fraction of pores below 4 nm). As compared to the 5 nm Membralox® membrane, we therefore conclude that our four-time coated membrane has a larger average pore size, or a tighter pore size distribution with fewer very small mesopores, or perhaps both.

5.3.3 Analytical Characterization

To further probe the microstructure of the membrane, several methods were employed. Fig. 5-5 shows a top-view FE-SEM image of a four-time coated membrane. The image clearly shows silica in the pores of the Anopore™ membrane. The FE-SEM image would seem to indicate that some of the pores appear empty. This is likely due to some pores not being filled with silica near the top of the membrane. Even the presence of a small amount of empty 200 nm pores would lead to clear differences in the permeation data as compared to what is shown in Fig. 5-3 and 5-4. TEM images were also obtained of the hybrid membrane (Fig. 5-6) and also indicate that the bulk of the pores (within the counting statistics of TEM) contain silica. EDX analysis indicates the Al/Si ratio is approximately 4.8. The elemental maps are also shown in Fig. 5-7, and

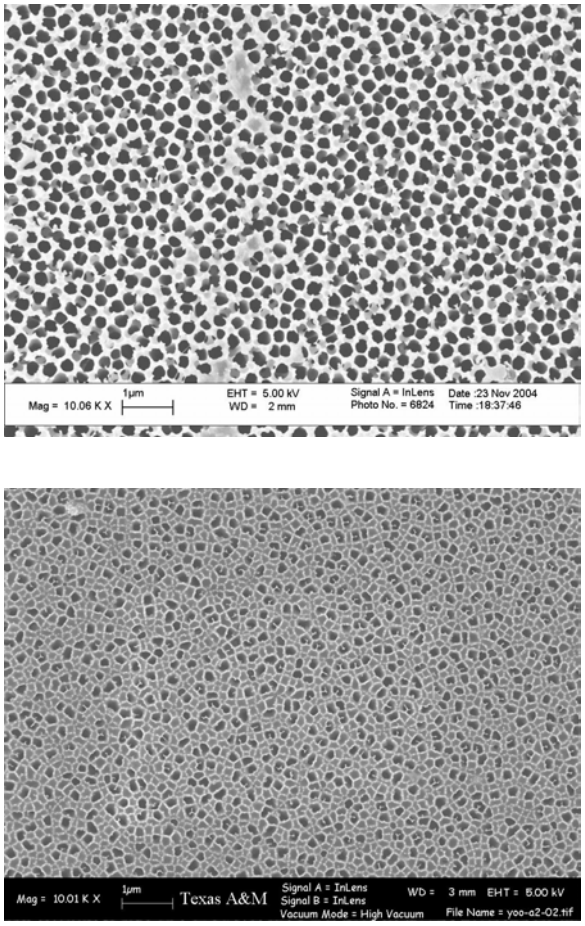

Fig. 5-5. FE-SEM images of Aopore^{TM}-MS composite membranes. (Top) Untreated membrane and (Bottom) four-time coated composite membrane.

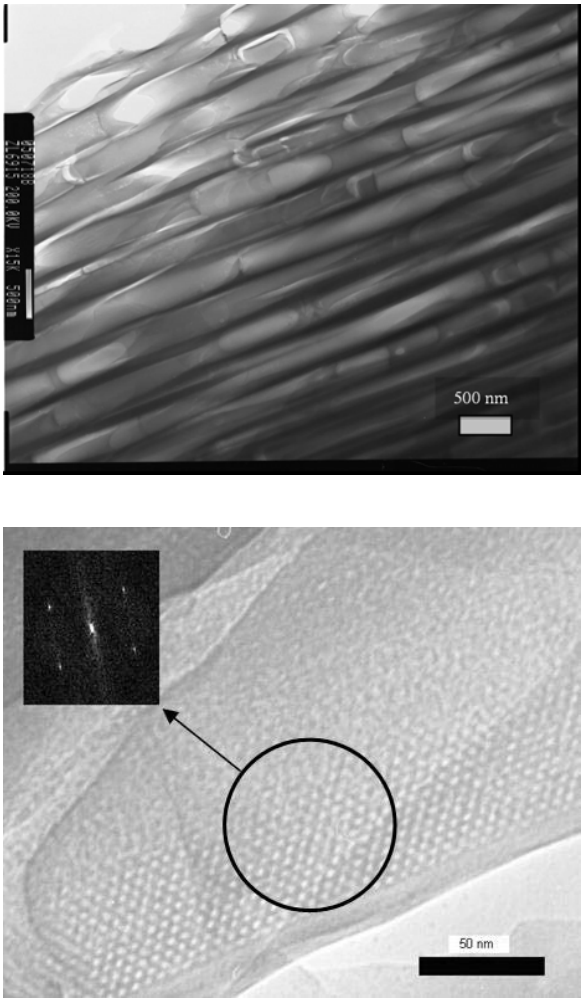

Fig. 5-6. TEM image of the Anopore^{TM}-MS composite membrane. (Bottom) High-magnification image showing the silica phase and (inset) FFT of the image area circled.

Spectrum processing :
Peaks possibly omitted : 0.514, 8.031 keV

Quantitation method : Cliff Lorimer thin ratio section.
Processing option : All elements analyzed
Number of iterations = 1

Standardless

Element	Weight%	Atomic%
Al K	82.15	82.73
Si K	17.85	17.27
Totals	100.00	

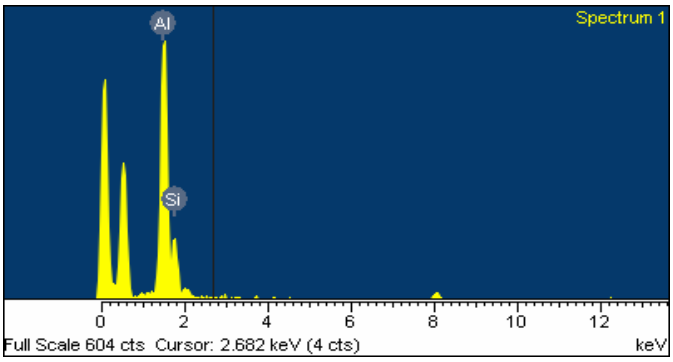

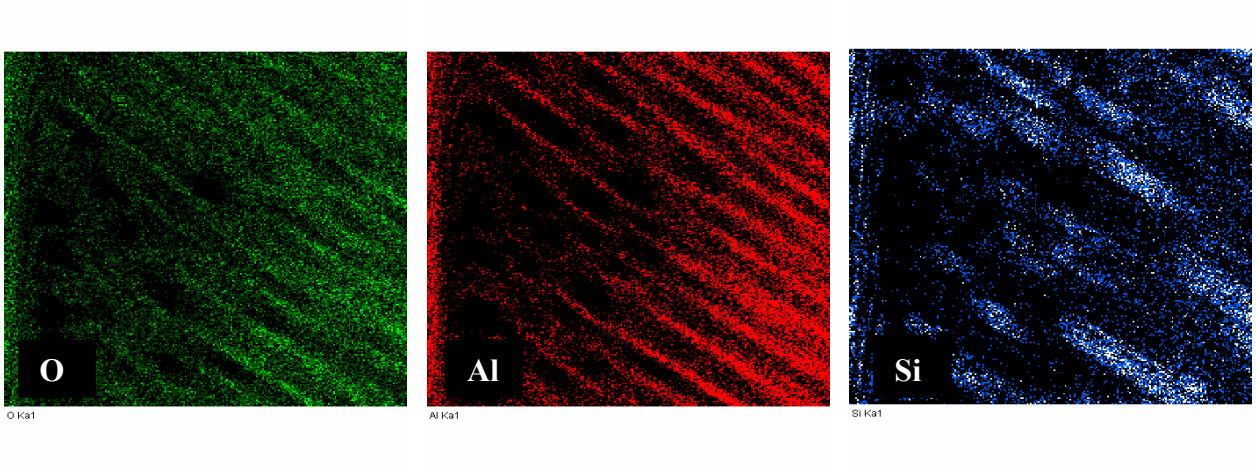

Fig. 5-7. Element mapping from TEM images of cross-section view of Anopore^{TM}-MS composite membrane.

are consistent with the TEM results showing the pores of the Anopore^{TM} membrane contain silica.

Fig. 5-6 shows a high-resolution TEM image of the composite membrane. The pores of the silica can be clearly observed in the image and are approximately 5 nm in diameter. Attempts to perform electron diffraction to unambiguously determine the pore topology were unsuccessful due to the poor stability of the silica in the electron beam. A Fast Fourier Transform (FFT) of the image shown in Fig. 5-6 indicates the presence of four-fold symmetry.

A more exhaustive analysis of several domains within the sample as well as of different samples indicates domains of six-fold symmetry as well, suggesting the likely presence of both cubic and hexagonal silica (see below). The TEM images are consistent with the permeation data in that many of the pores appear to contain silica, the pores of which are in the 5 nm size range. The EDX analysis in Figure 5-7 is of the images/sample shown in Figure 5-6.

PXRD analysis was also performed directly on the composite membrane (Fig. 5-8). PXRD of the composite membrane before extraction shows two peaks, consistent with a mixture of cubic and lamellar phases. The peak positions are consistent with a bicontinuous cubic $Ia\bar{3}d$ phase structure [81, 82]. A unit cell parameter of 13.1 nm is estimated from the position of the (211) reflection consistent with the original report [106].

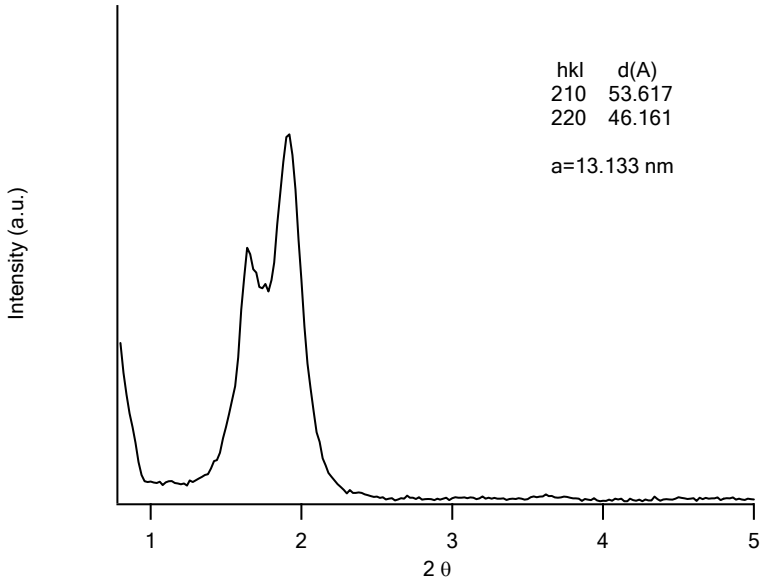

Fig. 5-8. Powder X-ray Diffraction (PXRD) patterns of Anopore^{TM}-MS composite membrane before ethanol extraction.

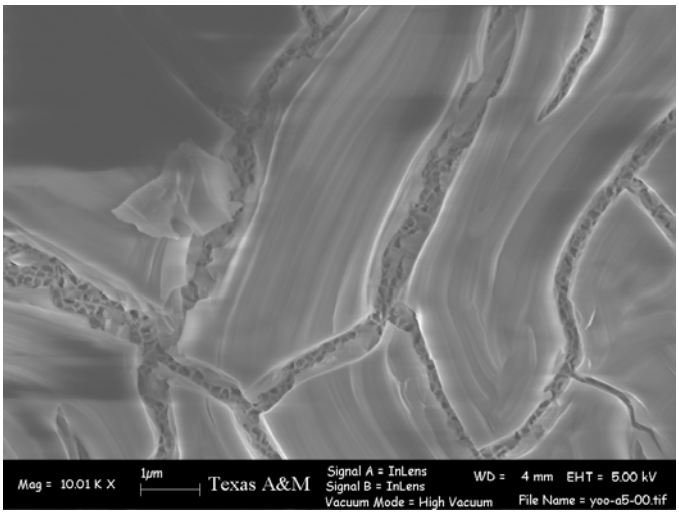

Fig. 5-9. FE-SEM image of Anopore^{TM}-MS membrane before surfactant extraction.

However, the intensities of peaks are different than is observed for the $Ia\bar{3}d$ bicontinuous structure. The intensity of the (220) peak is larger than the (211) peak; one possibility is due to the presence of lamellar phases that could be attributed to the surfactant deposited on top of the membrane [198]. After extraction, however, no peaks are observed in the PXRD pattern. This would seem to indicate that a silica/surfactant over layer on the membrane is the source of the PXRD peaks for the sample before extraction. FE-SEM images of the membranes before extraction (Fig. 5-9) are consistent with the presence of an over layer, likely containing silica, on the top of the Anopore^{TM}. The absence of peaks for the composite after extraction is inconsistent with the TEM data and was further probed by dissolution of the alumina matrix.

The silica fibers obtained after dissolution of the alumina matrix in phosphoric acid were also analyzed by TEM. Fig. 5-10 shows TEM images of silica fibers after the dissolution of the Anopore^{TM} matrix. The fibers are approximately 200 nm in diameter and of variable length. The diameter of the fibers is consistent with the permeation results indicating the 200 nm pores contain mesoporous silica nanowires of comparable size to the original pores of the membrane. Figure 5-11 shows additional TEM images of the fibers at different positions along the fiber and the FFTs of the images. As can be seen the FFTs suggest the presence of both cubic and hexagonal silica given the presence of four-fold and six-fold symmetry. The presence of hexagonal silica is inconsistent with the work by Hayward [106]. This result can be explained in two contexts. First, Wu and coworkers showed that the OMS pore topology can be modulated by using similar (though smaller diameter) alumina membranes as a confined

space for OMS growth [118]. That work also showed that the pore topology varied as the confinement effect was increased, or as the pore diameter decreased, from coiled cylindrical pore topologies to spherical cavities. In the current work the surface curvature, or alumina pore diameter, is a function of the dip-coating cycle, and so one might anticipate the pore topology changing as one scans across the silica wires formed in the alumina pores. The presence of six- and four-fold symmetry domains would thus be consistent with their work. Ongoing work is investigating this in more detail. The second possibility is related to the phase behavior of the mixture. The cubic V_1 phase is only present in a very small portion of the binary Brij-56/water phase diagram [199], and hexagonal liquid crystalline phases are observed at lower surfactant contents. The pores having an effective surfactant concentration below that of the bulk concentration could be invoked as a means to explain the presence of hexagonal phases, though we have no evidence for this. PXRD shows that the over layer on the membrane surface possesses cubic and lamellar domains, and the lamellar domains are observed in the phase diagrams at high surfactant contents. At this point we cannot quantify the relative proportions of the hexagonal and cubic phases, as well as whether the silica is a "core-shell" structure of hexagonal-cubic silica or vice versa. However, the presence of pores 4-5 nm in size are observed in the TEM and this is consistent with the permeation results and the numerical calculations described above. The gas permeation results and TEM appear consistent in that both indicate the presence of 5 nm size pores that are uniform in size.

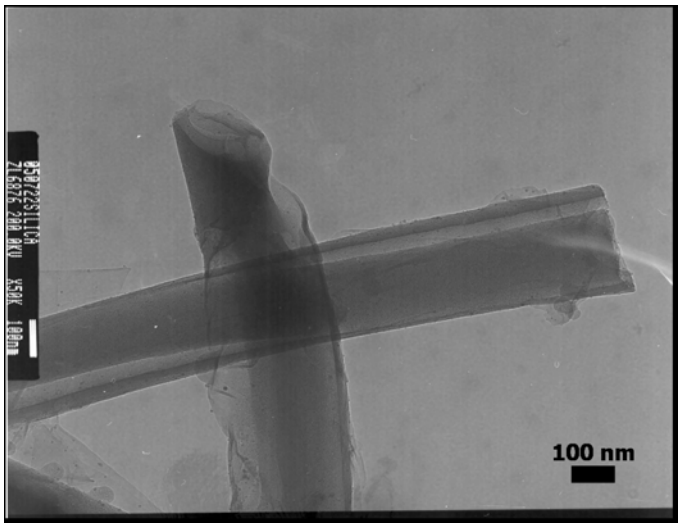

Fig. 5-10. TEM image of silica fibers after dissolution of the Anopore^{TM} membrane.

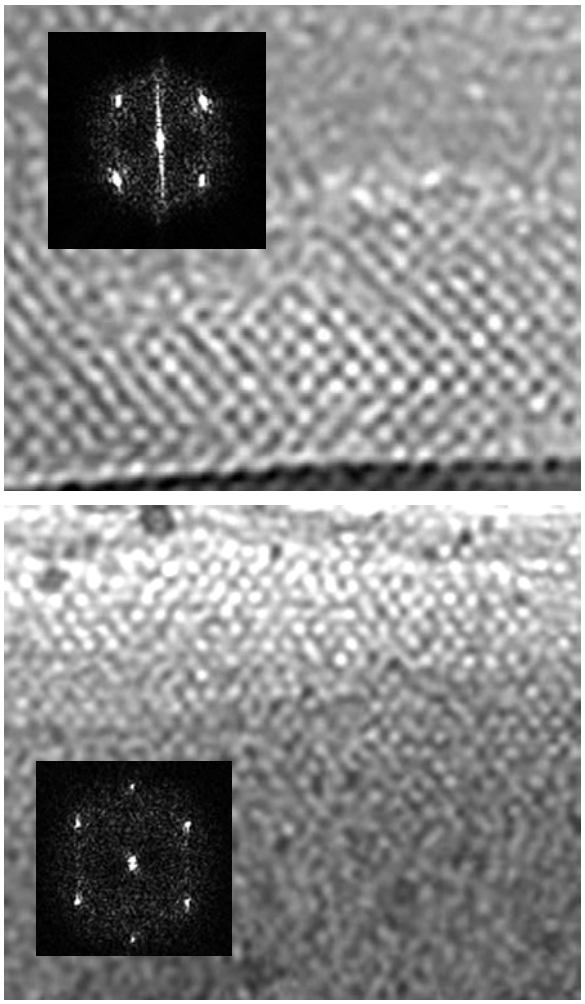

Fig. 5-11. High-magnification TEM images of the silica fibers. The FFTs of the images show domains of four- (top) and six-fold (bottom) symmetry.

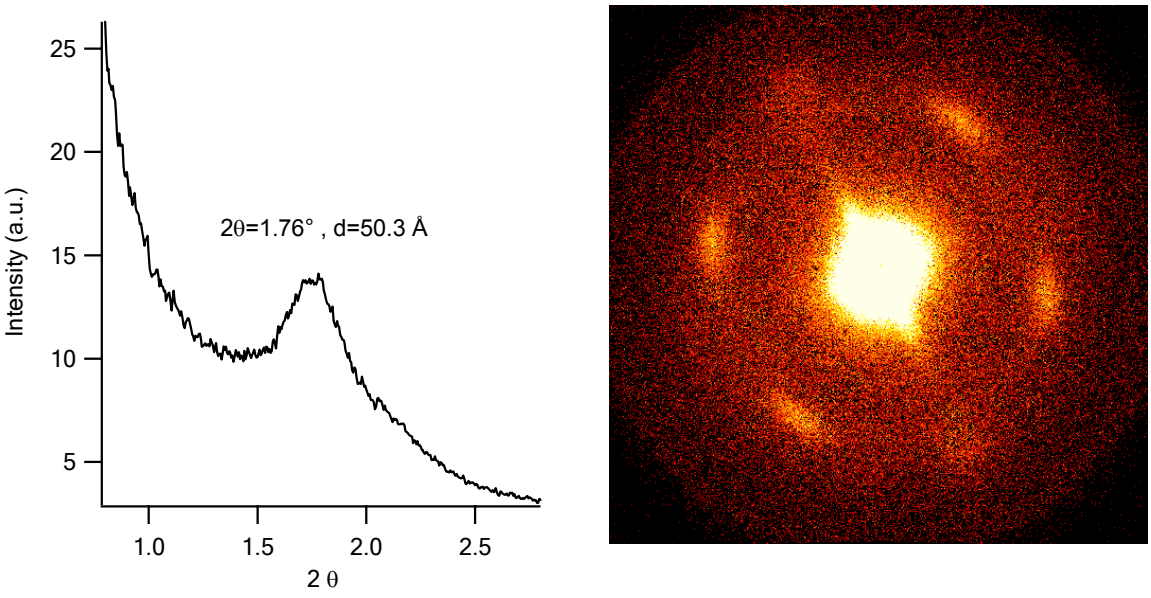

Fig. 5-12. Powder X-ray Diffraction (PXRD) patterns of silica obtained after dissolution of the Anopore^{TM} membrane. (Right) raw data before integration, indicating likely sample orientation effects (spots versus rings).

Powder X-ray diffraction and nitrogen porosimetry were also attempted. The X-ray diffraction data (Fig. 5-12) exhibits one peak at a comparable two-theta value to that observed for the $Ia\bar{3}d$ phase. Further, the raw data from the 2D area detector is also included and is consistent with preferred orientation effects for the powder sample given that spots, not rings are observed on the area detector for the powdered sample.

However, the data is insufficient to draw conclusions about the mesostructure of the silica. Given the low quantity of silica recovered after membrane dissolution (~ 1 mg) insufficient sample was present to obtain nitrogen adsorption data. This is consistent with previous reports that have also focused on electron microscopy [115, 118, 120], likely in part it seems due to the low amount of silica one recovers after matrix dissolution. The conclusion from the TEM/FE-SEM/PXRD work is that we cannot conclusively state the silica has a single well-defined pore topology (e.g. cubic versus hexagonal). However, the pore sizes observed by TEM are consistent with the permeation data. As such it is reasonable to conclude that the pore sizes are in the 4-5 nm range and that they are uniform.

5.4 Conclusions

The current work reports a synthesis route and permeation data for mesoporous silica-Anopore™ hybrid membranes. The permeation data for helium, nitrogen, and propane gases indicates several important points. First, the effective pore size of the membrane can be manipulated based on the number of dip-coating cycles. Four dip-coating cycles result in permeation data that are consistent with the expected pore size of

the target mesoporous silica phases incorporated. Further dip-coating cycles result in a dramatic loss of mechanical properties. Second, the He/N_2 permselectivity of the four-time dip-coated membranes is higher than for existing 5 nm commercial membranes, which typically contain pinhole defects. The He/N_2 permselectivity values of the mesoporous silica-Anopore™ membranes reported here are at the theoretical Knudsen limit and thus indicate the practical absence of pinhole defects. Furthermore, the C_3H_8/N_2 permselectivity data indicate the absence of very small mesopores (< 4 nm) with enhanced surface flow of propane, at least in comparison to the 5 nm Membralox® membrane. Characterization of the silica phase in the membrane is challenging, but electron microscopy data is consistent with the presence of mesopores 4-5 nm in size. TEM indicates that both cubic and hexagonally ordered domains are present. On the balance of the evidence, we have formed hybrid alumina-silica membranes that are practically free of defects and have a tight pore size distribution centered around 5 nm. The results indicate these materials possess the desirable properties of mesoporous silica thin films (uniform porosity) and as such are a potentially interesting alternative to OMS thin films grown on porous supports for membrane applications. They are also a potentially interesting replacement for commercial slip-cast amorphous ceramic membranes in the small mesopore (2-10 nm) size range, since the greater uniformity of pore size should result in sharper separations in ultrafiltration applications. Ongoing work is exploring the use of other templates (e.g. Pluronic P123) [16] and organic-functionalized membranes and will be reported elsewhere.

CHAPTER VI

DENDRIMER-CERAMIC NANOCOMPOSITE MEMBRANES FOR GAS SEPARATIONS

This chapter describes the synthesis of dendrimer-ceramic nanocomposite membranes and their application to solubility-based separations. Composite membranes were prepared by growing a melamine-based dendrimer directly off a commercial alumina membrane with 5 nm mesopores. We engineered the nanostructure of the composite membranes by controlling the structure and chemistry of the dendrimers to achieve high permselectivity. These composite membranes show extraordinarily high selectivities of propane over nitrogen up to 70. This separation performance is remarkable because the propane/nitrogen selectivity is much higher than that of PDMS, the current benchmark.

6.1 Introduction

Solubility-based membrane separations, where the more soluble species preferentially permeates across the membrane, have attracted considerable recent attention due to both economic and environmental concerns [1-3]. This mode is particularly attractive in applications where the heavier species are present in dilute concentrations, such as the removal of volatile compounds (VOCs) from effluent streams or the removal of higher hydrocarbons from natural gas. Freeman and Pinnau

outlined the design criteria for solubility-selective polymeric membranes [6]. In any membrane separation the selectivity of one component (*A*) over another (*B*), defined as the ratio of permeabilities, contains contributions from both diffusivity and solubility as shown in eq 1.

$$\alpha_{A/B} = \frac{\overline{P_A}}{\overline{P_B}} = \frac{D_A}{D_B}\frac{S_A}{S_B} \tag{6-1}$$

Freeman and Pinnau point out that to achieve solubility-based separation, the polymer needs not only a high solubility ratio but also a large free volume to drive the diffusivity ratio of the permeating species as close to unity as possible. Such a membrane will be reverse-selective, preferentially permeating the larger species. Solubility-selective materials can enable a positive correlation between permeability and selectivity, which is in contrast to the conventional Robeson trade-off rule [40] that suggests an upper bound in diffusivity-based separations. Many studies have focused on developing materials which can separation performance above Robeson's upper bound and thus become economically attractive (Fig. 2-1) [10, 57, 58].

Nanocomposites are a viable route to improved membrane materials for solubility-selective separations. Polymers doped with some type of inorganic nanophase are a popular approach [41, 59-65, 200, 201]. In a recent example, Merkel *et al.* doped poly(4-methyl-2-pentyne) with nanoscale fumed silica particles and studied them for a prototype solubility-selective separation: *n*-butane from methane [201]. With increasing weight % silica, they observed simultaneous increases in *n*-butane permeability and *n*-

butane / methane selectivity. The main reason was a change in the polymer packing, and thus the free vvvolume distribution, due to the presence of nanoparticles.

Another approach employs nanocomposites comprising organic moieties deposited onto a mesoporous ceramic framework. This approach allows one to design and build membranes that simultaneously deliver the desired chemistry and the desired free volume thereby making the membrane formation process quite versatile. This approach of forming organic-inorganic composites has shown great promise in creating materials for solubility-based separations [11-15, 48, 80, 202, 203]. Work in our group [11, 14, 15, 80] and that of J.D. Way [12] has led to structure-property relationships for membranes comprising organosilanes attached to porous silica and alumina. This work demonstrated that we can rationally modify permeation properties by choosing pore size, and type and amount of organic group deposited. The Martin group has used similar nanocomposites to carry out enantiomeric separations in the liquid phase [204].

In this study, we further develop this concept of engineering the membrane nano-architecture by exploring a new type of organic molecule architecture and chemistry, melamine-based dendrimers. Dendrimers are a promising class of organic molecules for this purpose due to their wide range of structural and chemical diversity [71, 76]. Dendrimer-ceramic nanocomposite membranes were synthesized by growing several generations of dendrimers with diverse functional groups directly off the surface of mesoporous alumina membrane. We have achieved extraordinarily high reverse selectivities by engineering the dendrimeric organic phase and carefully screening the effects of the pore size of the mesoporous substrate.

6.2 Experimental Section

6.2.1 Materials

Ethanol and toluene (ACS reagent grade) were purchased from EM Science. 3-aminopropyldimethyethoxysilane (APDMES, 99%) was purchased from Gelest Inc. Piperazine (P, 99%) and N,N-diisopropylethylamine (DIPEA, 99%) were purchased from Aldrich. Cyanuric chloride (CC, 99%) was purchased from ACROS. Tetrahydrofuran (THF), methanol, and dichloromethane (DCM) (all ACS reagent grade) were purchased from EMD. All chemicals were used as received. Water was purified using a Barnstead EASY pure water purification system. The membranes used in this research were Membralox ® T1-70-25G-Bare, γ-alumina membranes with an average pore size of 5 nm (Part# S700-01227). They were obtained from US Filter Ceramic Membrane Products, DeLand, Florida.

6.2.2 Synthesis of Dendrimer-Ceramic Nanocomposite Membrane

Details about the procedure of the growth of melamine-based dendrimer on the surface of the mesoporous alumina membrane were described in the section 3.3 and Fig. 3-3. This concept of melamine-based dendrimer was proposed first by Simanek's group in the chemistry department at Texas A&M University [76]. Dendrimers were grown directly off the surface of mesoporous alumina membranes by the stepwise synthesis [123, 205]. First, 3-aminopropyldimethylethoxysilane is attached on the porous support to provide the anchor group where dendrimer structures can be extended. These surface

amines were then allowed to react with cyanuric chloride (trichlorotriazine) to give the dichlorotriazine intermediate, branch-point. The dichlorotriazine was then allowed to react with either a monoamine or a diamine. The monoamine acted as a capping group that provided function to the membranes, while the diamine acted as a reactive spacer that continued the polymerization process. The treatment with triazine and diamine linker such as piperazine will be repeated alternately to reach the each generation. Finally, the functional monoamine molecules such as dodecyl amine or p-amino benzyl amine will be attached to provide the specific chemical diversity. In this manner, generation 1, 2 and 3 dendrons capped with either dodecyl amine or p- amino benzyl amine groups were produced. Our previous work proved the feasibility of the growth of this dendrimer inside the mesopores by doing the model study with dendrimer/SBA-15 hybrids [123, 205].

Fig. 6-1 shows two representative dendrimer structures we prepared here; piperazine is used as a diamine linker molecule in both cases but the different chemical adjustments are brought by the different functional groups, such as dodecyl amine or p-amino benzyl amine that we expect to be appropriate for the particular separations. G2-C12 is the second generation dendrimer capped with dodecyl amine and G2-B is the second generation dendrimer capped with p-amino benzyl amine. The G2-C12 was expected to show better performance in propane/nitrogen gas separation than G2-B because the dodecyl chains are expected to increase the solubility for the target component, propane.

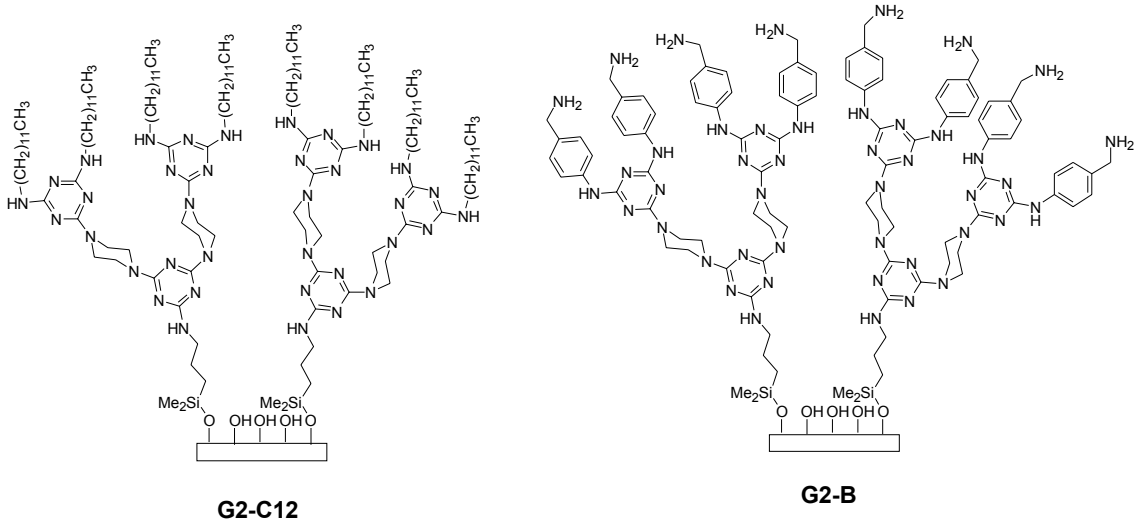

Fig. 6-1. Dendrimers structures of G2-C12 and G2-B.

The organic molecule size is controlled based on dendrimer generation. The number of the functional groups per dendron increases as the dendrimer generation increases. These rational modifications on the molecular architecture and chemistry by using the structural and chemical diversity of dendrimers finally lead to the development of the membrane which is customized for its application.

6.2.3 Procedure for Single Gas Permeation Test

Permeation measurements on the individual gases were performed using an in-house unit. Details of the single gas permeation experiments can be found in section 3.4. Pure helium (99.996%), nitrogen (99.998%), and propane (99.5%) gases were used as received from Praxair Distribution, Inc. The ambient temperature ranged from 20 to 22 ºC. The pressure was ambient on the permeate side. The pressure on the feed side was regulated up to 90 psig by a pressure regulator. The volumetric flow rate was measured at several pressure differences ranging from 5 to 90 psi. All data presented here were obtained using a pressure difference of 20 psi. The average value of the final four measurements at each pressure was taken in order to get the reported value for a permeate flow rate after it reached the steady-state. We noted that permeance typically required some time to reach steady-state under propane testing. It usually took a longer stabilization time, up to 24 hrs, for the organic treated membrane than for the bare membrane, which took around 15 min. This is not unusual for solubility-based separations with polymeric membranes and is attributed to conformational changes in the polymer over time [68, 69].

6.3 Results

6.3.1 Effect of Chemical Functionality

Pure-gas permeation studies were done with propane and nitrogen. Several dendrimer-Membralox® nanocomposite membranes with melamine-based dendrimer of different generations and chemical functionalities were tested. Fig. 6-2 shows the effect of chemical functionality on the separation performance. The third generation of each dendrimer showed a large difference in permeance performance with propane recovery. Propane permeance decreases as the mesopores are filled with both kinds of dendrimers, compared with the bare membrane. But, permselectivity of propane over nitrogen shows very different features depending on which dendrimer is attached. The aliphatic dodecyl functionalized membrane, G3-C12, shows a high propane/nitrogen selectivity around 50, while aromatic benzyl functionalized membranes, G3-B, show no change of selectivity compared with bare membrane. It is believed that the aliphatic dodecyl functional groups of G3-C12 increase the solubility of propane resulting in a high selectivity. This result indicates that we can adjust the chemical functionality of nanocomposite membranes to tailor membrane characteristics to specific applications.

6.3.2 Effect of Dendrimer Generations

We also see how permeance performance changes as dendrimer generation increases. Dodecylamine-capped dendrimers of different generations were tested for

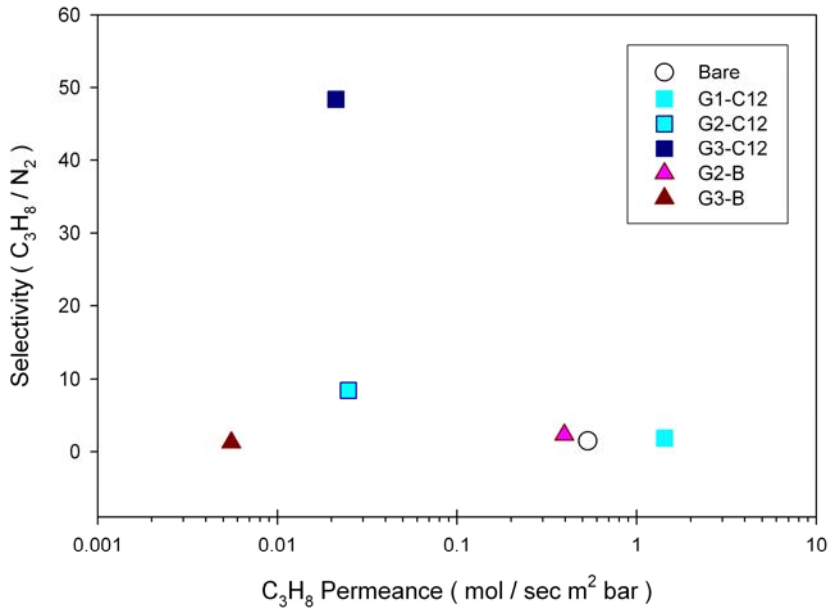

Fig. 6-2. Effect of chemical functionality of dendrimer.

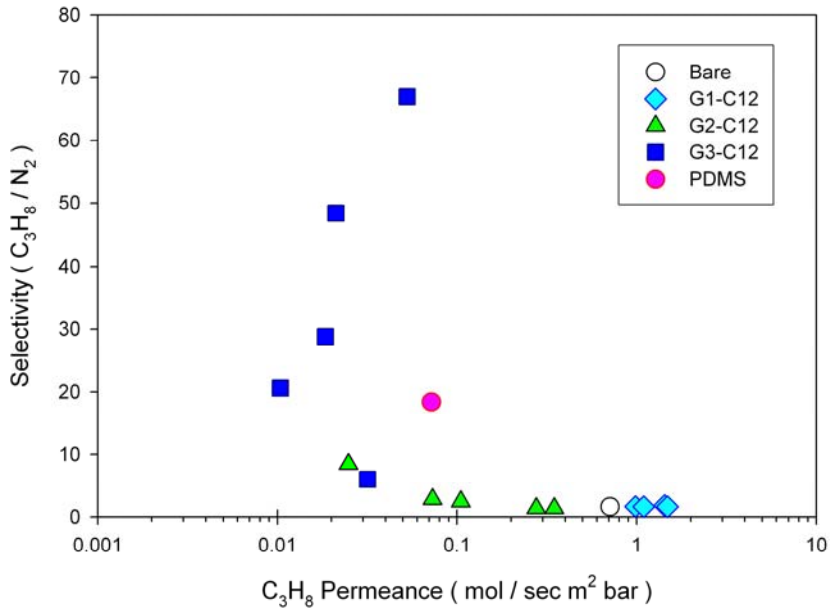

Fig. 6-3. Effect of dendrimer generation.

propane/nitrogen gas separation. Fig. 6-3 shows a summary of our selectivity-permeance data in the usual form of a selectivity *vs*. permeance (Robeson) plot. As the dendrimer generation increases from zero (bare membrane) to the first and second generation, it shows a slight increase of selectivity of propane over nitrogen with the decrease of propane permeance. The first generation dendrimer capped with dodecyl functional group, G1-C12, shows slightly enhanced permeance with negligible change in selectivity relative to the untreated support. G1-C12 is too small to have much effect on transport through the mesopores, except near the pore surface where it may enhance adsorption and surface flow. The second generation dendrimer, G2-C12, yields a reduction in permeance with slight increase in selectivity. This large molecule is starting to fill the pores, which has the simultaneous effects of reducing permeance and solubilizing the propane to enhance selectivity. Finally, the G3-C12 samples show dramatic increases of selectivity, up to 70. By contrast, a commonly used commercial polymer membrane, polydimethylsiloxane (PDMS), shows a selectivity of 18 [206]. One of our G3-C12 dendrimer-ceramic nanocomposite membranes thus shows a selectivity nearly 4 times higher than a standard industry benchmark, a remarkably promising result. As the dendrimer generation increases the number of functional groups increases as the mesopore of the inorganic support fill, which increase the solubility effect, resulting in increase of propane/nitrogen selectivity. To view this from another perspective, we estimated the solubility-selectivity (last term on the right-hand-side of eq 1) using correlations based on the vapor pressure of propane/nitrogen [207] and on the solubilities of these two gases fit across a wide range of liquids and polymers

[208]; the results were 46 and 59 respectively. Also, bulk polyethylene exhibits a propane/nitrogen solubility-selectivity of 55 for HDPE and 93 for LDPE [209]. Our best G3-C12 membranes are thus showing an overall performance at or near the upper limit of theoretical expectations; presumably the hyperbranched structure of the dendritic groups brings both high solubility-selectivity and a high enough free volume so that the ratio of diffusivities of the two species is driven close to unity.

However, the wide range of selectivities shown across the five (identically prepared) G3-C12 samples requires deeper investigation. We further develop our understanding of the structure-performance relationship in these membranes by re-plotting the data in Fig. 6-3 as propane permeance *vs*. nitrogen permeance (Fig. 6-4). The diagonal in Fig. 6-4 corresponds to a selectivity of one and the most selective membranes are now represented by the points that are farthest from the diagonal. The overall shape of the data is now like a fishhook with the most selective G3-C12 membrane at the tip. Two conclusions are supported by Fig. 6-4. First, *the ability of the organic phase to reduce the light gas (nitrogen) flow appears to be key in making membranes that are selective for the heavy gas (propane)*. Only in the region where the nitrogen permeance drops most sharply does the selectivity become appreciable; furthermore, the trend of decreasing nitrogen permeance correlates with increasing physical size of the dendrimers employed. Second, *once the light gas (nitrogen) flow is sufficiently restricted, the ability of the organic phase to solubilize the heavy gas (propane) appears to be key in creating the most selective membranes*. Within the G3-

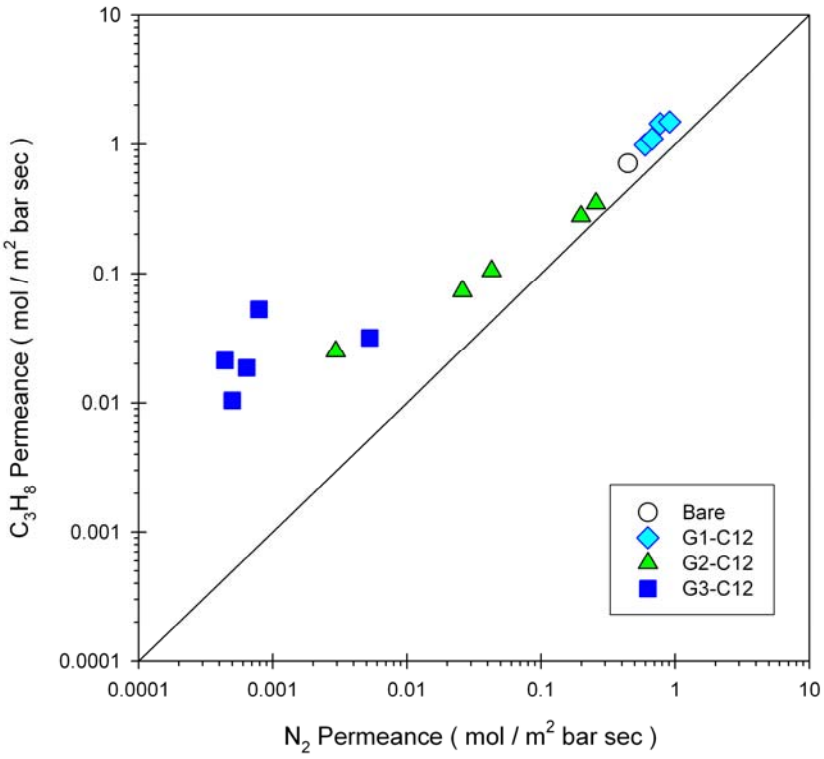

Fig. 6-4. Propane permeance vs. nitrogen permeance.

C12 data on the far left in Fig. 6-4, differences in selectivity correlate more strongly with differences in propane permeance than nitrogen permeance; the underlying cause is most likely based on solubility effects.

6.3.3 Effect of Inorganic Porous Support

Our nanocomposite membrane is promising enough in the membrane separation application due to its high performance in G3-C12 membrane. However, in order to produce the high performance dendrimer-ceramic nanocomposite membrane with high reproducibility, the following question should be considered: why is the raaange of selectivities for the G3 membranes is large when the synthesis procedure applied is apparently identical in each case? The effect of inorganic porous support, specifically the effective pore size, shows the origin of this. Fig. 6-5 shows the selectivity of different G3 treated membranes correlated against the nitrogen permeance of its untreated membrane support (as measured for each piece before treatment). Clearly there is a strong positive correlation between the permeance of the bare substrate that one starts with, and the selectivity of the final treated membrane. Our hypothesis is that the pore size variance of the untreated mesoporous substrate has a critical effect on the separation performance of the treated membranes.

The nitrogen permeance of the untreated mesoporous membrane is a proxy for the average pore size. In this study, we used the commercial available Membralox® membranes whose general purpose is filtering out objects greater than 5 nm. Previous

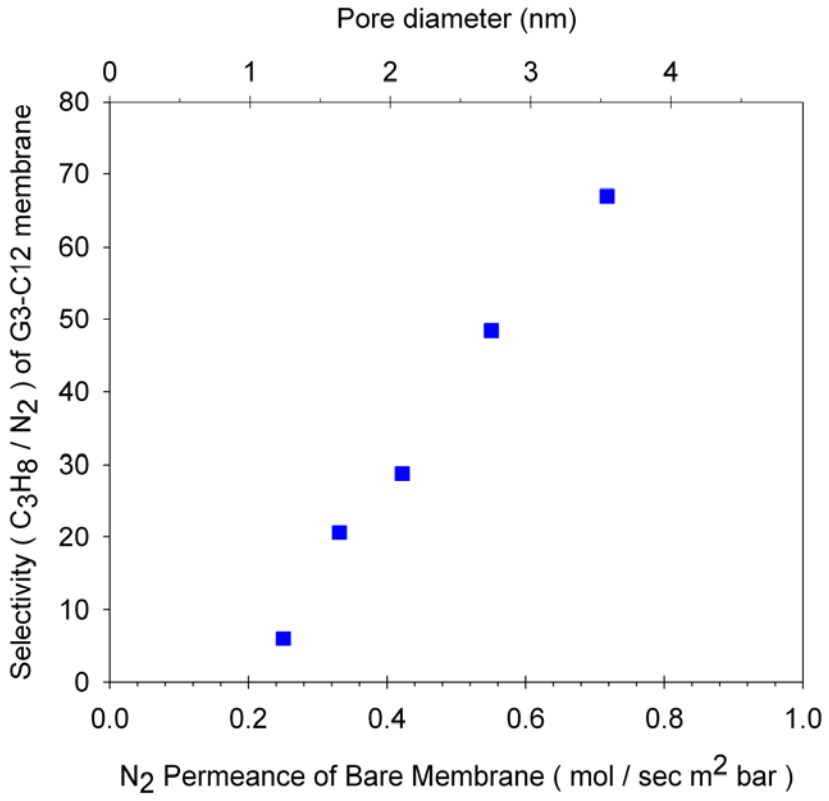

Fig. 6-5. Effect of the inorganic porous support.

literature characterization has shown that the active γ-alumina layer in these membranes has a distribution of pore sizes between 2 and 6 nm, with a maximum near 4 nm [130]. Using a Knudsen flow model for nitrogen and assuming that the active layer provides the only transport resistance, we calculated the average pore sizes of our untreated mesoporous supports (top horizontal axis in Fig. 4) which ranged from 1.2 to 3.5 nm. (Including the transport resistance of the supporting α-alumina layers, which have larger pores, would effectively increase our predictions of average pore size by 5-20 %. Our particular membrane pieces therefore had a somewhat smaller average pore size than that reported in the literature.) Figure 4 shows that the inorganic supports with larger pore sizes lead to higher selectivity of propane over nitrogen. We believe this correlation is related to the ability to grow the dendrimers in the pore spaces.

Dendrimers in this study were grown directly off the inorganic support by the stepwise synthesis. Each generation of dendrimers were grown divergently from the surface amines by the iterative synthesis of trichloro triazine and piperazine until the dichlorotriazine intermediate are left. Finally these dichlorotriazines are capped with dodecylamine, the functional group which has the high solubility effect for the target component. This final capping treatment with dodecylamine is important in the synthesis of organic-inorganic composite membranes because it ultimately provides the chemical functionality of the membrane. If the C12 capping is inefficient, the permeance of target component (propaaane) will be reduced due to a decrease in its solubility, resulting in a lower selectivity. The attachment of the functional group is affected by the space available in the mesopores during the capping step. Previous

studies of the synthesis of comparable dendrimers on mesoporous silica SBA-15 show clearly, by several analysis methods, that the 7.5 nm pores were highly filled after attaching the third generation dendrimer [205]. This indicates potential transport limitations for the C12 functional group attachment in the current G3-C12 synthesis. The growth to the third generation likely fills much of the membrane mesopores, thus restricting the diffusion of dodecylamine to the dichlrotriazine branch in the final step, resulting in the incomplete reaction of dichlorotriazine and a small number of functional groups attached in the final composite membrane. This effect will be strongly sensitive to small changes in the pore sizes of the support. As mentioned previously, the 5 nm membranes have a distribution of pore sizes between 2 and 6 nm. The bare porous substrate with the smaller initial pore size will have less porosity than the bigger pore support after the third dendrimer generation growth. Because of the reason discussed above, the composite membranes with smaller initial pore size likely have a small number of dodecyl groups, which decreases the solubility of propane. This incomplete reaction with dodecylamine will leave space which is not enough for the diffusion of dodecylamine but is big enough for nitrogen permeation, which facilitates the transport of the small permeates and deteriorate the propane/nitrogen selectivity. But, G3 membranes from the large initial pore substrate can have the opposite features. The more space availability enables the complete reaction of dichlorotriazine to leave the more dodecyl groups attached. It increases the solubility of propane and block nitrogen more efficiently. Finally it provides the high propane/nitrogen selectivity. In summary, supports with smaller pores will lead to fewer attached dodecyl groups and lower

propane/nitrogen selectivity, while supports with larger pore sizes will lead to more dodecyl groups and a greater solubility effect. High selectivity is achieved in cases where the pore size is large enough to accommodate all of the functional groups of the dendrimer but not too large to allow free flow of the light gas through the pores.

Work is ongoing to verify the correlation between the porosity characteristics of inorganic substrates and the performance of treated membrane and to enhance the reproducibility of high permselectivity. We are currently using a pre-screening step of the bare substrate: we choose new untreated membrane pieces based on their N_2 permeance and treat the membrane in the same way. If result shows they fall in the same place along the line in Fig. 6-5, it is further support of the above hypothesis. Another approach is using smaller capping molecules with similar chemical functionality instead of dodecylamines. For example, butylamine will be good choice for this purpose. The alkyl amine with the short chain length as a capping molecule can transport more easily in the same environment of the restricted space and reach to dichlorotriazine branch more readily to increase mesopore filling. But, this method also requires the pre-screening step of the bare substrate to determine the role of the porosity of the inorganic support.

These results show that the uniformity of inorganic porous support is very important to get the good membrane separation performance of composite membranes. The supported ordered mesoporous thin film (SOMTF) membranes, which were suggested in the chapter V [210], will be promising substrates for organic-inorganic composite membranes due to several advantages over Membralox® membranes.

SOMTF membranes have a well ordered pore structure with a narrow pore size distribution. This uniformity of SOMTF membranes can produce the sharper separation performance than commercial slip-cast amorphous ceramic membranes. Because of these reasons, SOMTF membranes will be explored as our new inorganic support for the synthesis of organic-inorganic nanocomposite membranes in the future study in our group.

6.4 Conclusions

The current work reports a synthesis of dendrimer-ceramic nanocomposite membrane and its application to propane/nitrogen separation. Composite membranes were prepared by growing the melamine-based dendrimer directly off the commercial alumina membrane with 5 nm mesopores. We engineered the nanostructure of composite membranes by introducing different organic structure and chemistry. Dendrimers are a promising class of organic molecules for this purpose due to this wide range of structural and chemical diversity. In this study, we control the molecule size and the number of the functional groups by increasing dendrimer generation. And the chemical functionality was adjusted for each application by attaching different capping molecules, aliphatic molecules such as dodecyl amine or aromatic molecules such as p-amino benzyl amine. Composite membranes were applied to the prototype separation of propane from nitrogen, and the effects of structure and chemistry of organic molecules on separation performance were explored. The permselectivity of propane over nitrogen shows very different features depending on which dendrimer is attached. Aliphatic

dodecyl functionalized membrane, G3-C12, shows the high propane/nitrogen selectivity up to 70, while aromatic benzyl functionalized membrane, G3-B, shows no change of selectivity. This indicates that we can adjust the chemical functionality of nanocomposite membranes to tailor membrane characteristics to specific application. Aliphatic dodecyl functional groups of G3-C12 increase the solubility of target component, propane, to get high selectivity. This effect is enhanced dramatically in the higher generation dendrimer because number of functional groups increases with filling mesopore of inorganic support as dendrimer generation increases. The increase of functional groups enhances the solubility for the target component, propane, and the organic filling of the mesopores increases the blocking effect of nitrogen (smaller molecules); both effects are combined and increase propane/nitrogen selectivity. Especially the ability of the organic phase to reduce the light gas (nitrogen) flow is important to making a membrane that is highly selective for the heavy gas (propane). The separation performance of G3-C12 membrane is remarkable because it shows the propane/nitrogen selectivity more than three times that of PDMS, the current industrial benchmark. The wide distribution of the permselectivity is a problem to be solved. The positive correlation between the nitrogen permeance of the bare substrate and the selectivity of the final treated membrane indicates that the uniformity of inorganic porous support is very important to get the good membrane separation performance of composite membranes. Several ways are currently being explored to enhance the reproducibility of high permselectivity: introducing the pre-screening step of the bare substrate, using the small functional group with the same chemistry and applying

supported ordered mesoporus thin film (SOMTF) membrane as new support. SOMTF membranes are promising as an inorganic porous support for the synthesis of organic-inorganic nanocomposite membranes because of several advantages about uniformity such as the well ordered pore structure and the narrow pore size distribution.

CHAPTER VII

CONCLUSIONS AND SUMMARY

Solubility-based separation with membranes has attracted considerable recent attention due to both economic and environmental concerns. This mode enables the preferential permeation of larger and heavier species by solubility differences. So, it is particularly attractive over diffusivity-selective mode in applications where the heavier and the more condensable species are present in dilute concentration; the removal of volatile compounds (VOCs) from effluent streams or the removal of higher hydrocarbons from natural gas are two examples.

Recently, nanocomposites have shown great promise as possible membrane materials for solubility-selective separations. The chemical derivatization of inorganic mesoporous substrates has been explored to synthesize organic-inorganic nanocomposite membranes. Several research works including ours showed that the composite membranes had significantly different (better) permselectivity properties than their pure-polymer analogues, proving the viability of this design concept of composite materials for solubility based separation. The most exciting feature of this approach is that it enables the rational engineering of membrane nano-architecture with independent control over the free volume and chemistry to create membranes with highly customizable permselectivity properties. The materials engineering variables include the

pore size and structure of porous inorganic support, organic filler size and chemistry, and surface coverage.

In this study, we further develop this concept of engineering the membrane nano-architecture by exploring new organic molecule architecture and chemistry, melamine-based dendrimers, and new inorganic support, ordered mesoporous thin film. Dendrimers are particularly attractive for the present application due to their hyperbranched nature and structural and chemical diversity. Surfactant-templated ordered mesoporous inorganic thin films shows promising characteristics as inorganic porous support for composite membranes because of their well ordered pore structure and uniform pore size distribution, which can lead to precise control of membrane performance.

First, we did a model study to verify the feasibility of dendrimer growth inside mesopores by using ordered mesoporous silica, SBA-15. Various dendrimers were grown on SBA-15 by varying the dendrimer generation, the linker molecule, and the surface amine loading. Porosimetry measurements indicate that the effective pore size of the composite and the total pore volume of the material can be controlled independently. Results demonstrate that dendrimers can be grown inside mesopores and that these composite materials have potential use in many areas including separations, sensing, and catalysis, given the ability to tune chemistry and porosity independently.

We also prepared supported ordered mesoporous thin film membranes as new inorganic porous substrates. Alumina-ordered mesoporous silica (alumina-OMS) hybrid membranes were synthesized by depositing ordered mesoporous silica thin film on

commercial macoporous alumina membranes. Several analytical methods such as SEM and TEM indicate that ordered mesoporous thin films with uniform 4-5 nm pores are filled inside the macropores of Anopore™ membrane. The permeation data for helium, nitrogen, and propane gases indicates that the effective pore size of the membrane can be manipulated based on the number of dip-coating cycles and that four dip-coating cycles result in permeation data that are consistent with the expected pore size of the target mesoporous silica phases incorporated. The He/N_2 permselectivity values of the mesoporous silica-Anopore™ membranes are at the theoretical Knudsen limit and thus indicate the practical absence of pinhole defects. The results indicate these materials possess the desirable properties of mesoporous silica thin films (uniform porosity) and as such are a potentially interesting alternative to OMS thin films grown on porous supports for membrane applications.

Finally, we synthesized dendrimer-ceramic nanocomposite membrane by growing the melamine-based dendrimer directly off the commercial alumina membrane with 5 nm mesopores. We engineered the nanostructure of composite membranes by introducing several generations of dendrimers with diverse functional groups. Composite membranes show very high propane/nitrogen selectivity up to 70.

Especially, the separation performance of G3-C12 membrane in the propane recovery is remarkable because the propane/nitrogen selectivity is much higher than that of PDMS, which is the material usually used in industry. But its wide distribution of the permselectivity is a problem to be solved. The positive correlation between the nitrogen permeance of the bare substrate and the selectivity of the final treated membrane

indicates that the uniformity of inorganic porous support is very important to obtain the good membrane separation performance in composite membranes. These results indicate that SOMTF membranes could be a promising inorganic porous support for the synthesis of organic-inorganic nanocomposite membranes because of several advantages about uniformity such as the well ordered pore structure and the narrow pore size distribution.

This study shows that we can modify permeation properties of nanocomposite membranes by rationally choosing dendrimer structure and chemistry to tailor membrane characteristics to the recovery of the higher hydrocarbon from air. For future study, we will evaluate composite membranes for the removal of trace VOCs from air or water by exploring the impact of organic oligomer size, chemistry, and surface coverage, as well as substrate pore size and structure, on membrane performance. SOMTF membrane will be explored as new inorganic porous substrate for the precise control of pore size and structure. And also in the near future, we will employ molecular simulation to provide a molecular-level explanation for the permselectivity performance of the membrane.

REFERENCES

[1] W. S. W. Ho, K. K. Sirkar, Membrane handbook, Van Nostrand Reinhold, New York, 1992.

[2] M. Mulder, Basic principles of membrane technology, Kluwer Academic Publishers, Dordrecht, 1996.

[3] N. A. Downie, Industrial gases, Blackie Academic & Professional, London, 1997.

[4] W. J. Koros, G. K. Fleming, Membrane-based gas separation, J. Membr. Sci. 83 (1993) 1-80.

[5] S. A. Stern, Polymers for gas separations - the next decade, J. Membr. Sci. 94 (1994) 1-65.

[6] B. Freeman, I. Pinnau, Separation of gases using solubility-selective polymers, Trends in Polym. Sci. 5 (1997) 167-173.

[7] M. B. Rao, S. Sircar, Nanoporous carbon membranes for separation of gas-mixtures by selective surface flow, J. Membr. Sci. 85 (1993) 253-264.

[8] M. B. Rao, S. Sircar, Performance and pore characterization of nanoporous carbon membranes for gas separation, J. Membr. Sci. 110 (1996) 109-118.

[9] P. Huang, N. Xu, J. Shi, Y. S. Lin, Recovery of volatile organic solvent compounds from air by ceramic membranes, Ind. Eng. Chem. Res. 36 (1997) 3815-3820.

[10] J. Schultz, K. V. Peinemann, Membranes for separation of higher hydrocarbons from methane, J. Membr. Sci. 110 (1996) 37-45.

[11] A. Javaid, M. P. Hughey, V. Varutbangkul, D. M. Ford, Solubility-based gas separation with oligomer-modified inorganic membranes, J. Membr. Sci. 187 (2001) 141-150.

[12] K. C. McCarley, J. D. Way, Development of a model surface flow membrane by modification of porous γ-alumina with octadecyltrichlorosilane, Sep. Purif. Technol. 25 (2001) 195-210.

[13] J. Randon, R. Paterson, Preliminary studies on the potential for gas separation by mesoporous ceramic oxide membranes surface modified by alkyl phosphonic acids, J. Membr. Sci. 134 (1997) 219-223.

[14] A. Javaid, D. M. Ford, Solubility-based gas separation with oligomer-modified inorganic membranes - Part II. Mixed gas permeation of 5 nm alumina membranes modified with octadecyltrichlorosilane, J. Membr. Sci. 215 (2003) 157-168.

[15] A. Javaid, D. A. Krapchetov, D. M. Ford, Solubility-based gas separation with oligomer-modified inorganic membranes - Part III. Effects of synthesis conditions, J. Membr. Sci. 246 (2005) 181-191.

[16] M. P. Tate, B. W. Eggiman, J. D. Kowalski, H. W. Hillhouse, Order and orientation control of mesoporous silica films on conducting gold substrates formed by dip-coating and self-assembly: A GISAXS and FE-SEM study, Langmuir 21 (2005) 10112-10118.

[17] N. Nishiyama, D. H. Park, A. Koide, Y. Egashira, K. Ueyama, A mesoporous silica (MCM-48) membrane: Preparation and characterization, J. Membr. Sci. 182 (2001) 235-244.

[18] G. Xomeritakis, C. M. Braunbarth, B. Smarsly, N. Liu, R. Kohn, Z. Klipowicz, C. J. Brinker, Aerosol-assisted deposition of surfactant-templated mesoporous silica membranes on porous ceramic supports, Micropor. Mesopor. Mater. 66 (2003) 91-101.

[19] E. E. Simanek, S. O. Gonzalez, Dendrimers: Branching out of polymer chemistry, J. Chem. Edu. 79 (2002) 1222-1231.

[20] T. Graham, On the law of the diffusion of gases, Philos. Mag. 32 (1866) 401-420.

[21] A. Fick, Über diffusion, Ann. Phys. Chem. 94 (1855) 59-86.

[22] H. Benchold, Ultrafiltration, Biochem. Z. 6 (1907) 379-408.

[23] F. Erbe, Die bestimmung der porenverteilung nach ihrer größe in filtern und ultrafiltern, Kolloid. Z. 63 (1933) 277-285.

[24] S. Loeb, S. Sourirajan, Sea water demineralization by means of an osmotic membrane, Adv. Chem. Ser. 38 (1963) 117-132.

[25] J. M. S. Henis, M. K. Tripodi, A novel approach to gas separation using composite hollow fiber membranes, Sep. Sci. Technol. 15 (1980) 1059.

[26] J. Karger, D. M. Ruthven, Diffusion in zeolites and other microporous solids, Wiley, New York, 1992.

[27] S. Morooka, K. Kusakabe, Microporous inorganic membranes for gas separation, MRS Bulletin March (1999) 25-29.

[28] M. Tsapatsis, G. R. Gavalas, Synthesis of porous inorganic membranes, MRS Bulletin March (1999) 30-35.

[29] B. N. Nair, K. Keizer, W. J. Elferink, M. J. Gilde, H. Verweij, A. J. Burggraaf, Synthesis, characterisation and gas permeation studies on microporous silica and alumina-silica membranes for separation of propane and propylene, J. Membr. Sci. 116 (1996) 161-169.

[30] R. S. A. de Lange, J. H. A. Hekkink, K. Keizer, A. J. Burggraaf, Formation and characterization of supported microporous ceramic membranes prepared by sol-gel modification techniques, J. Membr. Sci. 99 (1995) 57-75.

[31] R. S. A. de Lange, K. Keizer, A. J. Burggraaf, Analysis and theory of gas transport in microporous sol-gel derived ceramic membranes, J. Membr. Sci. 104 (1995) 81-100.

[32] P. Blanc, A. Larbot, J. Palmeri, M. Lopez, L. Cot, Hafnia ceramic nanofiltration membranes. Part I: Preparation and characterization, J. Membr. Sci. 149 (1998) 151-161.

[33] P. J. Davis, C. Jeffrey Brinker, D. M. Smith, Pore structure evolution in silica gel during aging/drying I. Temporal and thermal aging, J. Non-Crystalline Solids 142 (1992) 189-196.

[34] A. Singh-Ghosal, W. J. Koros, Air separation properties of flat sheet homogeneous pyrolytic carbon membranes, J. Membr. Sci. 174 (2000) 177-188.

[35] A. F. Ismail, L. I. B. David, A review on the latest development of carbon membranes for gas separation, J. Membr. Sci. 193 (2001) 1-18.

[36] Z. A. E. P. Vroon, K. Keizer, M. J. Gilde, H. Verweij, A. J. Burggraaf, Transport properties of alkanes through ceramic thin zeolite mfi membranes, J. Membr. Sci. 113 (1996) 293-300.

[37] Z. A. E. P. Vroon, K. Keizer, A. J. Burggraaf, H. Verweij, Preparation and characterization of thin zeolite mfi membranes on porous supports, J. Membr. Sci. 144 (1998) 65-76.

[38] A. J. Burggraaf, Z. A. E. P. Vroon, K. Keizer, H. Verweij, Permeation of single gases in thin zeolite mfi membranes, J. Membr. Sci. 144 (1998) 77-86.

[39] R. E. Kesting, A. K. Fritzsche, Polymeric gas separation membranes, John Wiley & Sons, Inc., New York, 1993.

[40] L. M. Robeson, Correlation of separation factor versus permeability for polymeric membranes, J. Membr. Sci. 62 (1991) 165-185.

[41] M. Moaddeb, W. J. Koros, Gas transport properties of thin polymeric membranes in the presence of silicon dioxide particles, J. Membr. Sci. 125 (1997) 143-163.

[42] W. J. Koros, R. Mahajan, Pushing the limits on possibilities for large scale gas separation: Which strategies?, J. Membr. Sci. 175 (2000) 181-196.

[43] D. E. Fain, Membrane gas separation principles, MRS Bulletin April (1994) 40-43.

[44] S. V. Sotirchos, V. N. Burganos, Transport of gases in porous membranes, MRS Bulletin 24 (1999) 41-45.

[45] R. J. R. Uhlhorn, K. Keizer, A. J. Burggraaf, Gas and surface diffusion in modified γ-alumina systems, J. Membr. Sci. 46 (1989) 225-241.

[46] K. Keizer, R. J. R. Uhlhorn, R. J. Van vuren, A. J. Burggraaf, Gas separation mechanisms in microporous modified γ-Al_2O_3 membranes, J. Membr. Sci. 39 (1988) 285-300.

[47] R. J. R. Uhlhorn, K. Keizer, A. J. Burggraaf, Gas transport and separation with ceramic membranes. Part I. Multilayer diffusion and capillary condensation, J. Membr. Sci. 66 (1992) 259-269.

[48] M. Leemann, G. Eigenberger, H. Strathmann, Vapour permeation for the recovery of organic solvents from waste air streams: Separation capacities and process optimization, J. Membr. Sci. 113 (1996) 313-322.

[49] M. H. Hassan, J. Douglas Way, P. M. Thoen, A. C. Dillon, Single component and mixed gas transport in a silica hollow fiber membrane, J. Membr. Sci. 104 (1995) 27-42.

[50] R. W. Baker, N. Yoshioka, J. M. Mohr, A. J. Khan, Separation of organic vapors from air, J. Membr. Sci. 31 (1987) 259-271.

[51] I. Blume, P. J. F. Schwering, M. H. V. Mulder, C. A. Smolders, Vapour sorption and permeation properties of poly (dimethylsiloxane) films, J. Membr. Sci. 61 (1991) 85-97.

[52] T. Masuda, E. Isobe, T. Higashimura, Polymerization of 1-(trimethylsilyl)-1-propyne by halides of niobium (v) and tantalum (v) and polymer properties, Macromolecules 18 (1985) 841-845.

[53] R. Srinivasan, S. R. Auvil, P. M. Burban, Elucidating the mechanism(s) of gas transport in poly[1-(trimethylsilyl)-1-propyne] (PTMSP) membranes, J. Membr. Sci. 86 (1994) 67-86.

[54] Y. Ichiraku, S. A. Stern, T. Nakagawa, An investigation of the high gas permeability of poly (1-trimethylsilyl-1-propyne), J. Membr. Sci. 34 (1987) 5-18.

[55] N. A. Plate, A. K. Bokarev, N. E. Kaliuzhnyi, E. G. Litvinova, V. S. Khotimskii, V. V. Volkov, Y. P. Yampol'skii, Gas and vapor permeation and sorption in poly (trimetylsilylpropyne), J. Membr. Sci. 60 (1991) 13-24.

[56] I. Pinnau, L. G. Toy, Transport of organic vapors through poly(1-trimethylsilyl-1-propyne), J. Membr. Sci. 116 (1996) 199-209.

[57] T. C. Merkel, R. P. Gupta, B. S. Turk, B. D. Freeman, Mixed-gas permeation of syngas components in poly(dimethylsiloxane) and poly(1-trimethylsilyl-1-propyne) at elevated temperatures, J. Membr. Sci. 191 (2001) 85-94.

[58] Y. P. Yampol'skii, S. M. Shishatskii, V. P. Shantorovich, E. M. Antipov, N. N. Kuzmin, S. V. Rykov, V. L. Khodjaeva, N. A. Plat, Transport characteristics and other physicochemical properties of aged poly(1-(trimethylsilyl)-1-;propyne), J. App. Polym. Sci. 48 (1993) 1935-1944.

[59] I. F. J. Vankelecom, E. Merckx, M. Luts, J. B. Uytterhoeven, Incorporation of zeolites in polyimide membranes, J. Phys. Chem. 99 (1995) 13187-13192.

[60] I. F. J. Vankelecom, C. Dotremont, M. Morobe, J. B. Uytterhoeven, C. Vandecasteele, Zeolite-filled pdms membranes. 1. Sorption of halogenated hydrocarbons, J. Phys. Chem. B 101 (1997) 2154-2159.

[61] M. V. Chandak, Y. S. Lin, W. Ji, R. J. Higgins, Sorption and diffusion of vocs in day zeolite and silicalite-filled pdms membranes, J. Membr. Sci. 133 (1997) 231-243.

[62] M. Smaihi, T. Jermoumi, J. Marignan, R. D. Noble, Organic-inorganic gas separation membranes: Preparation and characterization, J. Membr. Sci. 116 (1996) 211-220.

[63] Q. Hu, E. Marand, S. Dhingra, D. Fritsch, J. Wen, G. Wilkes, Poly(amide-imide)/tio2 nano-composite gas separation membranes: Fabrication and characterization, J. Membr. Sci. 135 (1997) 65-79.

[64] C. Joly, S. Goizet, J. C. Schrotter, J. Sanchez, M. Escoubes, Sol-gel polyimide-silica composite membrane: Gas transport properties, J. Membr. Sci. 130 (1997) 63-74.

[65] W. I. Sohn, D. H. Ryu, S. J. Oh, J. K. Koo, A study on the development of composite membranes for the separation of organic vapors, J. Membr. Sci. 175 (2000) 163-170.

[66] X. Zhao, R. Kopelman, Mechanism of organosilane self-assembled monolayer formation on silica studied by second-harmonic generation, J. Phys. Chem. 100 (1996) 11014-11018.

[67] J. Randon, P. Blanc, R. Paterson, Modification of ceramic membrane surfaces using phosphoric acid and alkyl phosphonic acids and its effects on ultrafiltration of bsa protein, J. Membr. Sci. 98 (1995) 119-129.

[68] C. Leger, H. D. L. Lira, R. Paterson, Preparation and properties of surface modified ceramic membranes. Part II. Gas and liquid permeabilities of 5 nm alumina membranes modified by a monolayer of bound polydimethylsiloxane (pdms) silicone oil, J. Membr. Sci. 120 (1996) 135-146.

[69] C. Leger, H. D. L. Lira, R. Paterson, Preparation and properties of surface modified ceramic membranes. Part III. Gas permeation of 5 nm alumina membranes modified by trichloro-octadecylsilane, J. Membr. Sci. 120 (1996) 187-195.

[70] J. R. Miller, W. J. Koros, The formation of chemically modified γ-alumina microporous membranes, Sep. Sci. Technol. 25 (1990) 1257.

[71] O. A. Matthews, A. N. Shipway, J. F. Stoddart, Dendrimers--branching out from curiosities into new technologies, Prog. Polym. Sci. 23 (1998) 1-56.

[72] M. F. Neerman, W. Zhang, A. R. Parrish, E. E. Simanek, *In vitro* and *in vivo* evaluation of a melamine dendrimer as a vehicle for drug delivery, Inter. J. Pharm. 281 (2004) 129-132.

[73] W. Zhang, S. O. Gonzalez, E. E. Simanek, Structure-activity relationships in dendrimers, based on triazines: Gelation depends on choice of linking and surface groups, Macromolecules 35 (2002) 9015-9021.

[74] W. Zhang, J. Jiang, C. H. Qin, L. M. Perez, A. R. Parrish, S. H. Safe, E. E. Simanek, Triazine dendrimers for drug delivery: Evaluation of solubilization properties, activity in cell culture, and in vivo toxicity of a candidate vehicle, Supramol. Chem. 15 (2003) 607.

[75] W. Zhang, D. T. Nowlan, L. M. Thomson, W. M. Lackowski, E. E. Simanek, Orthogonal, convergent syntheses of dendrimers based on melamine with one or two unique surface sites for manipulation, J. Am. Chem. Soc. 123 (2001) 8914-8922.

[76] W. Zhang, E. E. Simanek, Dendrimers based on melamine. Divergent and orthogonal, convergent syntheses of a G3 dendrimer, Org. Lett. 2 (2000) 843-845.

[77] W. Zhang, E. E. Simanek, Synthesis and characterization of higher generation dendrons based on melamine using p-aminobenzylamine. Evidence for molecular recognition of Cu(ii), Tetra. Lett. 42 (2001) 5355-5357.

[78] W. Zhang, S. E. Tichy, L. M. Perez, G. C. Maria, P. A. Lindahl, E. E. Simanek, Evaluation of multivalent dendrimers based on melamine: Kinetics of thiol-disulfide exchange depends on the structure of the dendrimer, J. Am. Chem. Soc. 125 (2003) 5086-5094.

[79] S. A. Bell, M. E. McLean, S. K. Oh, S. E. Tichy, W. Zhang, R. M. Corn, R. M. Crooks, E. E. Simanek, Synthesis and characterization of covalently linked single-stranded DNA oligonucleotide-dendron conjugates, Bioconj. Chem. 14 (2003) 488-493.

[80] A. Javaid, S. O. Gonzalez, E. E. Simanek, D. M. Ford, Nanocomposite membranes of chemisorbed and physisorbed molecules on porous alumina for environmentally important separations, J. Membr. Sci. 275 (2006) 255-260.

[81] C. T. Kresge, M. E. Leonowicz, W. J. Roth, J. C. Vartuli, J. S. Beck, Ordered mesoporous molecular-sieves synthesized by a liquid-crystal template mechanism, Nature 359 (1992) 710-712.

[82] J. S. Beck, J. C. Vartuli, W. J. Roth, M. E. Leonowicz, C. T. Kresge, K. D. Schmitt, C. T. W. Chu, D. H. Olson, E. W. Sheppard, S. B. McCullen, J. B. Higgins, J. L. Schlenker, A new family of mesoporous molecular-sieves prepared with liquid-crystal templates, J. Am. Chem. Soc. 114 (1992) 10834-10843.

[83] A. Firouzi, D. Kumar, L. M. Bull, T. Besier, P. Sieger, Q. Huo, S. A. Walker, J. A. Zasadzinski, C. Glinka, J. Nicol, D. Margolese, G. D. Stucky, B. F. Chmelka, Cooperative organization of inorganic-surfactant and biomimetic assemblies, Science 267 (1995) 1138-1143.

[84] P. T. Tanev, T. J. Pinnavaia, A neutral templating route to mesoporous molecular-sieves, Science 267 (1995) 865-867.

[85] P. T. Tanev, M. Chibwe, T. J. Pinnavaia, Titanium-containing mesoporous molecular-sieves for catalytic-oxidation of aromatic-compounds, Nature 368 (1994) 321-323.

[86] S. A. Bagshaw, E. Prouzet, T. J. Pinnavaia, Templating of mesoporous molecular-sieves by nonionic polyethylene oxide surfactants, Science 269 (1995) 1242-1244.

[87] Q. S. Huo, D. I. Margolese, U. Ciesla, P. Y. Feng, T. E. Gier, P. Sieger, R. Leon, P. M. Petroff, F. Schuth, G. D. Stucky, Generalized synthesis of periodic surfactant inorganic composite materials, Nature 368 (1994) 317-321.

[88] D. Y. Zhao, J. L. Feng, Q. S. Huo, N. Melosh, G. H. Fredrickson, B. F. Chmelka, G. D. Stucky, Triblock copolymer syntheses of mesoporous silica with periodic 50 to 300 angstrom pores, Science 279 (1998) 548-552.

[89] S. Inagaki, Y. Fukushima, K. Kuroda, Synthesis and characterization of highly ordered mesoporous material - FSM-16, from a layered polysilicate, in: J. Weitkamp, H.G. Karge, H. Pfeifer, Hölderich (Eds.), Zeolites and related microporous materials: State of the art 1994, Elsvier Science, Amsterdam, 1994, pp. 125-132.

[90] S. Inagaki, Y. Fukushima, K. Kuroda, Synthesis of highly ordered mesoporous materials from a layered polysilicate, J. Chem. Soc. Chem. Comm. (1993) 680-682.

[91] Q. S. Huo, D. I. Margolese, U. Ciesla, D. G. Demuth, P. Y. Feng, T. E. Gier, P. Sieger, A. Firouzi, B. F. Chmelka, F. Schuth, G. D. Stucky, Organization of organic-molecules with inorganic molecular-species into nanocomposite biphase arrays, Chem. Mater. 6 (1994) 1176-1191.

[92] Q. S. Huo, D. I. Margolese, G. D. Stucky, Surfactant control of phases in the synthesis of mesoporous silica-based materials, Chem. Mater. 8 (1996) 1147-1160.

[93] R. Ryoo, J. M. Kim, C. H. Ko, C. H. Shin, Disordered molecular sieve with branched mesoporous channel network, J. Phys. Chem. 100 (1996) 17718-17721.

[94] W. Z. Zhou, J. Klinowski, The mechanism of channel formation in the mesoporous molecular sieve MCM-41, Chem. Phys. Lett. 292 (1998) 207-212.

[95] D. Y. Zhao, Q. S. Huo, J. L. Feng, B. F. Chmelka, G. D. Stucky, Nonionic triblock and star diblock copolymer and oligomeric surfactant syntheses of highly ordered, hydrothermally stable, mesoporous silica structures, J. Am. Chem. Soc. 120 (1998) 6024-6036.

[96] H. Yang, N. Coombs, I. Sokolov, G. A. Ozin, Registered growth of mesoporous silica films on graphite, J. Mater. Chem. 7 (1997) 1285-1290.

[97] G. Wirnsberger, P. D. Yang, B. J. Scott, B. F. Chmelka, G. D. Stucky, Mesostructured materials for optical applications: From low-k dielectrics to sensors and lasers, Spectrochimica Acta Part A - Molecular and Biomolecular Spectroscopy 57 (2001) 2049-2060.

[98] A. Bearzotti, J. M. Bertolo, P. Innocenzi, P. Falcaro, E. Traversa, Relative humidity and alcohol sensors based on mesoporous silica thin films synthesised from block copolymers, Sensors and Actuators B - Chemical 95 (2003) 107-110.

[99] T. Hyodo, S. Abe, Y. Shimizu, M. Egashira, Gas-sensing properties of ordered mesoporous SnO_2 and effects of coatings thereof, Sensors and Actuators B - Chemical 93 (2003) 590-600.

[100] T. Yamada, H. S. Zhou, H. Uchida, M. Tomita, Y. Ueno, I. Honma, K. Asai, T. Katsube, Application of a cubic-like mesoporous silica film to a surface photovoltage gas sensing system, Micropor. Mesopor. Mater. 54 (2002) 269-276.

[101] T. Yamada, H. S. Zhou, H. Uchida, M. Tomita, Y. Ueno, T. Ichino, I. Honma, K. Asai, T. Katsube, Surface photovoltage no gas sensor with properties dependent

on the structure of the self-ordered mesoporous silicate film, Adv. Mater. 14 (2002) 812-815.

[102] Y. Shioya, K. Ikeue, M. Ogawa, M. Anpo, Synthesis of transparent Ti-containing mesoporous silica thin film materials and their unique photocatalytic activity for the reduction of CO_2 with H_2O, Applied Catalysis A - General 254 (2003) 251-259.

[103] B. D. Hatton, K. Landskron, W. Whitnall, D. D. Perovic, G. A. Ozin, Spin-coated periodic mesoporous organosilica thin films - towards a new generation of low-dielectric-constant materials, Adv. Func. Mater. 15 (2005) 823-829.

[104] A. R. Balkenende, F. K. de Theije, J. C. K. Kriege, Controlling dielectric and optical properties of ordered mesoporous organosilicate films, Adv. Mater. 15 (2003) 139-143.

[105] P. C. A. Alberius, K. L. Frindell, R. C. Hayward, E. J. Kramer, G. D. Stucky, B. F. Chmelka, General predictive syntheses of cubic, hexagonal, and lamellar silica and titania mesostructured thin films, Chem. Mater. 14 (2002) 3284-3294.

[106] R. C. Hayward, P. C. A. Alberius, E. J. Kramer, B. F. Chmelka, Thin films of bicontinuous cubic mesostructured silica templated by a nonionic surfactant, Langmuir 20 (2004) 5998-6004.

[107] F. Cagnol, D. Grosso, G. Soler-Illia, E. L. Crepaldi, F. Babonneau, H. Amenitsch, C. Sanchez, Humidity-controlled mesostructuration in CTAB-templated silica thin film processing. The existence of a modulable steady state, J. Mater. Chem. 13 (2003) 61-66.

[108] D. Grosso, F. Cagnol, G. Soler-Illia, E. L. Crepaldi, H. Amenitsch, A. Brunet-Bruneau, A. Bourgeois, C. Sanchez, Fundamentals of mesostructuring through evaporation-induced self-assembly, Adv. Funct. Mater. 14 (2004) 309-322.

[109] M. Ogawa, N. Masukawa, Preparation of transparent thin films of lamellar, hexagonal and cubic silica-surfactant mesostructured materials by rapid solvent evaporation methods, Micropor.Mesopor. Mater. 38 (2000) 35-41.

[110] S. Besson, C. Ricolleau, T. Gacoin, C. Jacquiod, J. P. Boilot, A new 3d organization of mesopores in oriented ctab silica films, J. Phys. Chem. B 104 (2000) 12095-12097.

[111] C. J. Brinker, G. W. Scherer, Sol-gel science. The physis and chemistry of sol-gel processing, Academic Press, Boston, 1990.

[112] I. Honma, H. S. Zhou, D. Kundu, A. Endo, Structural control of surfactant-templated hexagonal, cubic, and lamellar mesoporous silicate thin films prepared by spin-casting, Adv. Mater. 12 (2000) 1529-1533.

[113] D. Zhao, P. Yang, N. Melosh, J. Feng, B. F. Chmelka, G. D. Stucky, Continuous mesoporous silica films with highly ordered large pore structures, Adv. Mater. 10 (1998) 1380-1385.

[114] Y. F. Lu, R. Ganguli, C. A. Drewien, M. T. Anderson, C. J. Brinker, W. L. Gong, Y. X. Guo, H. Soyez, B. Dunn, M. H. Huang, J. I. Zink, Continuous formation of supported cubic and hexagonal mesoporous films by sol gel dip-coating, Nature 389 (1997) 364-368.

[115] Z. Yang, Z. Niu, X. Cao, Z. Yang, Y. Lu, Z. Hu, C. C. Han, Template synthesis of uniform 1d mesostructured silica materials and their arrays in anodic alumina membranes, Angew. Chem. Int. Ed. 42 (2003) 4201-4203.

[116] B. Yao, D. Fleming, M. A. Morris, S. E. Lawrence, Structural control of mesoporous silica nanowire arrays in porous alumina membranes, Chem. Mater. 16 (2004) 4851-4855.

[117] Q. Lu, F. Gao, S. Khomarneni, T. E. Mallouk, Ordered SBA-15 nanorod arrays inside a porous alumina membrane, J. Am. Chem. Soc. 126 (2004) 8650-8651.

[118] Y. Y. Wu, G. S. Cheng, K. Katsov, S. W. Sides, J. F. Wang, J. Tang, G. H. Fredrickson, M. Moskovits, G. D. Stucky, Composite mesostructures by nano-confinement, Nature Mater. 3 (2004) 816-822.

[119] Y. Y. Wu, T. Livneh, Y. X. Zhang, G. S. Cheng, J. F. Wang, J. Tang, M. Moskovits, G. D. Stucky, Templated synthesis of highly ordered mesostructured nanowires and nanowire arrays, Nano Letters 4 (2005) 2337-2342.

[120] D. Wang, R. Kou, Z. Yang, J. He, Z. Yang, Y. Lu, Hierarchical mesoporous silica wires by confined self-assembly, Chem. Comm. (2005) 166-167.

[121] A. Yamaguchi, F. Uejo, T. Yoda, T. Uchida, Y. Tanamura, T. Yamashita, N. Teramae, Self-assembly of a silica-surfactant nanocomposite in a porous alumina membrane, Nature Mater. 3 (2004) 337-341.

[122] B. A. McCool, N. Hill, J. DiCarlo, W. J. DeSisto, Synthesis and characterization of mesoporous silica membranes via dip-coating and hydrothermal deposition techniques, J. Membr. Sci. 218 (2003) 55-67.

[123] E. J. Acosta, C. S. Carr, E. E. Simanek, D. F. Shantz, Engineering nanospaces: Iterative synthesis of melamine-based dendrimers on amine-functionalized SBA-15 leading to complex hybrids with controllable chemistry and porosity, Adv. Mater. 16 (2004) 985-989.

[124] M. Platt, R. A. W. Dryfe, E. P. L. Roberts, Voltammetry with liquid/liquid microarrays: Characterization of membrane materials, Langmuir 19 (2003) 8019-8025.

[125] L. Palacio, P. Pradanos, J. I. Calvo, A. Hernandez, Porosity measurements by a gas penetration method and other techniques applied to membrane characterization, Thin Solid Films 348 (1999) 22-29.

[126] A. Hernandez, J. I. Calvo, P. Pradanos, L. Palacio, M. L. Rodriguez, J. A. de Saja, Surface structure of microporous membranes by computerized SEM image analysis applied to anopore filters, J. Membr. Sci. 137 (1997) 89-97.

[127] G. P. Crawford, L. M. Steele, R. Ondriscrawford, G. S. Iannacchione, C. J. Yeager, J. W. Doane, D. Finotello, Characterization of the cylindrical cavities of anopore and nucleopore membranes, J. Chem. Phys. 96 (1992) 7788-7796.

[128] M. P. Thomas, R. R. Landham, E. P. Butler, D. R. Cowieson, E. Barlow, P. Kilmartin, Inorganic ultrafiltration membranes prepared by a combination of anodic film and sol-gel technologies, J. Membr. Sci. 61 (1991) 215-225.

[129] R. C. Furneaux, W. R. Rigby, A. P. Davidson, The formation of controlled-porosity membranes from anodically oxidized aluminum, Nature 337 (1989) 147-149.

[130] G. R. Gallaher, P. K. T. Liu, Characterization of ceramic membranes. 1. Thermal and hydrothermal stabilities of commercial 40 angstrom membranes, J. Membr. Sci. 92 (1994) 29-44.

[131] C. L. Lin, D. L. Flowers, P. K. T. Liu, Characterization of ceramic membranes II. Modified commercial membranes with pore size under 40 Å, J. Membr. Sci. 92 (1994) 45-58.

[132] C. H. Cheng, D. F. Shantz, Silicalite-1 growth from clear solution: Effect of the structure-directing agent on growth kinetics, J. Phys. Chem. B 109 (2005) 13912-13920.

[133] S. J. Gregg, K. S. W. Sing, Adsorption, surface area, and porosity, Academic Press, London, 1982.

[134] F. Rouquerol, J. Roquerol, K. Sing, Adsorption by powders and porous solids, Academic, San Diego, 1999.

[135] E. P. Barrett, L. G. Joyner, P. P. Halenda, The determination of pore volume and area distributions in porous substances. I. Computations from nitrogen isotherms, J. Am. Chem. Soc. 73 (1951) 373-380.

[136] M. Kruk, M. Jaroniec, A. Sayari, Application of large pore MCM-41 molecular sieves to improve pore size analysis using nitrogen adsorption measurements, Langmuir 13 (1997) 6267-6273.

[137] D. A. Loy, K. J. Shea, Bridged polysilsesquioxanes - highly porous hybrid organic-inorganic materials, Chem. Rev. 95 (1995) 1431-1442.

[138] N. K. Raman, M. T. Anderson, C. J. Brinker, Templated-based approaches to the preparation of amorphous, nanoporous silicas, Chem. Mater. 8 (1996) 1682-1701.

[139] R. J. P. Corriu, Ceramics and nanostructures from molecular precursors, Angew. Chem. Int. Ed. 39 (2000) 1376-1398.

[140] C. Sanchez, B. Lebeau, F. Chaput, J. P. Boilot, Optical properties of functional hybrid organic-inorganic nanocomposites, Adv. Mater. 15 (2003) 1969-1994.

[141] U. Ciesla, F. Schuth, Ordered mesoporous materials, Micropor. Mesopor. Mater. 27 (1999) 131-149.

[142] M. E. Davis, Ordered porous materials for emerging applications, Nature 417 (2002) 813-821.

[143] F. Schuth, W. Schmidt, Microporous and mesoporous materials, Adv. Mater. 14 (2002) 629-638.

[144] A. Stein, Advances in microporous and mesoporous solids - highlights of recent progress, Adv. Mater. 15 (2003) 763-775.

[145] K. Moller, T. Bein, Inclusion chemistry in periodic mesoporous hosts, Chem. Mater. 10 (1998) 2950-2963.

[146] S. L. Burkett, S. D. Sims, S. Mann, Synthesis of hybrid inorganic-organic mesoporous silicas by co-condensation of siloxane and organosiloxane precursors, Chem. Comm. (1996) 1367-1368.

[147] M. H. Lim, C. F. Blanford,A. Stein, Synthesis and characterization of a reactive vinyl-functionalized MCM-41: Probing the internal pore structure by a bromination reaction, J. Am. Chem. Soc. 119 (1997) 4090-4091.

[148] C. E. Fowler, S. L. Burkett,S. Mann, Synthesis and characterization of ordered organo-silica-surfactant mesophases with functionalized MCM-41-type architecture, Chem. Comm. (1997) 1769-1770.

[149] M. H. Lim, A. Stein, Comparative studies of grafting and direct syntheses of inorganic-organic hybrid mesoporous materials, Chem. Mater. 11 (1999) 3285-3295.

[150] M. Alvaro, B. Ferrer, H. Garcia, S. Hashimoto, M. Hiratsuka, T. Asahi, H. Masuhara, Photochemistry of charge-transfer complexes in a viologen periodic mesoporous organosilica: Time evolution from femtoseconds to minutes, ChemPhysChem 5 (2004) 1058-1062.

[151] H. Juvaste, E. I. Iiskola, T. T. Pakkanen, Preparation of new modified catalyst carriers, J. Mol. Catal. A 150 (1999) 1-9.

[152] R. J. P. Corriu, A. Mehdi, C. Reye, C. Thieuleux, A. Frenkel, A. Gibaud, Preparation of ordered SBA-15 mesoporous silica containing chelating groups. Study of the complexation of eu(iii) inside the pore channels of the materials, New. J. Chem. 28 (2004) 156-160.

[153] M. W. McKittrick, C. W. Jones, Towards single-site functional materials - preparation of amine-functionalized surfaces exhibiting site-isolated behavior, Chem. Mater. 15 (2003) 1132-1139.

[154] M. W. McKittrick, C. W. Jones, Toward single-site, immobilized molecular catalysts: Site-isolated ti ethylene polymerization catalysts supported on porous silica, J. Am. Chem. Soc. 126 (2004) 3052-3053.

[155] K. Yu, M. W. McKittrick, C. W. Jones, Role of amine structure and site isolation on the performance of aminosilica-immobilized zirconium CGC-inspired ethylene polymerization catalysts, Organometallics 23 (2004) 4089-4096.

[156] S. Huh, J. W. Wiench, J.-C. Yoo, M. Pruski, V. S. Y. Lin, Organic functinalization and morphology control of mesoporous silicas via a co-condensation synthesis method, Chem. Mater. 15 (2003) 4247-4256.

[157] S. A. Kanan, W. T. Y. Tze, C. P. Tripp, Method to double the surface concentration and control the orientation of adsorbed (3-aminopropyl)dimethylethoxysilane on silica powders and glass slides, Langmuir 18 (2002) 6623-6627.

[158] I. Haller, Covalently attached organic monolayers on semiconductor surfaces, J. Am. Chem. Soc. 100 (1978) 8050-8055.

[159] C. W. Jones, M. W. McKittrick, J. V. Nguyen, K. Yu, Design of silica-tethered metal complexes for polymerization catalysis, Top. Catal. 34 (2005) 67-76.

[160] J. C. Hicks, C. W. Jones, Controlling the density of amine sites on silica surfaces using benzyl spacers, Langmuir 22 (2006) 2676-2681.

[161] J. D. Bass, S. L. Anderson, A. Katz, The effect of outer-sphere acidity on chemical reactivity in a synthetic heterogeneous base catalyst, Angew. Chem. Int. Ed. 42 (2003) 5219-5222.

[162] J. D. Bass, A. Katz, Thermolytic synthesis of imprinted amines in bulk silica, Chem. Mater. 15 (2003) 2757-2763.

[163] J. D. Bass, A. Katz, Bifunctional surface imprinting of silica: Thermolytic studies and characterization of discrete thiol-amine functional group pairs, Chem. Mater. 18 (2006) 1611-1620.

[164] J. L. Defreese, A. Katz, Shape-selective covalent binding in bulk, microporous imprinted silica, Micropor. Mesopor. Mater. 89 (2006) 25-32.

[165] A. W. Bosman, H. M. Janssen, E. W. Meijer, About dendrimers: Structure, physical properties, and applications, Chem. Rev. 99 (1999) 1665-1688.

[166] S. K. Grayson, J. M. J. Frechet, Convergent dendrons and dendrimers: From synthesis to applications, Chem. Rev. 101 (2001) 3819-3867.

[167] D. A. Tomalia, J. M. J. Frechet, Discovery of dendrimers and dendritic polymers: A brief historical perspective, J. Polym. Sci. A. 40 (2002) 2719-2728.

[168] I. Díaz, B. García, B. Alsonso, C. M. Casado, M. Morán, J. Losada, J. Pérez-Pariente, Ferrocenyl dendrimers incorporated into mesoporous silica: New hybrid redox-active materials, Chem. Mater. 15 (2003) 1073-1079.

[169] M. F. Ottaviani, N. J. Turro, S. Jockbush, D. A. Tomalia, Epr investigations of the adsorption of dendrimers on porous surfaces, J. Phys. Chem. B 107 (2003) 2046-2053.

[170] I. Díaz, B. García, B. Alsonso, C. M. Casado, M. Morán, J. Losada,J. Pérez-Pariente, Ferrocenyl dendrimers incorporated into mesoporous silica: New hybrid redox-active materials, Chem. Mater. 15 (2003) 1073-1079.

[171] J. P. K. Reynhardt, Y. Yang, A. Sayari, H. Alper, Periodic mesoporous silica-supported recyclable rhodium-complexed dendrimer catalysts, Chem. Mater. 16 (2004) 4095-4102.

[172] J. P. K. Reynhardt, Y. Yang, A. Sayari, H. Alper, Rhodium complexed c2-pamam dendrimers supported on large pore davisil silica as catalysts for the hydroformylation of olefins, Adv. Synth. Catal. 347 (2005) 1379-1388.

[173] J. P. K. Reynhardt, Y. Yang, A. Sayari, H. Alper, Polyamidoamine dendrimers prepared inside the channels of pore-expanded periodic mesoporous silica, Adv. Funct. Mater. 15 (2005) 1641-1646.

[174] M. F. Ottaviani, S. Bossmann, N. J. Turro, D. A. Tomalia, Characterization of starburst dendrimers by the epr technique. 1. Copper complexes in water solution, J. Am. Chem. Soc. 116 (1994) 661-671.

[175] M. F. Ottaviani, F. Montalti, N. J. Turro, D. A. Tomalia, Characterization of starburst dendrimers by the epr technique. Copper(ii) ions binding full-generation dendrimers, J. Phys. Chem. B 101 (1997) 158-166.

[176] H. Yang, N. Coombs, I. Sokolov, G. A. Ozin, Free-standing and oriented mesoporous silica films grown at the air-water interface, Nature 381 (1996) 589-592.

[177] P. D. Yang, D. Y. Zhao, D. I. Margolese, B. F. Chmelka, G. D. Stucky, Generalized syntheses of large-pore mesoporous metal oxides with semicrystalline frameworks, Nature 396 (1998) 152-155.

[178] A. Gibaud, D. Grosso, B. Smarsly, A. Baptiste, J. F. Bardeau, F. Babonneau, D. A. Doshi, Z. Chen, C. J. Brinker, C. Sanchez, Evaporation-controlled self-assembly of silica surfactant mesophases, J. Phys. Chem. B 107 (2003) 6114-6118.

[179] E. L. Crepaldi, G. J. D. A. Soler-Illia, D. Grosso, F. Cagnol, F. Ribot, C. Sanchez, Controlled formation of highly organized mesoporous titania thin films: From mesostructured hybrids to mesoporous nanoanatase TiO_2, J. Am. Chem. Soc. 125 (2003) 9770-9786.

[180] D. A. Doshi, N. K. Huesing, M. C. Lu, H. Y. Fan, Y. F. Lu, K. Simmons-Potter, B. G. Potter, A. J. Hurd, C. J. Brinker, Optically defined multifunctional patterning of photosensitive thin-film silica mesophases, Science 290 (2000) 107-111.

[181] D. A. Doshi, A. Gibaud, V. Goletto, M. C. Lu, H. Gerung, B. Ocko, S. M. Han, C. J. Brinker, Peering into the self-assembly of surfactant templated thin-film silica mesophases, J. Am. Chem. Soc. 125 (2003) 11646-11655.

[182] H. Y. Fan, Y. F. Lu, A. Stump, S. T. Reed, T. Baer, R. Schunk, V. Perez-Luna, G. P. Lopez, C. J. Brinker, Rapid prototyping of patterned functional nanostructures, Nature 405 (2000) 56-60.

[183] D. Grosso, F. Babonneau, P. A. Albouy, H. Amenitsch, A. R. Balkenende, A. Brunet-Bruneau, An *in situ* study of mesostructure ctab-silica film formation during dip coating using time-resolved SAXS and interferometry, Chem. Mater. 14 (2002) 931-939.

[184] D. Grosso, F. Babonneau, C. Sanchez, G. J. D. A. Soler-Illia, E. L. Crepaldi, P. A. Albouy, H. Amenitsch, A. R. Balkenende, A. Brunet-Bruneau, A first insight in the mechanisms involved in the self-assembly of 2d-hexagonal templated SiO_2 and TiO_2 mesostructured films during dip-coating, J. Sol Gel Sci. Technol. 26 (2003) 561-565.

[185] M. Trau, N. Yao, E. Kim, Y. Xia, G. M. Whitesides, I. A. Aksay, Microscopic patterning of oriented mesoscopic silica through guided growth, Nature 390 (1997) 674-676.

[186] C. R. Martin, Nanomaterials - a membrane-based synthetic approach, Science 266 (1994) 1961-1966.

[187] M. Nishizawa, V. P. Menon, C. R. Martin, Metal nanotubule membranes with electrochemically switchable ion-transport selectivity, Science 268 (1995) 700-702.

[188] Y. M. Lin, S. B. Cronin, O. Rabin, J. Y. Ying, M. S. Dresselhaus, Transport properties of bi1-xsbx alloy nanowires synthesized by pressure injection, Appl. Phys. Lett. 79 (2001) 677-679.

[189] O. Rabin, P. R. Herz, Y. M. Lin, A. I. Akinwande, S. B. Cronin,M. S. Dresselhaus, Formation of thick porous anodic alumina films and nanowire arrays on silicon wafers and surfaces, Adv. Func. Mater. 13 (2003) 631-638.

[190] D. T. Mitchell, S. B. Lee, L. Trofin, N. C. Li, T. K. Nevanen, H. Soderlund, C. R. Martin, Smart nanotubes for bioseparations and biocatalysis, J. Am. Chem. Soc. 124 (2002) 11864-11865.

[191] S. F. Hou, J. H. Wang, C. R. Martin, Template-synthesized protein nanotubes, Nano Letters 5 (2005) 231-234.

[192] S. F. Hou, J. H. Wang, C. R. Martin, Template-synthesized DNA nanotubes, J. Am. Chem. Soc. 127 (2005) 8586-8587.

[193] A. Y. Ku, S. T. Taylor, S. M. Loureiro, Mesoporous silica composites containing multiple regions with distinct pore size and complex pore organization, J. Am. Chem. Soc. 127 (2005) 6934-6935.

[194] M. Trocha, W. J. Koros, A diffusion-controlled procedure to close pores in ceramic membranes, J. Membr. Sci. 95 (1994) 259-276.

[195] Y. S. Lin, A theoretical-analysis on pore-size change of porous ceramic membranes after modification, J. Membr. Sci. 79 (1993) 55-64.

[196] Y. S. Lin, A. J. Burggraaf, Experimental studies on pore-size change of porous ceramic membranes after modification, J. Membr. Sci. 79 (1993) 65-82.

[197] H. M. Alsyouri, J. Y. S. Lin, Gas diffusion and microstructural properties of ordered mesoporous silica fibers, J. Phys. Chem. B 109 (2005) 13623-13629.

[198] S. Pevzner, O. Regev, The *in situ* phase transitions occurring during bicontinuous cubic phase formation, Micropor. Mesopor. Mater. 38 (2000) 413-421.

[199] N. R. B. Coleman, G. S. Attard, Ordered mesoporous silicas prepared from both micellar solutions and liquid crystal phases, Micropor. Mesopor. Mater. 44-45 (2001) 73-80.

[200] H. Q. Lin, E. Van Wagner, B. D. Freeman, L. G. Toy, R. P. Gupta, Plasticization-enhanced hydrogen purification using polymeric membranes, Science 311 (2006) 639-642.

[201] T. C. Merkel, B. D. Freeman, R. J. Spontak, Z. He, I. Pinnau, P. Meakin, A. J. Hill, Ultrapermeable, reverse-selective nanocomposite membranes, Science 296 (2002) 519-522.

[202] J. S. Cha, V. Malik, D. Bhaumik, R. Li, K. K. Sirkar, Removal of VOCs from waste gas streams by permeation in a hollow fiber permeator, J. Membr. Sci. 128 (1997) 195-211.

[203] H. Paul, C. Philipsen, F. J. Gerner, H. Strathmann, Removal of organic vapors from air by selective membrane permeation, J. Membr. Sci. 36 (1988) 363-372.

[204] S. B. Lee, D. T. Mitchell, L. Trofin, T. K. Nevanen, H. Soderlund, C. R. Martin, Antibody-based bio-nanotube membranes for enantiomeric drug separations, Science 296 (2002) 2198-2200.

[205] S. Yoo, J. D. Lunn, S. Gonzalez, J. A. Ristich, E. E. Simanek, D. F. Shantz, Engineering nanospaces: OMS/dendrimer hybrids possessing controllable chemistry and porosity, Chem. Mater. 18 (2006) 2935-2942.

[206] S. A. Stern, V. A. Shah, V. J. Hardy, Structure-permeability relationship in silicon polymers, J. Polym. Sci. Part B: Polym. Phys 25 (1987) 1263.

[207] B. E. Poling, J. M. Prausnitz, J. P. O'Connell, The properties of gases and liquids, McGraw-Hill, New York, 2001.

[208] B. D. Freeman, Basis of permeability/selectivity tradeoff relations in polymeric gas separation membranes, Macromolecules 32 (1999) 375-380.

[209] J. Brandrup, E. H. Immergut, Polymer handbook, Wiley, New York, 1989.

[210] S. J. Yoo, D. M. Ford, D. F. Shantz, Synthesis and characterization of uniform alumina-mesoporous silica hybrid membranes, Langmuir 22 (2006) 1839-1845.

VITA

SUK JOON YOO

Suk Joon Yoo was born in Seoul, Korea. He received his B.S. in chemical engineering from Korea University, Seoul, Korea in 1997. In 2000, he joined Texas A&M University as a graduate student. He received his M.S. in chemical engineering from Texas A&M University in August 2002. He received his Ph.D. in chemical engineering from Texas A&M University in December 2006.

He can be contacted at:

C/o Dr. David M. Ford or Dr. Daniel F. Shantz

Department of Chemical Engineering

Texas A&M University

TAMU 3122

College Station, TX 77843-3122